TABLE OF CONTENTS

Report Documentation Page

Form Approved
OMB No. 0704-0188

1. REPORT DATE	2. REPORT TYPE	3. DATES COVERED
23 FEB 2010		**01-04-2007 to 30-11-2009**

4. TITLE AND SUBTITLE	5a. CONTRACT NUMBER
Polyacrylonitrile/Carbon Nanotube Composite: Precursor for Next Generation Carbon Fiber	**FA9550-07-1-0233**
	5b. GRANT NUMBER
	5c. PROGRAM ELEMENT NUMBER
6. AUTHOR(S)	5d. PROJECT NUMBER
	5e. TASK NUMBER
	5f. WORK UNIT NUMBER
7. PERFORMING ORGANIZATION NAME(S) AND ADDRESS(ES) **Georgia Institute of Technology,School of Polymer, Textile and Fiber Engineering,Atlanta,GA,30332-0295**	8. PERFORMING ORGANIZATION REPORT NUMBER
9. SPONSORING/MONITORING AGENCY NAME(S) AND ADDRESS(ES) **Aerospace, Chemical and Material Sciences Directorate, Air Force office of Scientific Research, 875 N. Randolph St, Arlington, VA, 22203**	10. SPONSOR/MONITOR'S ACRONYM(S)
	11. SPONSOR/MONITOR'S REPORT NUMBER(S)

12. DISTRIBUTION/AVAILABILITY STATEMENT
Approved for public release; distribution unlimited

13. SUPPLEMENTARY NOTES

14. ABSTRACT

15. SUBJECT TERMS

16. SECURITY CLASSIFICATION OF:			17. LIMITATION OF ABSTRACT	18. NUMBER OF PAGES	19a. NAME OF RESPONSIBLE PERSON
a. REPORT **unclassified**	b. ABSTRACT **unclassified**	c. THIS PAGE **unclassified**	**Same as Report (SAR)**	**107**	

Executive Summary

In the preliminary study it was reported that gel spun polyacrylonitrile (PAN) and PAN/single wall carbon nanotube (SWNT) composite fibers have been stabilized in air and subsequently carbonized in argon at 1100 ºC. Differential scanning calorimetry (DSC) and infrared spectroscopy suggested that the presence of single wall carbon nanotube affects PAN stabilization. Carbonized PAN/SWNT fibers exhibited 10 to 30 nm diameter fibrils embedded in brittle carbon matrix, while the control PAN carbonized under the same conditions exhibited brittle fracture with no fibrils. High resolution transmission electron microscopy and Raman spectroscopy suggests the existence of well developed graphitic regions in carbonized PAN/SWNT and mostly disordered carbon in carbonized PAN. Tensile modulus and strength of the carbonized fibers were as high as 250 N/tex and 1.8 N/tex for the composite fibers and 168 N/tex and 1.1 N/tex for the control PAN based carbon fibers, respectively. The addition of 1 wt% carbon nanotubes enhanced the carbon fiber modulus by 49% and strength by 64%. Carbon fiber diameter in this study was above 5 micrometer. In a follow up study, polyacrylonitrile (PAN) and PAN/carbon nanotube (CNT) composite (99/1) based carbon fibers with an effective diameter of about 1 μm have been processed using island-in-a-sea bi-component cross-sectional geometry and gel spinning. PAN/CNT (99/1) based carbon fibers processed using this approach exhibited a tensile strength of 4.5 GPa (2.5 N/tex) and tensile modulus of 463 GPa (257 N/tex), while these values for the control PAN-based carbon fiber processed under the similar conditions were 3.2 GPa (1.8 N/tex) and 337 GPa (187 N/tex), respectively. Properties of these 1 μm diameter carbon fibers have been compared to the properties of the larger diameter (> 6 μm) PAN and PAN/CNT based carbon fibers.

These and other published studies demonstrated the following: (1) PAN and PAN/CNT fibers can be gel spun. (2) these gel spun PAN and PAN/CNT fibers can be stabilized and carbonized to yield high strength and high modulus carbon fibers. (3) Small diameter (of the order of one micrometer diameter) PAN and PAN/CNT based carbon fibers can be processed using islands-in-a sea bi-component spinning approach. (4) Carbon nanotubes affect the order, orientation, stabilization, and carbonization behavior of PAN making PAN graphitizable at a relatively low temperature of 1100 °C. (4) Addition of 1 wt% CNT in PAN can increase the strength and modulus of the resulting carbon fibers by about 50%. (5) Carbon nanotubes act as a nucleating agent for polymer crystallization and a template for polymer orientation. Based on these studies it has been concluded that PAN/CNT can be a precursor for next generation carbon fiber. However, the development of the next generation carbon fiber requires, both the material and process optimization. Material optimization includes PAN copolymer composition and the its molecular weight, as well as the carbon nanotube type, its impurity as well as its structural perfection. Process optimization includes CNT dispersion methods, as well as PAN/CNT fiber spinning, stabilization, and carbonization parameters. Following studies summarize initial attempts on optimizing and understanding the fiber processing and stabilization behavior of PAN/CNT systems.

PAN/CNT fiber spinning: Poly(acrylonitrile-co-methacrylic acid) (PAN-co-MAA)/few-wall carbon nanotube (FWNT) solutions were prepared at the FWNT concentration of 0, 0.1, 0.5, and 1 wt%. Rheological behavior of the solutions has been studied using dynamic and steady shear test. The viscosity of PAN-co-MAA/FWNT composite solution is higher than that of control solution in low shear rate regime. For high shear rate regime, the viscosity of composite solution

became lower than that of control solution due to the alignment of FWNTs along the flow direction, suggesting that the FWNTs may facilitate the flow of polymer solution. PAN-co-MAA/FWNT fibers were gel spun followed by drawing at room temperature and subsequent drawing at 165 ºC. Using this approach, fibers with tensile strength of up to 1.15 GPa and tensile modulus of up to 31.7 GPa were processed. After each processing step, fibers were studied for their structure and morphology using X-ray diffraction and Raman spectroscopy. It was shown that carbon nanotube orientation develops much earlier than that of the polyacrylonitrile.

Stabilization: The effects of different types of CNTs on chemical, mechanical and structural evolution during the stabilization were studied. The optimal residence time for stabilization with the best orientation and chemical structure was determined by combining wide angle X-ray diffraction (WAXD), infrared spectroscopy (IR), and scanning electron microscopy (SEM) results. These different methods show comparable results and can be used as criteria to optimize stabilization. Additionally, applied stress during stabilization is very important for obtaining good properties. The detailed effects of applied stress during stabilization on chemical structure, physical parameter and mechanical properties of stabilized fibers are discussed. The addition of CNTs enhances the maximum stress that can be applied on fiber during stabilization. Differential scanning calorimetry (DSC), infrared spectroscopy (IR), wide angle x-ray diffraction (WAXD) and thermo-gravimetric analysis (TGA) studies suggest that individual reactions such as cyclization, oxidation, dehydrogenation, and cross-linking can be distinguished at different stabilization stages. It is also shown that the overall stabilization reaction is limited by cyclization reaction and oxygen diffusion because the oxidation preferentially occurs with cyclized structure. Shrinkage behavior of PAN/CNT composite fiber exhibited that CNT significantly reduces overall shrinkage and increases the maximum stress that can be applied to fiber, indicating good interaction with PAN matrix.

Published papers:

1. H. G. Chae, M. L. Minus, A. Rasheed, and S. Kumar, "Stabilization and Carbonization of Gel Spun Polyacrylonitrile/Single Wall Carbon Nanotube Composite Fibers", *Polymer*, **48**, 3781-3789 (2007).
2. S. Zhang, M. L. Minus, S. Kumar, L. Zhu, C. P. Wong, "Polymer Transcrystallinity Induced by Carbon Nanotubes", *Polymer*, 49, 1356-1364 (2008) .
3. H. G. Chae and S. Kumar, "Making Strong Fibers", *Science,* **319**, 908-909 (2008).
4. S. Zhang and S. Kumar, "Shaping Polymer Particles by Carbon Nanotubes", *Macromol. Rapid Commun.*, **29**, 557-561 (2008).
5. S. Zhang and S. Kumar, "Carbon Nanotubes as Liquid Crystals", *Small,* **4** (9), 1270-1283 (2008).
6. H. Guo, A. Rasheed, and S. Kumar, "Polyacrylonitrile/Vapor Grown Carbon Nano Fiber Composite Films", *J. Mater. Sci.*,**43**, 4363 - 4369 (2008).
7. G-W Lee, S. Jagannathan, H. G. Chae, M. L. Minus, S. Kumar, "Carbon Nanotube Dispersion and exfoliation in Polypropylene and Structure and Properties of the Resulting Composites", *Polymer*, **49**, 1831-1840 (2008).
8. W. Wang, N.S. Murthy, H. G. Chae, and S. Kumar, "Structural changes during deformation in carbon nanotube reinforced polyacrylonitrile fibers", *Polymer*, **49**, 2133-2145 (2008)
9. S. Zhang, L. Zhu, M. L. Minus, H. G. Chae, S. Jagannathan, C. P. Wong, J. Kowalik, L. B. Roberson, and S. Kumar, "Solid-State Spun Fibers and Yarns from 1mm Long Carbon Nanotube Forests Synthesized by Water-Assisted Chemical Vapor Deposition", *J. Mater. Sci.*,**43**, 4356-4362 (2008).
10. H. G. Chae, D. J. Delong, S. Kumar, "Next Generation Carbon Fiber", *Nanotechnology Law and Business*, **5** (3), 275 – 286 (2008).
11. S. Kumar, "Fibers in the Twenty First Century", *Indian Journal of Fiber and Textile Research,* **33** (4), 361 – 362 (2008).
12. J. Liu, A. Rasheed, Marilyn L. Minus, and S. Kumar, "Processing and Properties of Carbon Nanotubes/Poly (methyl methacrylate) Composite Films", *J. Appl. Polym. Sci.*, **112**(1), 142 – 156 (2009).
13. H. G. Chae, Y. H. Choi, M. L. Minus, and S. Kumar, "Carbon Nanotube Reinforced Small Diameter Polyacrylonitrile Based Carbon Fiber", *Composites Science and Technology*, **69**, 406-413 (2009).
14. B. G. Min, H. G. Chae, M. L. Minus, and S. Kumar, "Polymer/Carbon Nanotube Composite Fibers – An Overview", in *Functional Composites of Carbon Nanotubes and Applications,* Editors - K. P. Lee and A. I. Gopalan, and F. D. S. Marquis, p. 43 – 73 (2009) Research Signpost, Transworld Research Network, Trivandrum, Kerala, India.
15. M. L. Minus, H. G. Chae, S. Kumar, Interfacial Crystallization in Gel Spun Poly (vinyl alcohol) /Single-Wall Carbon Nanotube Composite Fibers", *Macromolecular Chemistry and Physics*, **210,** 1799 – 1808 (2009).

16. W. Wang, N. S. Murthy, H. G. Chae, and S. Kumar “Small-angle x-ray scattering investigation of carbon nanotube reinforced polyacrylonitrile fibers during deformation”, *Journal of Polymer Science Part B: Polymer Physics,* **47**, 2394 - 2409 (2009).

Key Manuscripts (to be published):

1. Young Ho Choi, Han Gi Chae, and Satish Kumar, “Poly(acrylonitrile-co-methacrylic acid)/ few-wall carbon nanotube composites: Solution rheology and development of structure and property during fiber spinning.
2. Yaodong Liu, Han Gi Chae, Satish Kumar, “Stabilization of Gel-spun Polyacrylonitrile/Carbon Nanotubes Composite Fibers. Part I: Effects of Carbon Nanotubes”.
3. Yaodong Liu, Han Gi Chae, Satish Kumar, “Stabilization of Gel-spun Polyacrylonitrile/Carbon Nanotubes Composite Fibers. Part II: Stabilization Kinetics and Effects of Various Chemical Reactions”.
4. Yaodong Liu, Han Gi Chae, Satish Kumar, “Stabilization of Gel-spun Polyacrylonitrile/Carbon Nanotubes Composite Fibers. Part III: Effect of stabilization conditions”

These four unpublished manuscripts are included in this report.

Ph.D. Theses (completed):

1. Han Gi Chae, “Polyacrylonitrile/carbon nanotube composite fibers: reinforcement efficiency and carbonization studies”, Ph.D. Thesis, Georgia Institute of Technology, 2008.
2. Marilyn L. Minus, The study of crystallization and interfacial morphology in polymer/carbon nanotube composites, Ph.D. Thesis, Georgia Institute of Technology, 2008.

Ph.D. Theses (in progress):

3. Yaodong Liu, “Stabilization and Carbonization Studies in Gel spun Polyacrylonitrile/carbon nanotube composite fibers”, Ph.D. Thesis, Georgia Institute of Technology, in progress.
4. Young Ho Choi, "Polyacrylonitrile / Carbon Nanotube Composite Fibers: Effect of various spinning parameters on fiber structure and properties". Ph.D. Thesis, Georgia Institute of Technology, in progress.

SECTION I

Poly(acrylonitrile-co-methacrylic acid)/ few-wall carbon nanotube composites: Solution rheology and development of structure and property during fiber spinning

Young Ho Choi, Han Gi Chae, Satish Kumar

School of Polymer, Textile & Fiber Engineering, Georgia Institute of Technology
Atlanta, GA 30332-0295

Abstract

Poly(acrylonitrile-co-methacrylic acid) (PAN-co-MAA)/few-wall carbon nanotube (FWNT) solutions were prepared at the FWNT concentration of 0, 0.1, 0.5, and 1 wt%. Rheological behavior of the solutions has been studied using dynamic oscillation and steady shear test. The viscosity of PAN-co-MAA/FWNT composite solution is higher than that of control solution in low shear rate regime. For high shear rate regime, the viscosity of composite solution became lower than that of control solution due to the alignment of FWNTs along the flow direction, suggesting that the FWNTs facilitate the flow of polymer solution. PAN-co-MAA/FWNT fibers were gel spun followed by cold-drawing at room temperature and hot-drawing at 165 ºC using glycerol bath. Control fibers experienced cold-drawing process, possessed tensile strength of 1.15 GPa and tensile modulus of 26.1 GPa, while composite fibers (1 wt% of FWNT) exhibited up to 31.7 GPa of tensile modulus. After each processing step, fibers were studied in terms of structure and morphology using X-ray diffraction and Raman spectroscopy. For as-spun and cold drawn fiber, the Herman's orientation factor of PAN-co-MAA crystal (f_c) is lower than that of CNTs (f_{CNT}).

Keywords: PAN; CNT; cold-drawing; rheology; orientation

1. Introduction

Polyacrylonitrile (PAN) is commercially important polymer for carbon fiber production as a precursor material[1]. PAN fibers have become major precursor due to the high tensile and compressive strength of the resulting carbon fibers[2,3]. Intensive researches have been carried out to improve mechanical properties of carbon fibers since 1960s. As a result, high strength carbon fibers with nearly 90% of the theoretical modulus[4] are available now in case of pitch-based carbon fiber, yet the tensile strength is still less than 10% of the theoretical value. Recent efforts to narrow down this gap between the theory and practice are: (i) gel-spinning of PAN fiber[5] and (ii) incorporation of carbon nanotubes (CNTs) in PAN fiber[5,6]. Gel spun PAN fiber showed high modulus and high strength as compared to conventional solution spun PAN fiber due to high molecular orientation of PAN and less defect structure. Furthermore, recent results show that the addition of 1 wt% CNTs can increase the tensile strength and tensile modulus of PAN-based carbon fibers by 64% and 49%, respectively due to the formation of highly graphitic structure in the vicinity of CNTs.

In this study, the rheological behavior of PAN/FWNTs solution, orientation of FWNTs and structural variation of PAN crystal were monitored in each processing steps such as solution

preparation, spinning, drawing (cold and hot). Mechanical properties and structural changes in cold drawn fibers were also compared with fibers without cold drawing.

2. Experimental

2.1. Materials

PAN-co-MAA (Polyacrilonitrile-co-methacrylic acid; 4 wt% of MAA content, molecular weight - 2.4×10^5 g/mol) was obtained from Japan Exlan, Co (Japan). Few-walled nanotube (FWNT: Lot # XO021UA with 2.4 wt% metallic impurity) were obtained from Carbon Nanotechnologies, Inc. (Houston, TX) and used as received. Dimethylacetamide (DMAc) from Aldrich co. and *N, N*-dimethylformamide (DMF) from BDH, Inc. were used after distillation.

2.2. Solution preparation

FWNTs were dispersed in DMAc or DMF by sonication method (Branson 3510R-MT, 100 W, 42 kHz) at a concentration of 37.5 mg/L for 24 hours. PAN-co-MAA polymer (12.5 g) was dried in vacuum oven at 100 °C and dissolved in DMAc (100 mL) at 80 °C. Dispersed FWNT/DMAc solution was added to PAN-co-MAA/DMAc solution and the excess amount of solvent was evaporated by vacuum distillation with mechanical stirring to meet desired solid content in solvent (12.5 g solids (PAN-co-MAA and FWNTs)/100 mL DMAc). Similarly, the other composite solutions are prepared at the CNTs concentration with respect to the polymer of 0, 0.1, 0.5, and 1 wt%, respectively.

2.3. Solution rheology

Frequency sweep tests were conducted using ARES rheometer (Rheometrics Scientific, Co.) with parallel plate geometry (25 mm of plate diameter and 1 mm of gap between plates) at room temperature. The angular frequency (ω) range was set from 0.5 to 500 rad/s at a fixed strain of 5% . The capillary rheometer measurements were carried out using Dynisco LCR7001 Rheometer with orifice of 29.97 L/D ratio (9.14 mm/0.305 mm) at two temperature levels of 40, and 110 °C. The apparent viscosity was monitored as a function of shear rate ranging from 500~50,000 1/s.

2.4. Fiber spinning

The PAN-co-MAA control and PAN-co-MAA/FWNTs composite fibers are gel-spun using Braford University spinning unit with single-hole spinneret (spinneret diameter - 250 μm). The prepared solution was spun into cold methanol gelation bath (-50 °C) with air gap of 2 - 3 cm. In some cases, the fibers were stretched during the spinning process by increasing the take-up speed with respect to linear throughput velocity of spun fibers. Prior to the drawing process, the as-spun fibers were immersed in the methanol bath at the temperature of -50 °C for 72 hours to ensure gelation. The two-step drawing process was carried out: (i) the as-spun fibers were stretched at room temperature (cold drawing). (ii) the cold drawn fibers were subsequently drawn by passing through hot glycerol bath of which temperature was maintained at 170 °C followed by washing in ethanol and vacuum drying at 50 °C for 3 days. The total draw ratio was determined by product of spin draw ratio, cold draw ratio, and hot draw ratio and expressed respectively in parenthesis (e.g. total draw ratio of 15 with spin draw ratio of 2, cold draw ratio of 1.5, and hot draw ratio of 5 is expressed as 15 ($2 \times 1.5 \times 5$)).

2.5 Characterization of fiber

The tensile properties were characterized by use of RSA III solids analyzer (Rheometric Scientific, Co.) at gauge length of 25.4 mm and crosshead speed of 0.25 mm/s. At least 16 specimens were tested for each sample. Wide-angle X-ray diffractions of PAN-co-MAA control and composite fibers were collected by Rigaku MicroMax 002 X-ray generator with confocal optics to produce Kα radiation (λ = 1.5418 Å) and equipped with a R-axis IV++ detector. The crystallinity was calculated by fitting the integrated scan using MDI Jade 6.1 software, and the crystal size was calculated by using Scherrer's equation. The Herman's orientation function pertains to the c axis crystals about fiber axis (f_c: Herman's orientation factor) was calculated using Wilchinsky's equation assuming even orientation distribution along the fiber radial direction. The detailed calculation method is given in previous literature.[7] Raman spectra were collected using Holoprobe Research 785 Raman microscopy (Kaiser optical system co, Ltd) equipped with excitation laser wavelength of 785 nm. Raman specimen was mounted on the angle stage of Raman spectroscopy. The intensity of laser source was adjusted to 40 mW to prevent the thermal decomposition of fiber. For orientation determination, the peak intensity (base line corrected by GRAMS/Al v7.01) of the tangential band (~ 1590 cm^{-1}) was read. For solving simultaneous equations to evaluate CNTs orientation as described elsewhere[8], VV (both laser source and analyzer are vertically polarized) and VH (laser source is vertically polarized and analyzer has horizontal polarization direction) mode spectra were collected at $\Phi = 0°$ (defined polarization direction of laser source is parallel to fiber axis) and $\Phi = 90°$ (defined polarized laser is perpendicular to fiber axis), respectively. The intensities at $\Phi = 0$ are obtained by changing analyzer from VV mode to VH mode. For the case of solution specimens, a droplet of each composite solution was carefully placed on silicon wafer to minimize flow induced orientation and characterized after ten minutes relaxation. The arbitrary point of droplet was set as $\Phi = 0$ and 90° rotation of angle stage as $\Phi = 90$.

3. Results and Discussion

3.1. Dynamic shear rheololgy of PAN and PAN/CNTs solution.

The changes in complex viscosity of PAN-co-MAA/FWNT solution are plotted in Figure 1 as a function of angular frequency. The complex viscosities of all solutions decreased with increasing angular frequency (shear thinning behavior). The CNTs containing composite solutions showed higher viscosity than control solution. The viscosity differences between various solutions are noticeable in low frequency regime, while comparable solution viscosity is observed in high frequency regime, indicating that the effect of CNTs on viscosity is significant at low frequency regime rather than at high frequency regime.

Figure 2 shows storage modulus (G') and loss modulus (G") behavior as a function of frequency for various solutions. Both moduli increase with frequency; the effect of nanotube content on storage modulus is higher at low frequency regime than at high frequency regime. At low frequency the storage modulus increased rapidly as nanotube loading increase. However, the contribution of nanotube loading on loss modulus is not as high as that on storage modulus even at low frequency regime. Since the nature of nanotubes is rigid rod, they can contribute storage modulus more than the loss modulus. Therefore, the storage modulus of PAN/CNT solution can be affected by nanotube loading dominantly at low frequency which is in good agreement with melt rheology of PP/MWNT[9,10]. At low shear rate, the CNTs remain randomly dispersed or a network structure in case above the percolation threshold and dominate the low frequency

response since CNTs are rigid as compared to polymer molecules[11]. On the other hand, polymer molecules start to respond and dominate at high frequency, since the CNTs are deformed or aligned along the shear direction.

Results for loss factor, tan δ, as a function of frequency are plotted in Figure 3. Lower tan δ value implies the more elastic behavior. In Figure 3, the tan δ values of all solutions are decreasing as a function of angular frequency which implies that PAN-co-MAA/FWNT solutions showed more elastic behavior at high deformation rate. By incorporating the nanotubes in the PAN-co-MAA solution system, the elastic modulus of the solution increases, resulting in reduced tan δ. It is also noted that the higher nanotube concentration solution showed the lower tan δ value. At low frequency regime, tan δ decreased by increasing nanotube content which implies that the formation of nanotube network in the composite solution contributes to an elastic response. However, the nanotube network started to deform and flow as the deformation rate increase, as a result the contribution of nanotube network on tan δ decreased. The solvent differences between DMF and DMAc on tan δ can be negligible by comparing the plots of 0.5 wt% DMAc and 0.5 wt% DMF. Again the differences mainly come from the amount of nanotube loading.

3.2 Steady shear rheology of PAN and PAN/CNT solution

The capillary steady shear tests were conducted to assess the rheological behavior of PAN-co-MAA control and composite solutions under high steady shear because polymer solution will experience more than 10,000 1/s shear rate in the case of fiber spinning process[1]. The apparent viscosity values are plotted as a function of shear rate in Figure 4 and PAN-co-MAA control and composite solution showed shear thinning behavior. The viscosity of composite solution is lower than that of control solution regardless of temperature which is opposite to the dynamic test results. Unlike the deformation under dynamic conditions, the fully developed laminar flow might help CNT orientation along the flow direction, leading to viscosity drop. Based on these observations, one can expect that CNTs can assist the flow of spinning solution during spinning process.

The dynamic (complex viscosity, η*) and steady (Rabinowitsch corrected viscosity, η) rheological behavior of PAN-co-MAA solution is compared and plotted together in Figure 5. According to the Cox-Merz rule[12] there is relationship between complex viscosity and shear viscosity and is expressed by

$$\eta(\dot{\gamma}) = \left|\eta^*(\omega)\right|_{\omega=\dot{\gamma}} = \eta'(\omega)\left[1+\left(\frac{\eta''}{\eta'}\right)^2\right]^{1/2}_{\omega=\dot{\gamma}} \quad \text{.....(1)}$$

There are discontinuous points that are observed between 100 and 1000. This discontinuity may come from the discrepancy of the rule, or overestimation of viscosity due to the entrance pressure drop in capillary. After this transition, PAN-co-MAA/FWNT composite solution showed lower viscosity than control one. As discussed earlier, this indicates that CNTs facilitate polymer solution flow.

[1] Shear rate calculation: $\left.\frac{\partial V_z}{\partial r}\right|_{r=R} = \dot{\gamma}_w = \frac{4Q}{\pi R^3}$,where V_z is velocity of polymer solution along the spinning direction, $\dot{\gamma}_w$ is shear rate, Q is flux across the spinneret, and R is radius of spinneret, respectively

3.3. Tensile properties

The tensile properties of PAN-co-MAA control and composite fibers are summarized in Table 1. Comparison of control fibers of various draw ratio revealed that the higher hot draw ratio contributes the higher tensile strength and modulus. The number of polymer molecular entanglements which act as defect during tensile test can be reduced by drawing (high draw ratio). However, fiber stretched 12.6 ($2\times1.8\times3.5$) times in total showed poor tensile properties as compared to the fiber with draw ratio of 9.45 ($1\times2.7\times3.5$). The former fiber was stretched 3.6 times prior to hot drawing by 2 times of spin drawing and 1.8 times of cold drawing, whereas the latter was stretched 2.7 times by cold drawing only. From these results, one can note that the cold drawing contributes the polymer molecule alignment more than spin drawing. This may be due to the fact that elongational shear stress in cold drawing stage is much higher than that in spin drawing stage because of the difference in amount of residual solvent molecules. In addition, the fiber only stretched during hot drawing ($1\times1\times11$) has poor tensile properties even though it experienced higher total draw ratio. Therefore, it can be noted that the cold drawing improves the polymer crystal structure very effectively similar to the strain hardening of metal by plastic deformation. The polymer may experience more elongational shear stress at a lower temperature with same draw ratio. For homopolymer PAN (molecular weight of 2.5×10^5 g/mol) cases[5], the tensile strength can be achieved to 0.9 GPa and tensile modulus of 22 GPa with total draw ratio of 51. In this study, the highest tensile strength of control fiber was 1.15 GPa at relatively low total draw ratio of 14.85. The effect of cold drawing is very significant, considering the low molecular weight of PAN-co-MAA (2.4×10^5 g/mol) as compared to that of homopolymer PAN (2.5×10^5 g/mol) and tendency of amorphous structure formation due to the methacrylic acid (MAA) component in PAN-co-MAA fiber. So the effects of the cold drawing process are; (i) to align the polymer molecules to the fiber axis more significantly and (ii) to remove the solvent from the fiber. The effect of spin, cold and hot drawing on crystal size, orientation and crystallinity will be discussed further with X-ray diffraction results. For the case of FWNT 1 wt% composite fibers, the tensile modulus was improved to 31.7 GPa due to the CNT reinforcement, yet the tensile strength was comparable to control fibers since the tensile strength is defect dependent property[13].

3.4. PAN crystal and CNT orientation characterization

The measured wide-angle X-ray diffraction patterns are shown in Figure 6 and analysis results of PAN-co-MAA control fibers are summarized in Table 2. The diffraction pattern of fully drawn PAN-co-MAA fibers showed four distinct peaks. The peak at around $2\theta=16.8°$ is correspond to (200,110) plane of PAN crystal and peak at $2\theta=29.3°$ is correspond to (310,020) plane[14]. The crystal size and Herman's orientation factor (f_c) are plotted as a function of draw ratio in Figure 7 to investigate the effect of drawing. It is well known that elongational shear stress during the drawing process can induce crystallization of polymer[15]. Based on WAXD results, the PAN molecules are aligned and crystallized along the stretching direction. The degree of orientation of polymer molecules starts to saturate at the draw ratio level above five while the crystal size does above seven. Though polymer molecules are well aligned to the fiber axis (f_c of 0.854) at the draw ratio of 5.4, but the fibers can be stretched more thereby crystal size and crystallinity can be increased. The orientation, crystal size and crystallinity increase very slowly above the draw ratio of seven while tensile strength kept increasing due to the reduced defective structure. Amorphous region can act as defect under stress and the tensile strength is

defect dependent property[13]. The fibers prepareted without cold drawing (blank triangle) have smaller crystal size of 12.3nm than fibers experienced cold drawing (solid triangle) of which crystal size of 14.7 even at higher draw ratio. In summary, the cold drawing process affects the tensile properties by structural change.

Herman's orientation factors (f_c) of PAN-co-MAA crystal as a function of processing step and CNT concentration are shown in Figure 8 and summarized in Table 3. The PAN crystallinity, and crystal size decrease as the amount of CNT loading increases. Also, Herman's orientation (f_c) showed the highest value at 0.1 wt% of CNT loading. The CNTs can act as nucleating agent for crystal growth. At the same time, the CNTs can cause spatial hindrance above certain concentration. Therefore, room for the polymer crystal growth, orientation of polymer crystal and CNT orientation should be considered all together to understand CNTs and polymer molecule behavior in the composite fiber during spinning and drawing processes. The PAN crystal information can be obtained from WAXD and CNT orientation can be monitored by using Raman spectroscopy. To evaluate the orientation of CNTs in composite fiber, the simultaneous equations below are used[8,16,17]:

$$\frac{I_{Fiber}^{VV}(\phi=0)}{I_{Fiber}^{VH}(\phi=0)}=\frac{I_{Fiber}^{VV}(\phi=0)}{I_{Fiber}^{VH}(\phi=90)}=-\frac{24<P_4(\cos\theta)>+60<P_2(\cos\theta)>+21}{12<P_4(\cos\theta)>-5<P_2(\cos\theta)>-7} \quad \text{……..(2)}$$

$$\frac{I_{Fiber}^{VV}(\phi=90)}{I_{Fiber}^{VH}(\phi=0)}=\frac{I_{Fiber}^{VV}(\phi=90)}{I_{Fiber}^{VH}(\phi=90)}=\frac{-9<P_4(\cos\theta)>+30<P_2(\cos\theta)>-21}{12<P_4(\cos\theta)>-5<P_2(\cos\theta)>-7} \quad \text{……(3)}$$

where, I_{Fiber}^{VV} is Raman G-band intensity measured under VV mode, I_{Fiber}^{VH} is Raman G-band intensity measured under VH mode, $<P_2(\cos\theta)>$ is 2nd order Legendre polynomials, $<P_2(\cos\theta)>$ is 4th order Legendre polynomials, respectively.

The intensities obtained by changing analyzer from VV mode to VH mode at Φ=0 are substituted in equation (2) and (3). Likewise, the intensities obtained at Φ=90 are also plugged in equations (2) and (3). Theoretically, the first and second depolarization ratio terms in equation (2) should be same. Practically the depolarization ratios can be slightly different due to the experimental error, so the 2nd and 4th order Legendre polynomials are obtained by solving two simultaneous equations with first depolarization ratio terms in equations (2) and (3) and second depolarization ratio terms in equations (2) and (3), respectively and the calculated 2nd order parameters are listed in Table 4. The solutions from 1st depolarization ratio term and 2nd one are almost same. Those two solutions are averaged up to minimize the experimental error. The solutions of 2nd order Legendre polynomials are in reasonable range and have expected trend as plotted in Figure 9. In composite solution, the nanotubes are randomly oriented (isotropic state). The orientation of CNT in as-spun fibers depends on the nanotube concentration. The 0.1 wt% nanotubes are well aligned along the fiber axis. However, as nanotube concentration goes higher the degree of orientation goes down. Also, it should be noted that the PAN crystal orientation is affected adversely as nanotube loading increases (the Herman's orientation factor of fully drawn control, 0.1 wt%, 0.5 wt%, and 1 wt% are 0.902, 0.895, 0.877, and 0.866, respectively (Table 3 and 4)). It is believed that the orientational motion of nanotube is hindered by neighboring nanotubes as nanotube concentration goes higher, thereby shows less orientation along the fiber

axis. Considering very high shear rate of 40,000 1/s during spinning process, the orientation of 1 wt% CNT is quite low. The CNT orientation order of 0.403 is similar to that of the bucky paper prepared under 26 Tesla magnetic field[8]. For this reason, one can expect that very high external forces are necessary to align the nanotubes in polymer matrix. The orientation of CNT in cold drawn fiber is almost same as in fully drawn fibers, indicating that the degree of CNT orientation is almost saturated by cold drawing process. Based on WAXD and Raman results, the orientation of CNT and polymer molecules can be illustrated as shown in Figure 10.

In the as-spun composite fiber, the nanotubes start to align along the fiber axis, while PAN crystals have much lower orientation. At the as-spun stage, the PAN crystal structure is not perfect hexagonal one judging from the *d*-spacing ratio of 1.63 between 17° and 30° of equatorial scan (Figure 11). After composite fibers experienced cold drawing, the nanotubes are well aligned along the fiber axis and PAN molecules start to form extended-chain structure yet crystals are not well aligned along the fiber axis. The fully drawn fibers show good CNT and PAN crystal orientation. In the fully drawn fiber, PAN crystal exhibits hexagonal packing as the *d*-spacing ratio between 17° and 30° of equatorial scan is close to $\sqrt{3}$ (1.732). Based on meridional peak position of fully drawn fiber(Figure 12), it can be also noted that the PAN molecules became more extended chain structure[5].

4. Conclusions

In low shear rate regime, the viscosity of PAN-co-MAA/FWNT composite solution is higher than that of control solution due to the network of CNTs. However, in high shear rate regime, composite solution viscosity is lower than viscosity of control solution, suggesting that CNTs facilitate polymer solution flow. During fiber spinning and drawing, it was found that cold drawing process was effective to produce high strength and high modulus PAN fiber. The tensile strength and modulus of cold drawn control fiber was as high as 1.15 GPa and 26.1 GPa, respectively. For comparison, previous gel spinning study exhibited these tensile properties up to 0.90 GPa and 22.1 GPa, respectively. The highest tensile modulus of 31.7 GPa was obtained for PAN-co-MAA/FWNT (1 wt%) composite fibers. WAXD studies revealed that the large crystal size (16.2 nm) of cold drawn PAN-co-MAA fiber was obtained whereas typical crystal size of homopolymer PAN fiber is about 11~12 nm[5]. The fibers experienced only hot drawing (11 times) showed crystal size of 12.3 nm, while the cold drawing applied fibers demonstrated that of 13.8 nm at even lower draw ratio (7 times; cold drawing 2.7 times combined with 2.6 times hot drawing), indicating that cold drawing is very effective for increasing crystal size. Raman G-band analysis results showed that the Herman's orientation factor of CNTs in PAN-co-MAA/FWNT (1 wt %) as-spun fiber was as high as 0.406 which is relatively low value considering very high shear rate of fiber spinning (4.0×10^4 1/s for this study). However, CNT alignment increased significantly as drawing process progressed, suggesting that drawing process is very critical for obtaining high CNTs orientation as well as high polymer orientation.

References

(1) Masson, J. C. *Acrylic fiber technology and applications*; M. Dekker: New York :, 1995.
(2) Chung, D. D. L. *Carbon fiber composites*; Butterworth-Heinemann: Boston :, 1994.
(3) Gupta, A. K.; Paliwal, D. K.; Bajaj, P. *Journal of Macromolecular Science: Reviews in Macromolecular Chemistry & Physics* **1991**, *C31*, 1.
(4) Blakslee, O. L.; Proctor, D. G.; Seldin, E. J.; Spence, G. B.; Weng, T. *Journal of Applied Physics* **1970**, *41*, 3373.
(5) Chae, H. G.; Minus, M. L.; Kumar, S. *Polymer* **2006**, *47*, 3494.
(6) Chae, H. G.; Minus, M. L.; Rasheed, A.; Kumar, S. *Polymer* **2007**, *48*, 3781.
(7) Sreekumar, T. V.; Liu, T.; Min, B. G.; Go, H.; Kumar, S.; Hauge, R. H.; Smalley, R. E. *Advanced Materials* **2004**, *16*, 1583.
(8) Liu, T.; Kumar, S. *Chemical Physics Letters* **2003**, *378*, 257.
(9) Seo, M.-K.; Park, S.-J. *Chemical Physics Letters* **2004**, *395*, 44.
(10) Lee, S. H.; Cho, E.; Jeon, S. H.; Youn, J. R. *Carbon* **2007**, *45*, 2810.
(11) Xu, D.-H.; Wang, Z.-G.; Douglas, J. F. *Macromolecules* **2008**, *41*, 815.
(12) Cox, W. P.; Merz, E. H. *Journal of Polymer Science* **1958**, *28*, 619.
(13) Chae, H. G.; Kumar, S. *Science* **2008**, *319*, 908.
(14) Z. Bashir *Journal of Polymer Science Part B: Polymer Physics* **1994**, *32*, 1115.
(15) Guo, J.; Narh, K. A. *Advances in Polymer Technology* **2002**, *21*, 214.
(16) D. I. Bower *Journal of Polymer Science: Polymer Physics Edition* **1972**, *10*, 2135.
(17) Gurp, M. *Colloid & Polymer Science* **1995**, *273*, 607.

Table 1. Tensile properties of PAN-co-MAA control and composite fibers.

		Diameter (μm)	Strength (GPa)	Strain (%)	Modulus (GPa)	Work of rupture (MPa)
Control	1×2.7×2	28.0±0.3	0.58±0.04	8.4±0.4	16.2±1.0	29±3
	1×2.7×2.6	25.3±0.1	0.81±0.12	9.5±0.9	18.5±0.7	41±8
	1×2.7×3.5	21.5±0.0	1.11±0.07	9.0±0.4	22.5±1.5	50±5
	1×2.7×4.8	18.7±0.2	1.08±0.10	8.1±0.7	22.5±1.8	45±6
	1×2.7×5.5	17.6±0.2	1.15±0.13	8.0±0.6	22.3±1.3	46±8
	2×1.8×3.5	17.9±0.1	0.92±0.08	8.2±0.6	20.1±1.1	40±5
	1×1×11	20.6±0.1	0.57±0.07	7.1±0.8	15.8±0.6	23±4
0.1 wt%	1× 2.8×5.6	16.9±0.2	1.17±0.09	7.9±0.4	24.9±0.8	46±5
	1×2.9×5.4	16.7±0.3	1.14±0.13	8.0±0.6	23.3±1.4	45±7
0.5 wt%	1×2.3×5.0	20.5±0.2	0.95±0.08	7.3±0.5	22.3±2.0	37±5
1 wt%	1×2.0×6.0	20.4±0.2	1.03±0.08	7.7±0.3	23.1±1.1	42±4
	2.0×1.8×5	16.8±0.1	1.11±0.13	7.0±0.6	31.7±1.5	42±7

Table 2. Crystal structure of PAN-co-MAA in control fibers.

	Tot. Draw ratio	Crystallinity (%)	XS (nm)	f_c	$\Phi_{meridional}$
As spun	1.0	-	2.7	0.385	39.4
1×2.7×1	2.7	-	3.1	0.558	39.5
1×2.7×2	5.4	62	10.5	0.854	39.6
1×2.7×2.6	7.0	64	13.8	0.854	39.7
1×2.7×3.5	9.5	64	14.7	0.862	39.6
1×2.7×4.8	13.0	67	14.7	0.897	39.4
1×2.7×5.5	14.9	69	16.2	0.902	39.5
2×1.8×1	3.6	-	3.0	0.543	40.3
2×1.8×3.5	12.6	62	15.2	0.884	39.6
2×2×1	4.0	-	3.3	0.564	39.7
1×1×11	11.0	60	12.3	0.892	39.5
1×1.3×1	1.3	-	2.7	0.474	39.5

Table 3. Crystal structure of PAN-co-MAA in composite fibers.

	Total DR	Crystallinity (%)	XS (nm)	f_c	$\Phi_{meridional}$
As spun (0.1wt%)	1	-	3.0	0.343	39.22
1×2.8×1 (0.1wt%)	2.8	-	3.5	0.569	40.23
1×2.8×5.6 (0.1wt%)	15.68	76	15.8	0.895	39.37
As spun (0.5wt%)	1	-	2.9	0.302	39.64
1×2.3×1 (0.5wt%)	2.3	-	3.4	0.547	40.35
1×2.3×5.0 (0.5wt%)	11.5	65	16.2	0.877	39.37
As spun (1wt%)	1	-	3.0	0.320	38.84
1×2×1 (1wt%)	2	-	3.0	0.449	39.88
1×2×6 (1wt%)	12	63	14.5	0.866	39.14

Table 4. CNT orientation results from solving simultaneous equations.

CNT (wt %)	Draw Ratio	$\langle P_2(\cos\theta)\rangle$		
		1st D.P. ratio	2nd D.P. ratio	Average
0.1	Solution	0.0722	0.0730	0.0726
	As-spun	0.7889	0.8286	0.8087
	1×2.8×1	0.8460	0.8774	0.8617
	1×2.8×5.6	0.8404	0.8769	0.8586
0.5	Solution	0.1916	0.1899	0.1907
	As-spun	0.6243	0.6265	0.6254
	1×2.3×1	0.8359	0.8835	0.8597
	1×2.3×5.0	0.7993	0.8859	0.8426
1	Solution	0.0161	0.0214	0.0187
	As-spun	0.4032	0.4089	0.4061
	1×2.0×1	0.7841	0.8271	0.8056
	1×2.0×6.0	0.8270	0.9008	0.8639

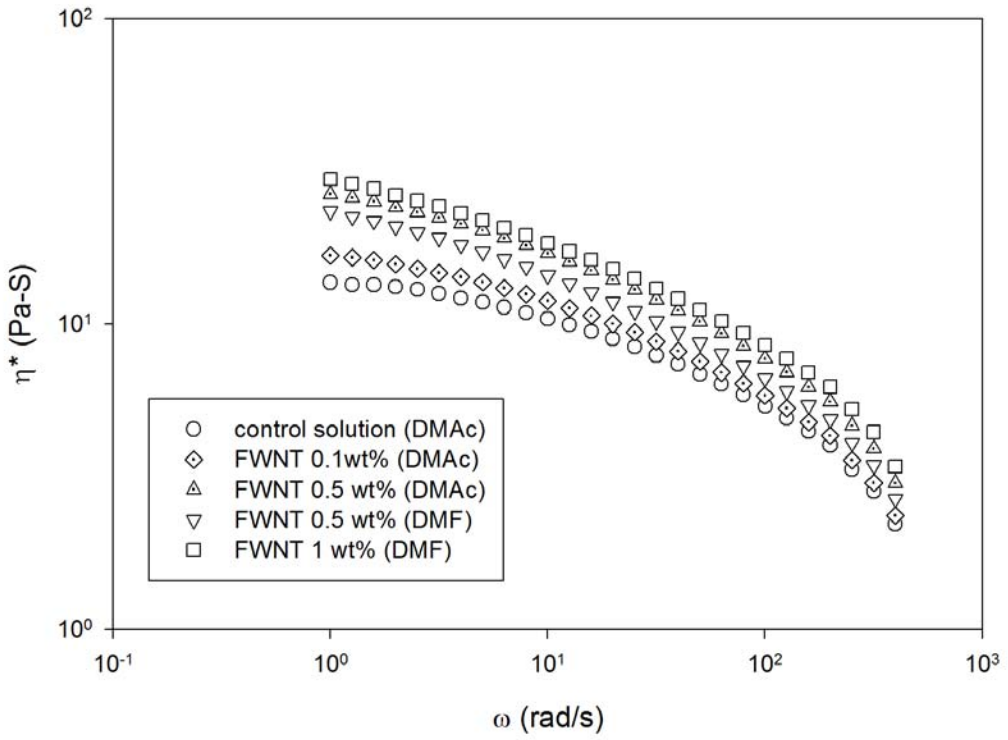

Figure 1. Frequency sweep test of complex viscosity of PAN-co-MAA/CNT solutions.

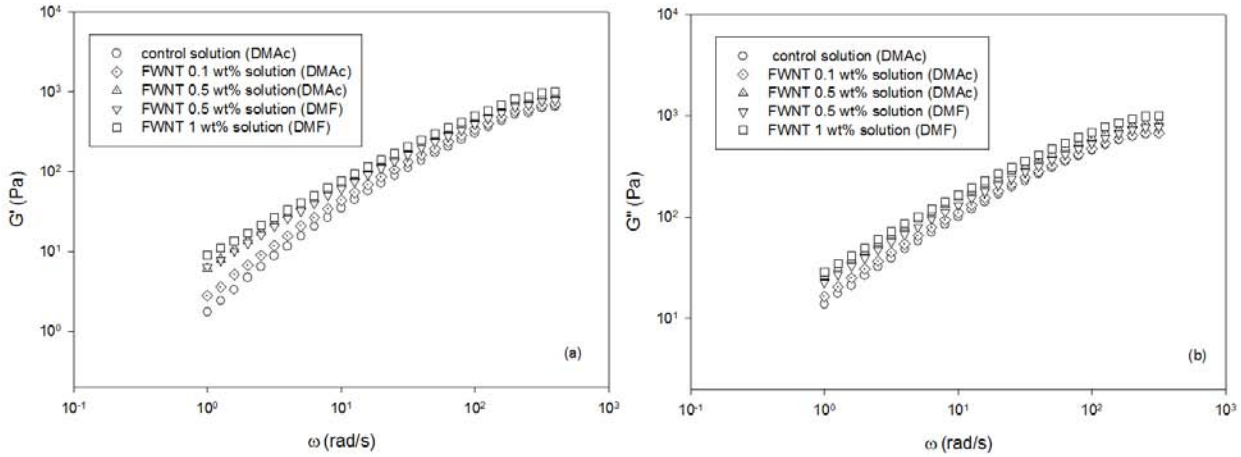

Figure 2. Storage modulus G' (a) and loss modulus G" (b) of PAN-co-MAA/CNT solutions as a function of frequency at 25 °C.

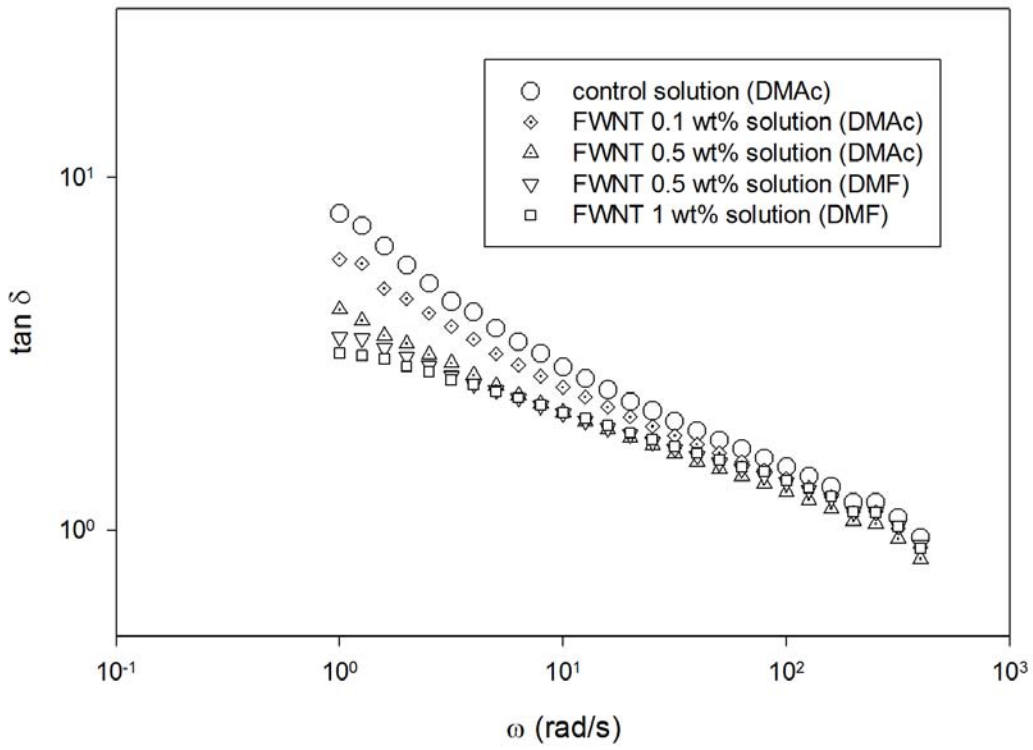

Figure 3. Tan δ of PAN-co-MAA solutions as a function of frequency.

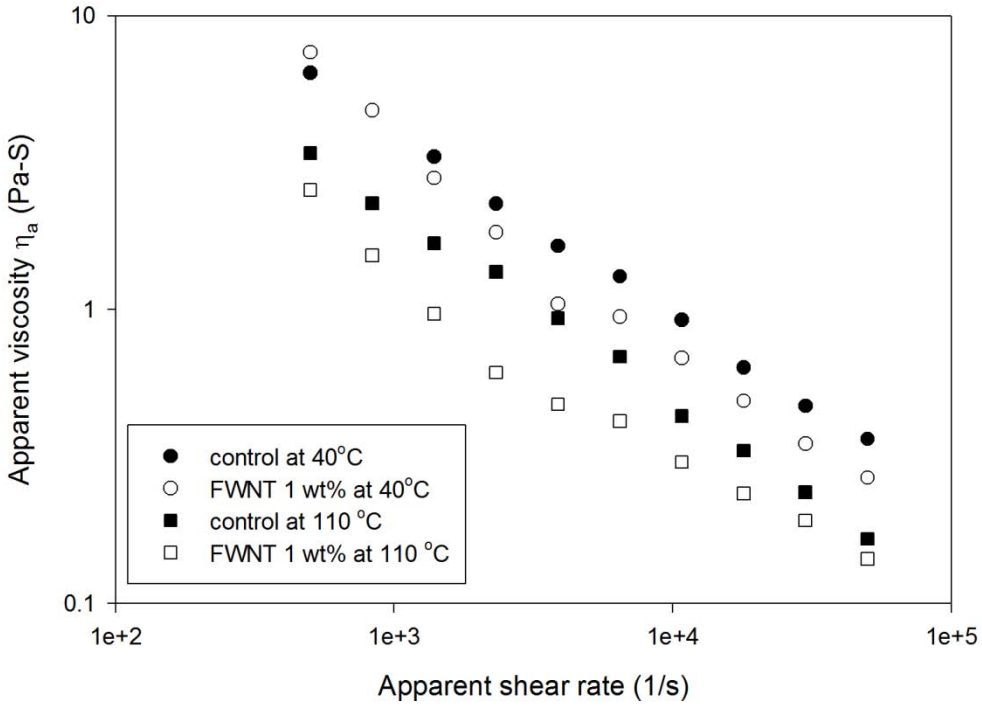

Figure 4. Apparent viscosity versus apparent wall shear rate by capillaries of PAN-co-MAA solutions.

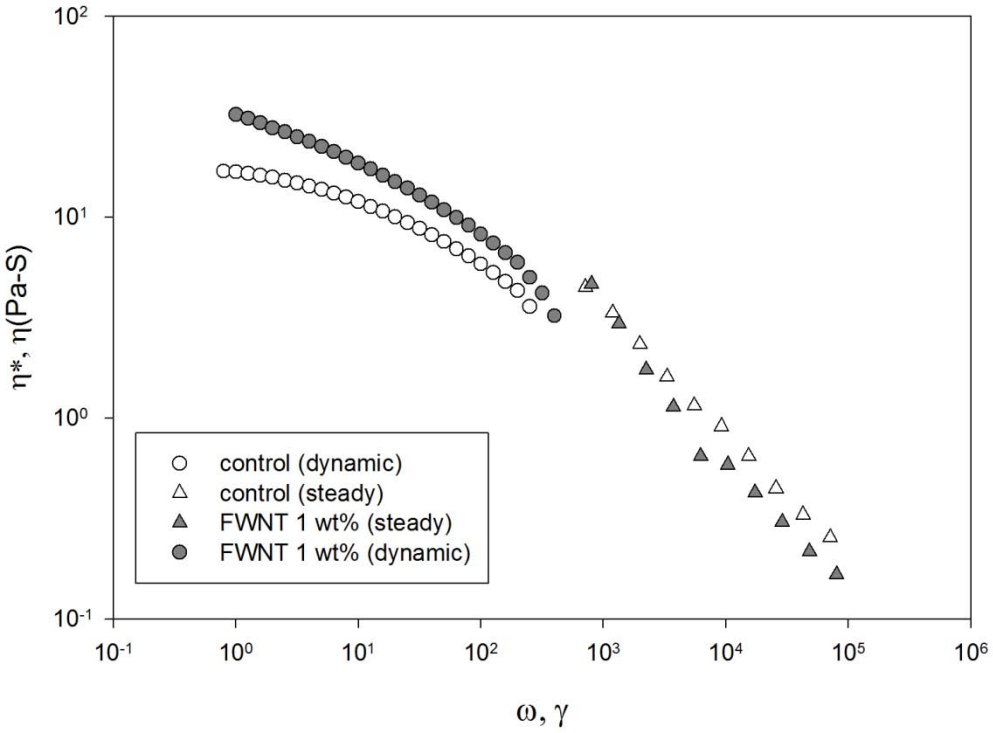

Figure 5. Comparison of viscous properties $\eta(\dot{\gamma})$ and $\eta'(\omega)$.

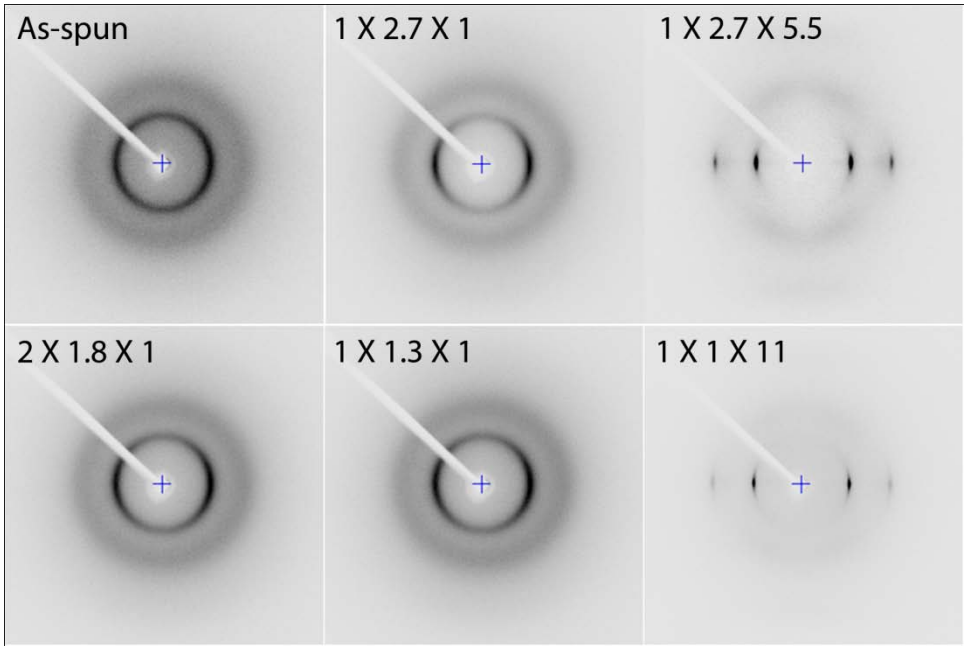

Figure 6. WAXD of selected control PAN-co-MAA fibers

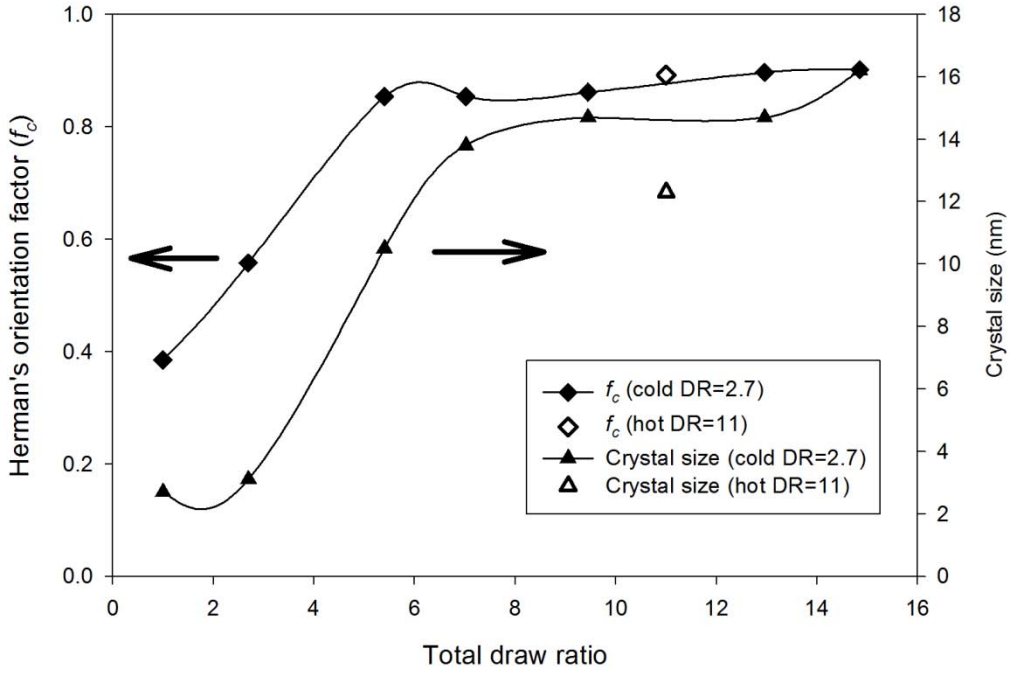

Figure 7. Crystal size and orientation of PAN-co-MAA control fibers as a function of draw ratio.

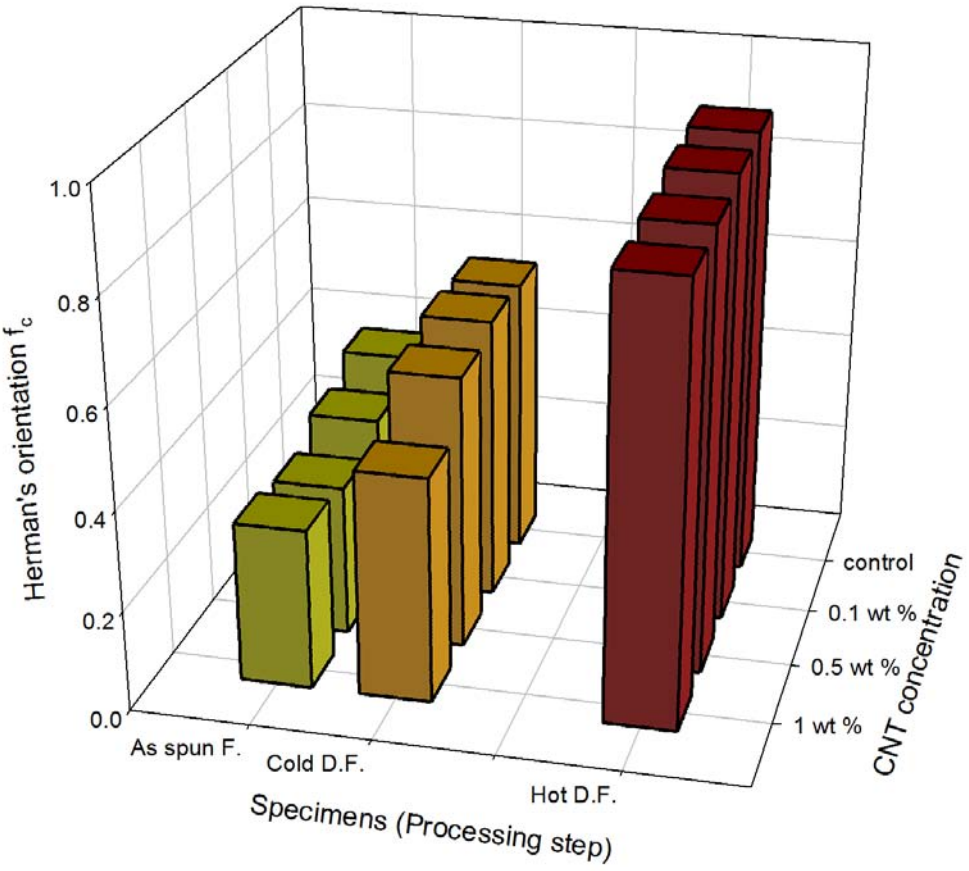

Figure 8. Herman's orientation factor (f_c) of PAN-co-MAA crystal as a function of processing step and CNT concentration.

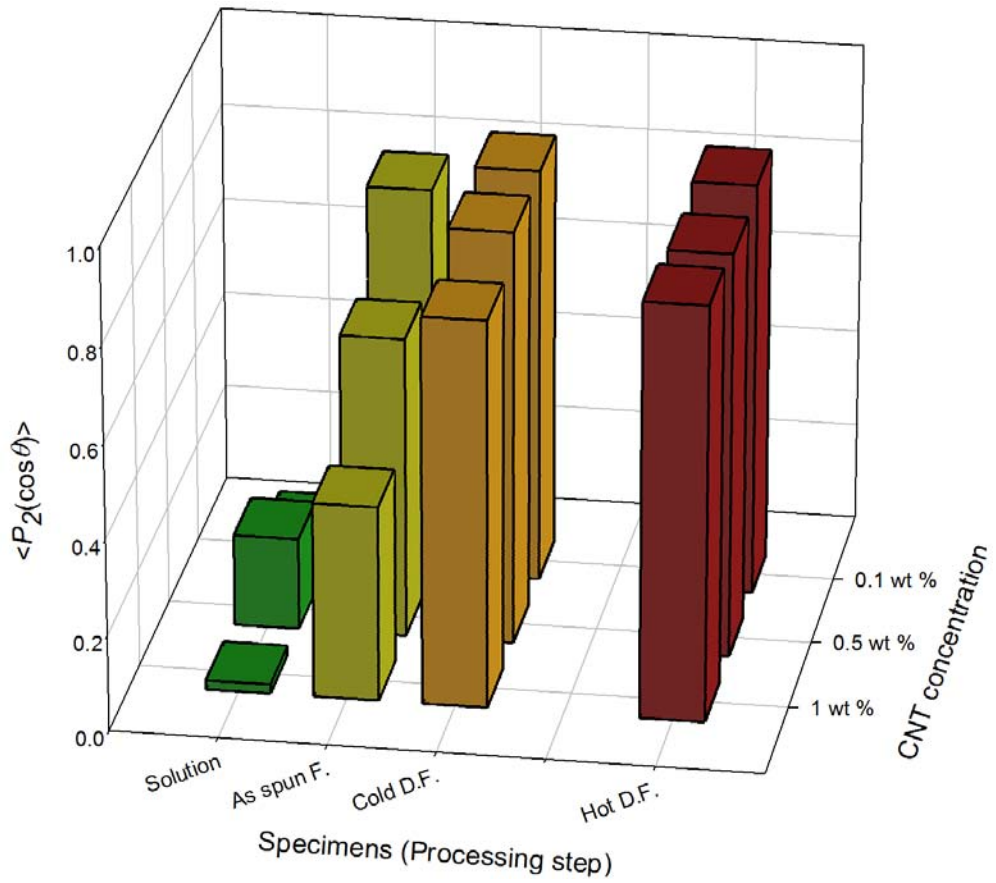

Figure 9. CNT orientation as functions of processing step and nanotube concentration.

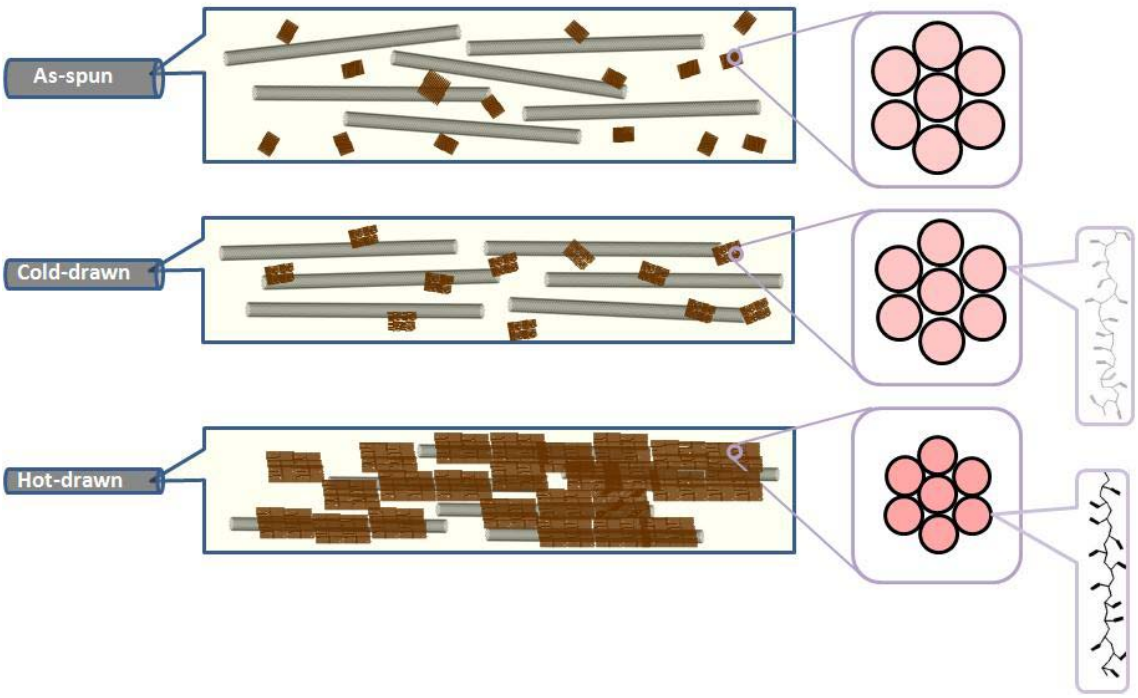

Figure 10. Schematic behavior of CNT and PAN in various fibers.

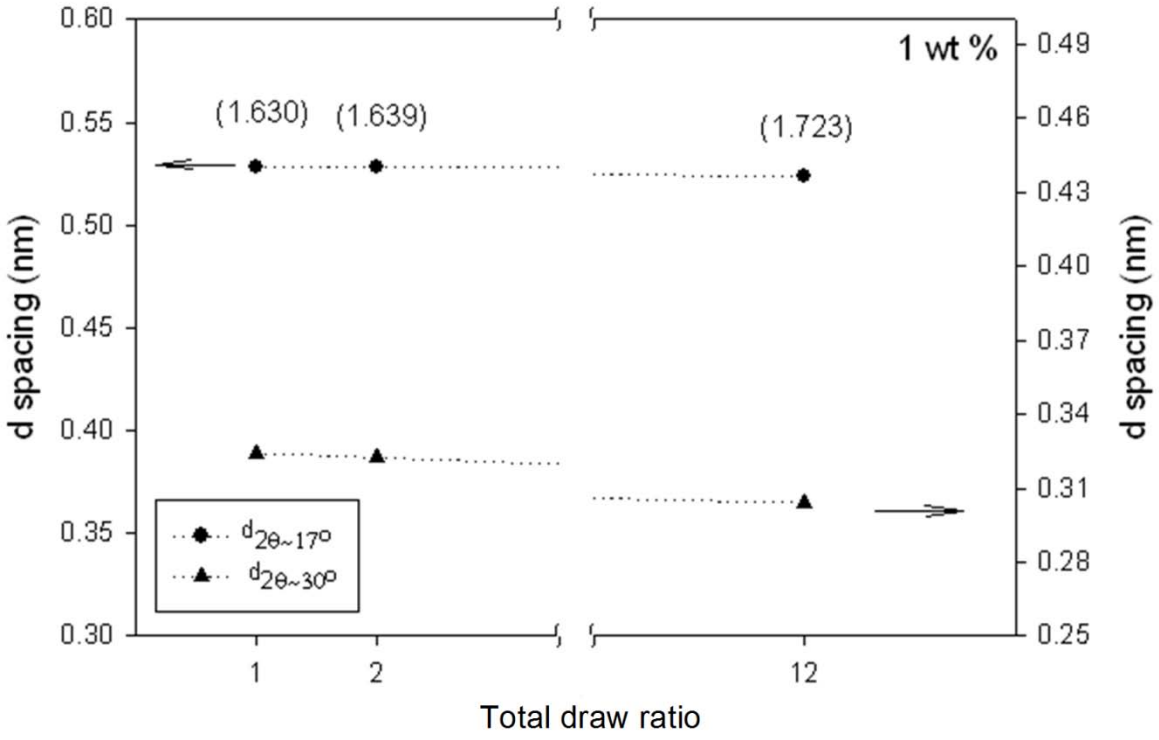

Figure 11. Effect of drawing on equatorial PAN-co-MAA *d*-spacings (for 2θ ~ 17° and 30° diffraction peaks). The values in parenthesis are the ratios of the two *d*-spacing.

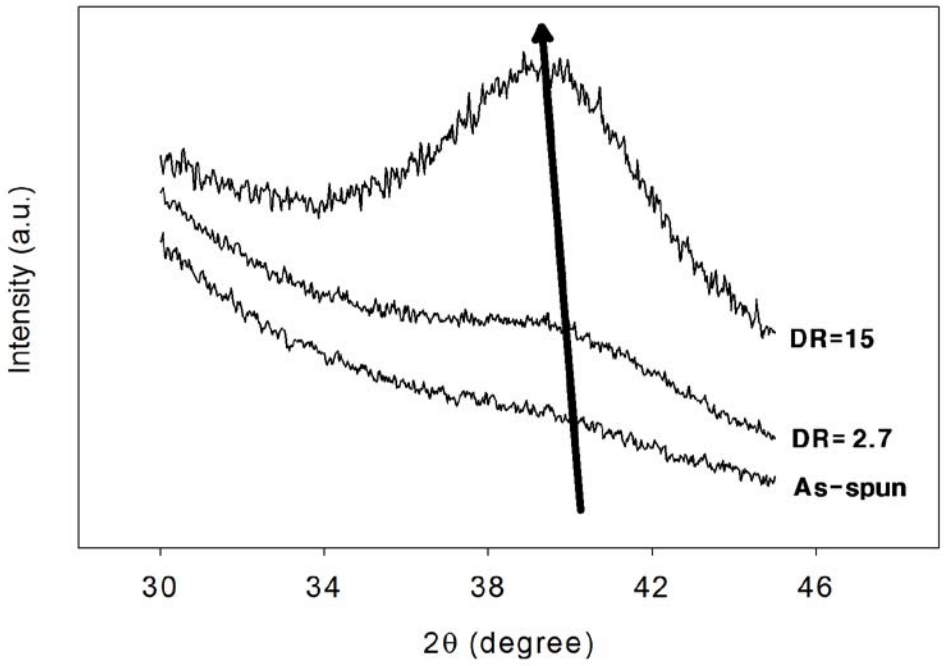

Figure 12. WAXD meridional scan

SECTION II

Stabilization of Gel-spun Polyacrylonitrile/Carbon Nanotubes Composite Fibers
Part I: Effects of Carbon Nanotubes

Yaodong Liu, Han Gi Chae, Satish Kumar

School of Polymer, Textile and Fiber Engineering, Georgia Institute of Technology,
801 Ferst Dr. NW, MRDC-1, Atlanta, GA 30332-0295, USA

Abstract

It has been found that addition of CNTs in polyacrylonitrile (PAN) fibers significantly improves the mechanical properties of the resulting carbon fibers and induces the formation of graphite-like structure at relatively low carbonization temperature. Since the ultimate carbon fiber properties are determined by the stabilized structure, this study focuses on the stabilization of PAN/CNT fibers in air. The effects of different types of CNTs on chemical, mechanical and structural evolution during the stabilization were studied. The optimal residence time for stabilization with the best orientation and chemical structure was determined by combining wide angle X-ray diffraction (WAXD), infrared spectroscopy (IR), and scanning electron microscopy (SEM) results. These different methods show comparable results and can be used as criteria to optimize stabilization. Additionally, applied stress during stabilization is very important for obtaining good properties. The detailed effects of applied stress during stabilization on chemical structure, physical parameter and mechanical properties of stabilized fibers are discussed. The addition of CNTs enhances the maximum stress that can be applied on fiber during stabilization. By studying the effects of CNTs on fiber shrinkage and stress, it was determined that two-phase structural model is suitable for PAN/CNTs composite fibers.

1. Introduction

Carbon fibers contain more than 90 wt. % carbon. The stiffness, strength and low density make carbon fibers an important reinforcement material for high performance composites. Currently, polyacrylonitrile (PAN) and meso-phase pitch are used as precursors [1-3]. Compared with meso-phase pitch-based carbon fibers, PAN-based carbon fibers [4, 5] have higher tensile and compressive strengths. In this study, PAN fibers were used to produce carbon fibers. In order to enhance the strength and modulus of carbon fibers, small amount of carbon nanotubes (CNTs) are added into PAN precursor fibers. Besides extraordinary mechanical properties of CNTs [6, 7], for example, the young's modulus of single wall carbon nanotubes (SWNT) is about 640 GPa, and tensile strength is over 20 GPa; it was found that the addition of CNTs strongly affected adjacent polymer molecules, such as, addition of CNTs makes adjacent PAN more compact [8], induces the formation of graphite-like structures even for fibers carbonized at a low temperature of 1100 ^{o}C [8, 9]. In general, PAN-based CFs is known to have graphitized structure only after carbonization at above 2500 ^{o}C. With the addition of as low as 1 wt. % CNTs in gel-spun PAN precursor fibers [8], strength and modulus of resulting carbon fibers were improved by 49 % and 64 % respectively.

To produce high performance carbon fibers, thermal treatment is very important for the final properties of resulting carbon fibers [10~13] and needs to be carefully optimized. In this study, chemical, structural and mechanical property evolutions during the thermal stabilization are studied. Effects of CNTs on stabilization were explored. Three kinds of CNTs were used to enhance PAN precursor fibers, and their effects on stabilization were compared. This study will help to better understand the effects of CNTs, choose the best kind of CNTs, and optimize the stabilization conditions.

2. Experimental

PAN used in is study is a homo-polymer (M_w ~ 250,000 g/mol) produced by Japan Exlan Company. CNT1 (lot no. XO122UA, 1 wt. % catalyst residual, walled number ~ 4), CNT2 (lot no. XO437UA, 1.2 wt. % catalyst residual, walled number ~ 6), and CNT3 (lot no. XB928, 4 wt. % catalyst residual, walled number ~ 6) were obtained from Unidym, Inc (Houston, TX). Based on manufacturer's information, CNT2 and CNT3 were prepared by same method and process, but only difference in these two CNTs was the residual catalyst content. Fiber spinning solutions were prepared following procedure as described elsewhere [8], the weight fraction of CNTs in all composite fibers was fixed at 1 %. Fibers were spun through a 120 μm diameter spinneret, and the as-spun draw ratio was 3. As-spun fibers were kept in methanol/dry ice bath for 2 days to ensure complete gelation. The gelated fibers were further drawn in a glycerol bath at 160 ^oC to a draw ratio of 4.5. Stabilization was carried in a box furnace (Lindberg, 51668-HR, Blue M Electric). Temperature of the furnace was calibrated by a temperature probe (Supporting information, S.Figure 1). Raman spectra (Supporting information, S.Figure 2) were collected using Holoprobe Research 785 Raman microscope (Kaiser Optical system). Raman excitation laser wavelength was 785 nm and spectra were collected using VV mode (polarizer and analyzer are parallel to each other). CNT orientation in the precursor fiber was calculated from the G band intensity using reported method [14]. Infrared spectra (IR) were collected using infrared microscope (Spectrum One, Perkin Elmer) with a resolution of 2 cm^{-1} and 256 scans. Peakfit software (Seasolve software Inc. v4.12) was used for peak fitting of IR spectra. Wide angle X-ray diffraction (WAXD) patterns were obtained by Rigaku micromax-002 (Cu K_α radiation) using Rigaku R-axis IV++ detector. The mechanical properties of single fiber were tested on RSA III solid analyzer (Rheometric Scientific Co.) at a gauge length of 25 mm and crosshead speed of 0.25 mm/s. Fiber morphologies were observed on scanning electron microscope (SEM, 1530, Leo Electron Microscopy Ltd) at an operating voltage of 10 kV on gold coated samples. The shrinkage and stress-temperature curves were recorded by thermal mechanical analyzer (TMA, Q-400, TA Instrument).

3. Results and discussion

The tensile properties and structural parameters of precursor PAN and PAN/CNT composite fibers are listed in Table 1. CNTs, especially CNT1, enhance PAN crystallinity and crystal size. The meridional scans of all composite fibers show peaks around 39^o which are lower than our previously reported results at ~ 39.7^o [15] and indicate more planar zigzag structure. CNT1 containing fibers exhibit the lowest peak position in meridional scan, which suggests it possesses the highest fraction of planar zigzag structure. All fibers showed very high orientation for PAN crystals along the fiber axis. For composite fibers, CNTs show better orientation than

PAN matrix. In precursor fibers, addition of CNT2 and CNT3 show similar reinforcement efficiencies, whereas CNT1 shows the best reinforcement efficiency. The porosity tests (supporting information, S.Figure 3) show that CNT2 and CNT3 have BET (Brunauer-Emmett-Teller) surface areas of 560 m^2/g and 546 m^2/g respectively, which are lower than that for CNT1, which has a BET surface area of 659 m^2/g. Comparing ratio of surface areas of CNT1/CNT2/CNT3 that is 1.21/1.02/1.00 and reinforcement efficiencies ratio of three CNTs that is 1.31/1.00/1.00[2]. CNTs reinforcement efficiency increases with CNTs surface area. The surface area of CNTs is proportional to the interfacial area of well dispersed CNTs in PAN matrix, and affects load transfer from matrix to CNTs. This is consistent with other reports [16-18] suggesting that the reinforcement efficiency of CNT correlates with CNT interfacial area.

Stabilized samples were collected at different stabilization stages as shown in Figure 1. A constant stress of 20 MPa was applied on fibers during whole stabilization process. Stabilized fibers were soaked in boiling DMF for 6 hr to remove unstabilized or decomposed PAN molecules. For PAN/CNT1 precursor fibers and fibers stabilized at 267 ^oC for 1 hr, stabilized fibers were completely dissolved in DMF. For the fibers stabilized for 2 hr, some fibers remained after DMF boiling test; uneven surfaces can be observed on residual fibers (supporting Information, S.Figure 4) which may be caused by swelling of under-stabilized PAN. For the fibers stabilized for 4 hr and longer, most fibers remained intact and fiber surface was relatively smooth. In addition, the color of DMF after boiling test became lighter with increasing stabilization time, indicating the increase in stabilized structure. The cross-sections of stabilized PAN fibers are shown in Figure 2. After stabilization at 267 ^oC for 2 hr, cross-section shows even features. After stabilization for 6 hr, pore structure can be observed in the fiber cross-section and their dimension increases with longer stabilization time, suggesting the decomposition of over-stabilized structure. For cross-section of PAN/CNT composite fiber (Supporting information, S.Figure 5), CNTs were pull out and showed fibrous structures.

Chemical structure of stabilized fibers was characterized by FTIR spectra. IR spectra of control PAN and PAN/CNT1 fibers stabilized at 267 ^oC for various times are shown in Figure 3. For precursor fibers, peak at 1673 cm^{-1} is assigned to C=O that is due to residual DMF, 2242 cm^{-1} band belongs to the C≡N groups, and 2938 cm^{-1} and 1456 cm^{-1} bands are assigned to C-H_2 [19]. During stabilization, peak at ~ 1600 cm^{-1} is evolved by formation of C=C and C=N bonds. A shoulder at ~ 1620 cm^{-1} is assigned to the carbonyl groups formation due to oxidation. The peak intensity at ~ 801 cm^{-1} is attributed to C=C-H increases during stabilization. When fibers are stabilized at 267 ^oC for 6 hr, the C-H_2 peak at 2938 cm^{-1} becomes very weak, and the C≡N peak position shifts to lower wavenumber as well as peak shape changes. The peaks in the range of 2180 ~ 2260 cm^{-1} are assigned to three kinds of nitrile groups: the un-reacted nitrile group at ~ 2242 cm^{-1}, conjugated nitrile at ~ 2215 cm^{-1}, and β-amino nitrile at ~ 2190 cm^{-1} [8, 20~24]. Mole fractions of different groups can be calculated by curve fitting method [8]. Figure 4 shows examples of nitrile band curve fitting. To fit the IR peak, peak positions were fixed at 2194 cm^{-1} for β-amino nitril, 2243 cm^{-1} for un-reacted nitrile, and 2218 cm^{-1} for conjugated nitrile respectively, while peak width and intensity were adjusted to get the best fitting. From the results of nitrile band peak fitting, approximate mole percentages of conjugated nitrile (ϕ_c) and β-amino (ϕ_a) nitrile are calculated by following equations:

[2] The reinforcement efficiency of CNT is calculated by $\frac{YM_{Composite} - YM_{Control} \cdot f_w(PAN)}{f_w(CNT)}$ (YM: Young's modulus (N/tex), f_w: Weight fraction (wt %)).

$$\phi_c = \frac{Area_{2218}}{Area_{2242} + Area_{2218} + Area_{2194}} \cdot 100\%$$

$$\phi_a = \frac{Area_{2194}}{Area_{2242} + Area_{2218} + Area_{2194}} \cdot 100\%$$

where $Area_{2218}$ etc are the areas for the corresponding fitted nitrile peak.

The nitrile band fitting results are listed in Table 2. Previous study [8] has shown that addition of CNTs lower the fraction of β-amino nitrile in stabilized fiber. The current study also exhibits similar results. In addition, the smallest diameter tube (CNT1) that gives the highest surface area reduces the formation of β-amino nitrile more than other tubes (CNT2 and CNT3). The β-amino nitrile can be formed by the termination of cyclization reaction [25]. The less β-amino nitrile indicates the less possibility of chain scission in stabilized fibers, and will improve properties of carbon fibers. The ratio of ϕ_c / ϕ_a is proportional to average unit number of conjugated nitrile segments. From Table 2, it was found that the ratio first increased; then decreased after a certain stabilization time. The mole ratio of ϕ_c / ϕ_a for fully stabilized PAN was 6.8, which is lower than the corresponding values for PAN/CNT composite fibers, which are 8.8, 8.0 and 7.9 for PAN/CNT1, PAN/CNT2 and PAN/CNT3 composite fibers respectively. The higher ratio means a longer conjugated nitrile segment. The time that ϕ_c / ϕ_a ratio reaches the maximum value is the optimal stabilization time, and stabilized fiber has optimal chemical structure. For even longer stabilization time, the ratio decreases due to over-stabilization (decomposition).

WAXD patterns and integrated scans of stabilized PAN/CNT1 composite fibers are shown in Figure 5. The diffraction peaks at $2\theta=16.7^o$ and 29.3^o corresponding to the (200, 110) and (310, 020) planes of PAN crystals respectively decrease during stabilization, and finally disappear. The evolution of PAN (200, 110) peak could be used to determine the stabilization degree [26]. The increase of peak intensity at $2\theta \sim 25.7^o$ can be attributed to the formation of ladder polymer. After stabilized at 267 ^{o}C for 10 hr, the (200, 110) peak of PAN in the integrated XRD scan completely disappeared for all the fiber samples, which indicated that all PAN crystals were disrupted. The crystal sizes and orientation factors of stabilized fibers calculated from XRD data are listed in Table 3.

An increase as high as 150 % of PAN crystal size was observed in the very early stabilization stage (Table 3). Same phenomenon was also reported by other researchers [29]. From an additional experiment, the increase of crystal size up as high as 140 % could be found when fibers were only heated from room temperature to 200 ^{o}C at a heating rate of 5 ^{o}C/min (Supporting information, S.Figure 6). The temperature strongly affected the reaction rate in stabilization as can be seen from the decrease of crystal size. When fibers were stabilized at 234 ^{o}C, PAN crystal size slightly decreased only after 4 hr; when fibers were stabilized at 267 ^{o}C, crystal size increases in the first hour, then decreases monotonically and finally totally disappears. For PAN/CNT1 composite fiber, comparing nitrile band fitting results in Table 2 and crystal size in Table 3. Based on IR data in Table 6, over 60 % nitrile band was reacted after fibers were stabilized at 267 ^{o}C for 4 hr. In comparison, PAN crystal size (Table 3) only slightly decreases from 14.7 nm (after 1 hr) to 13.4 nm (after 4 hr). Above results indicates that cyclization reactions mainly occurs in amorphous regions in early stabilization stage. For stabilization over 4 hr, PAN crystal size decreases rapidly. Above results suggest that stabilization reaction in crystal regions has a time lag as compared to the reactions in amorphous

regions. It is believed that stabilization is initiated in amorphous regions, and then diffuses into crystals [27, 28]; however, no direct evidence for this has been observed. Devasia et al. [19] also found slow down of stabilization by studying the absorbance of nitrile band in IR spectra. When cyclized ladder structure is formed in stabilization, helical chain of PAN needs to be uncoiled to form a planar structure. PAN molecule conformation can be more easily changed in amorphous regions than in crystallized regions. Also, stabilization involves complex reactions, including cyclization, oxidation, dehydrogenation, and cross-linking. Oxygen is an important reactant in stabilization reaction. It participates in oxidation reaction, leads to further dehydrogenation and may also initiate cyclization [11]. Oxygen can easily diffuse in amorphous regions as compared to crystalline regions, and facilitates stabilization. Thus, it is reasonable that stabilization reaction in amorphous region will be much faster than in the crystalline regions.

Azimuthal scans at $2\theta \sim 25.7^{o}$ for precursor and stabilized PAN, and PAN/CNT1 fibers are shown in Figure 6. Diffractions from PAN and formed ladder polymer overlap in the early stabilization stage. Along stabilization, PAN is converted to ladder polymer; azimuthal scan shows a single peak only from ladder polymer. The azimuthal scan peak of composite fibers is much sharper than that of control PAN, which suggests the formation of highly ordered stabilized structure induced by the addition of CNTs [9]. These highly ordered stabilized structure can form graphite-like structure after carbonization. Herman's orientation factors of ladder polymer calculated from azimuthal scan are listed in Table 3. Orientation of stabilized ladder polymer initially increased with increasing stabilization time, reached a maximum value and then decreased. Decrease in orientation may due to over-stabilization. The transition point indicates that optimally stabilized fibers have the best orientation. Comparing results in Tables 2 and 3, both IR and XRD data show similar trend and get the same optimal stabilization time. Before fibers are fully stabilized, ratio of ϕ_c / ϕ_a increases along stabilization. Since stabilization reactions are initiated from amorphous regions and then diffuse to crystallized regions, above results means that stabilized polymer from crystallized regions would have higher ϕ_c / ϕ_a ratio than that from amorphous regions. Therefore, higher crystallinity in PAN fiber will be more preferable to produce better carbon fibers.

The positions of PAN (200,110) peak and meridional peak are found to shift during stabilization as shown in Figure 7. The peak position of PAN (200, 110) planes in equatorial scan shifted to lower 2θ value, suggesting that PAN crystals became loose during stabilization. The meridional peaks exhibit obvious shift from $\sim 39^{o}$ (chain axis diffraction from PAN crystal) for precursor fibers to $\sim 43.3^{o}$ (in-plane diffraction from cyclized structure) for fully stabilized fibers (Figure 7b). Comparing with PAN crystal size shown in Table 3, shift of meridional peaks shows same trend as decrease of PAN crystal size.

Shrinkage behaviors of fibers were monitored in TMA (Figure 8), the temperature profile and applied tension were set to be same as in the experiments in box furnace. The shrinkage can be divided into two parts: entropic shrinkage and chemical shrinkage. If stress is high enough, a drawing can be observed. Due to the complexity of stabilization reaction, these different kinds of shrinkages may not be completely separated. Although final shrinkages of PAN and PAN/CNT1 fibers were in the comparable range, control PAN fiber was drawn more than PAN/CNT1 fiber, suggesting that CNT containing fiber has higher modulus even above the glass transition temperature as expected [18]. For a low stress at 4 MPa (Supporting information), no drawing occurred, and PAN fibers had larger entropic shrinkage than PAN/CNT1 composite fiber. From shrinkage curves in Figure 8, PAN/CNT1 fiber showed less chemical shrinkage (~ 8.5 %) than that of PAN fiber (~ 11 %) under 20 MPa stress.

Under the same stress of 20 MPa, fibers were stabilized in air at various temperatures, and shrinkage curves are shown in Figure 9. Higher temperature reduces the final shrinkage for both PAN and PAN/CNT1 composite fibers. Kim et al. [30] and Bahl et al. [31] also reported similar results for both homopolymer and copolymer PAN fibers. During cyclization, PAN molecules are converted into denser ladder polymer, density increases and fiber shrinks. When stabilization temperature is raised, cyclization reactions becomes much faster, and oxygen diffusion will limit further oxidation, dehydrogenation and cross-linking reactions. At higher temperature, stabilization reactions will tend to be limited by gas diffusion, which will lead to the difference of chemical shrinkage.

Table 4 shows tensile properties of stabilized fibers. For the modulus of stabilized fiber at 267 ^{o}C for 6 hr or longer, decrease of modulus were very slow. The elongation at break increased in the early stage, which can be due to the large shrinkage of fibers. For fully stabilized fibers, the elongation at break showed significant decrease compared with precursor fibers. After stabilized at 267 ^{o}C for 10 hr, the specific strength of all fibers decreased to about 0.2 N/tex. By comparison, the tensile strength of precursor fiber was about 0.8 N/tex. The specific modulus for fully stabilized fibers showed obvious improvement with the addition of CNTs. The reinforcement efficiencies of modulus for CNT1, CNT2 and CNT3 were 309 N/tex, 279 N/tex and 239 N/tex respectively, which was higher than the CNT reinforcement efficiencies in the precursor fibers. Similar to the case in precursor fibers, CNT1 that had the highest surface area to mass ratio showed the best reinforcement efficiency in the stabilized fibers as well.

Determining the end of stabilization is important to produce high quality carbon fibers; either under-stabilization or over-stabilization will lead to decrease of mechanical properties. For the fibers stabilized at 267 ^{o}C, XRD patterns showed that main PAN (200,110) peak at 17^{o} completely disappeared when stabilization time increased from 6 hr to 8 hr, indicating that all the PAN crystal structures are disrupted. From IR spectra, the mole ratios of ϕ_c / ϕ_a was found to decrease after reaching a maximum point, suggesting over-stabilization. It can be also noted that, for the same soaking time, Herman's orientation factor of ladder structure reached the maximum value, and then decreased. Cross-section of fibers after DMF boiling test showed an obvious increase in porosity after stabilization time increased from 8 hr to 10 hr at 267 ^{o}C. Different characterization methods showed same optimal time for stabilization. The optimal stabilization time at 267 ^{o}C for PAN, PAN/CNT1, PAN/CNT2 and PAN/CNT3 in this study is around 6 – 8 hr. However, this can be only verified upon further carbonization. Correlation between stabilized structure and properties of resulting carbon fibers needs to be studied to obtain the optimally stabilized PAN or PAN/CNT fibers.

In the following part, the stabilization time at 267 ^{o}C was fixed at 8 hr and the effects of applied stress on the structure and properties of PAN and PAN/CNT1 fibers were investigated. Various stresses were applied during the stabilization process, 2.1 MPa, 10 MPa, 15 MPa and 22 MPa. When stress was higher than 26 MPa, all fibers were broken during heating. The tensile properties and IR analysis results of stabilized fibers are shown in Tables 5 and 6. Higher stress improved the modulus and strength of stabilized fibers. When stress increased from 10 MPa to 22 MPa, the elongation at break of stabilized fibers was improved over 2 %. Under the same stress, CNT containing fiber showed better tensile properties than control PAN fibers. From Table 6, it can be noted that higher stress applied during stabilization will reduce the formation of β-amino nitrile in stabilized fibers, and significantly improve the ratio of ϕ_c / ϕ_a. Figure 10 shows azimuthal scans of stabilized PAN and PAN/CNT1 fibers under 22 MPa. Stabilized composite fibers show much sharper peak as compared with stabilized PAN fibers. This was

caused by the formation of highly oriented stabilized structures in the vicinity of CNT [9]. The azimuthal scans of stabilized PAN/CNT1 fibers were deconvoluted using two peaks fitting method [9] to obtain the orientation information of highly order regions. Herman's orientation factors of separated phase were calculated and listed in Table 7. Higher stress improved orientation of stabilized polymers. For composite fibers, highly oriented phase has an orientation factor over 0.9. The surrounding matrix in stabilized composite fibers still has a better orientation as compared with stabilized PAN fibers. The addition of CNT improves orientation of stabilized polymer, which will lead to better orientation and higher modulus of the resulting carbon fibers.

Fiber shrinkage under various stresses was monitored in TMA (Figure 11). For fibers stabilized with very low stress of 2.1 MPa, the final shrinkages for PAN fibers exceeded 30 %. Shrinkage is separated into three parts: entropic shrinkage, stretching (only under high stress), and chemical shrinkage, and the data is given in Table 8. Shrinkage is very sensitive to applied stress, and was greatly reduced if higher stress was applied. At low stress of 2.1 MPa, addition of CNTs reduces both entropic and chemical shrinkage. When stress was higher than 10 MPa, stretching of composite fibers was much less than that of PAN fibers. It can be also found that addition of CNTs improves the maximum stress that can be applied during stabilization. While the maximum stress of PAN fibers is 22 MPa, addition of CNT1 improves the maximum stress to 24 MPa.

Above results suggested that higher stress will benefit chemical structure and mechanical properties of stabilized fibers. For stabilization, the maximum stress without breaking fibers should be considered. Most fiber breakage during stabilization was found to happen when temperature was raised to around 200 ^{o}C. At this temperature range, fibers became plasticized and applied high stress would stretch the fibers before chemical reactions made fibers stiffer and cause breakage. To further improve the properties of stabilized fibers, stress should be changed in different stabilization stages.

The structure of PAN fibers was proposed to be two-phases [32, 33], ordered regions and disordered regions. For precursor fibers, CNTs were aligned along the fiber axis and PAN formed ordered and amorphous layered structure. According to above model, CNTs will penetrate many layers of crystal and amorphous regions, and affect fiber's thermo-mechanical properties. The stress-temperature evolution was detected in TMA at iso-strain mode (pre-strain = 0.3 %). Temperature was raised from 25 ^{o}C to 175 ^{o}C, and then cooled down to 25 ^{o}C at a rate of 5 ^{o}C/min. The process was repeated twice. Stress – temperature curves of PAN and PAN/CNT1 fibers are shown in Figure 12.

In the first cycle, entropic relaxation was observed when temperature was higher than 70 ^{o}C. The entropic stress was caused by the entropic relaxation of amorphous chains or segments. The entropic relaxation from recoil of polymer chains can not be reversed during cooling process. The irreversible process means that stretched amorphous chains or segments re-coiled and their conformations were permanently altered. Although both PAN and PAN/CNT fibers were spun under same process with same draw ratio, the maximum and minimum stresses showed obvious differences. PAN fiber has much higher entropic stress and much lower remaining stress than PAN/CNT1 fiber, which suggested more stretched polymer chains recoiled in PAN fibers. In the second and third cycles, the stress became reversible that indicated fiber structure was very stable. The minimum stresses in the second and third cycles appeared at around 100 ^{o}C, same temperature range as the glass transition temperature of PAN molecules. When temperature is higher than 100 ^{o}C, stress changes are caused by entropic force of stretched chains which act as springs. When temperature is lower than 100 ^{o}C, fibers is in glassy state, and

length will change according to intrinsic thermal shrinkage; cooling will reduce length and increase stress. In the second and third cycles in the temperature range from 100 to 175 ^{o}C , entropic stress amplitude of PAN/CNT1 fiber is smaller, 13 MPa, than that of PAN fiber, 16 MPa; while for intrinsic thermal shrinkage stress in the temperature range from 25 to 100 ^{o}C, its amplitude of PAN/CNT1 fiber is larger, 9 MPa, than that of PAN fiber, 8 MPa. Above changes of stress can be explained by the suggested PAN/CNT model. While temperature increases from 100 to 175 ^{o}C, the shrinking force caused by entropic relaxation is shared by CNTs, both maximum entropic stress (cycle 1) and entropic stress amplitude (cycle 2&3) are reduced by addition of CNTs. While temperature cools from 100 to 25 ^{o}C, assuming PAN and PAN/CNT1 fibers have same coefficient of thermal expansion (CTE), stress of PAN/CNT1 fibers will increase larger than PAN fibers, since composite fibers have better mechanical properties than PAN fibers. The shrinkage behaviors in Figure 11 can also be explained by this model. At low stress, addition of CNTs retains the original structure of fibers, and reduces both the entropic and chemical shrinkages; while under high stress, the same effect will makes fiber difficult to be drawn.

4. Conclusions

In summary, during the stabilization of gel-spun PAN and PAN/CNT composite, changes of structural, chemical and mechanical properties were studied, and the reinforcement of different kinds of CNTs were compared. The stabilization can be divided into a fast stage mainly in amorphous regions at the early stabilization process and a slow stage mainly in crystal regions at the late stabilization process. For stabilization rate of fibers, no obvious difference was found with or without the addition of CNTs. For fully stabilized fiber, addition of CNTs will reduce the fraction of β-amino nitrile, and enhances stress resistance. Ordered PAN structure or PAN crystals facilitated to form longer conjugated nitrile segments after stabilization; addition of CNTs was found to enhance the crystallinity of PAN and also affect crystal structure of interphase PAN. This led to the formation of highly ordered stabilized polymer in the inter-phase regions and improved the overall orientation of stabilized PAN matrix. Comparing different kinds of CNTs, the surface area played an important role on the reinforcement efficiency. The stress applied during stabilization also played an important role on the properties of stabilized fibers. Higher stress led to better mechanical properties, longer segment length of conjugated nitrile and better orientation of stabilized structure. The final shrinkage of fibers is very sensitive to applied stress, and can be reduced by higher stress or higher stabilization temperature. Addition of CNTs reduces both chemical and entropic shrinkages of PAN fibers during stabilization. Also, addition of CNTs improves the maximum applied stress during stabilization, which is very important for the properties of resulting carbon fiber properties. For the structure of fibers, it is believed that the two phase structure is suitable, and CNTs penetrated many layers of crystal and amorphous regions that improved the stress resistance and reduced entropic stress and shrinkage.

References

[1] Fitzer E. PAN-based carbon fiber present state and trend of the technology from the viewpoint of possibilities and limits to influence and to control the fiber properties by the process parameters. Carbon 1989; 27(5): 621-45.

[2] Chand S. Review carbon fibers for composite. Journal of Materials Science 2000; 35(6): 1303-13.

[3] Minus ML, Kumar S. The processing, properties, and structure of carbon fibers. JOM 2005; 57(2): 52-8.

[4] Kumar S, Anderson DP, Crasto AS. Carbon fiber compressive strength and its dependence on structure and morphology. Journal of Materials Science 1993; 28(2):423-39.

[5] Prandy JM, Hahn HT. Compressive strength of carbon fiber. Sampe Quarterly-Society for the Advancement of Material and Process Engineering 1991; 22(2): 47-52.

[6] Treacy MMJ, Ebbesen TW, Gibson JM. Exceptionally high young's modulus observed for individual carbon nanotubes. Nature 1996; 381(6584): 678-80.

[7] Dumitrica T, Hua M, Yakobson I. Symmetric-, time-, and temperature-dependent strength of carbon nanotubes. PNAS 2006; 103(16): 6105-9.

[8] Chae HG, Minus ML, Rasheed A, Kumar S. Stabilization and carbonization of gel spun polyacrylonitrile/single wall carbon nanotube composite fibers. Polymer 2007; 48(13): 3781-9.

[9] Chae HG, Choi YH, Minus ML, Kumar S. Carbon nanotube reinforced small diameter polyacrylonitrile based carbon fiber. Composites Science and Technology. 2009;69(3-4):406-13.

[10] Rahaman MSA, Ismail AF, Mustafa A. A review of heat treatment on polyacrylonitrile fiber. Polymer Degradation and Stability 2007; 92(8): 1421-32.

[11] Fitzer E, Frohs W, Heine M. Optimization of stabilization and carbonization treatment of PAN fibers and structural characterization of the resulting carbon-fibers. Carbon 1986; 24(4): 387-95.

[12] Dalton S, Heatley F, Budd PM. Thermal stabilization of polyacrylonitrile fibers. Polymer 1999; 40(20): 5531-43.

[13] Jing M, Wang CG, Zhu B, Wang YX, Gao XP, Chen WN. Effects of preoxidation and carbonization technologies on tensile strength of PAN-based carbon fiber. Journal of Applied Polymer Science 2008; 108(2): 1259-64.

[14] Liu T. and Kumar S. Quantitative characterization of SWNT orientation by polarized Raman spectroscopy. Chemical Physics Letters 2003; 378(3-4): 257-62.

[15] Chae HG, Minus ML, and Kumar S. Oriented and exfoliated single wall carbon nanotubes in polyacrylonitrile. Polymer 2006; 47(10): 3494-504.

[16] Cadek M, Coleman JN, Ryan KP, Nicolosi V, Bister G, Fonseca A, Nagy JB, Szostak K, Béguin F, Blau WJ. Reinforcement of polymers with carbon nanotubes: The role of nanotube surface area. Nano Letters 2004; 4(2): 353-6.

[17] Barber AS, Cohen SR, and Wagner HD. Measurement of carbon nanotube-polymer interfacial strength. Applied Physics Letter 2003; 82(23): 4140-2.

[18] Chae HG, Sreekumar TV, Uchida T, A comparison of reinforcement efficiency of various types of carbon nanotubes in polyacrylonitrile fiber. Kumar S. Polymer. 2005; 46(24):10925-35.

[19] Devasia R, Nair CPR, Sadhana R, Babu NS, Ninan KN. Fourier transform infrared and wide-angle X-ray diffraction studies of the thermal cyclization reactions of high-molar-

mass poly(acrylonitrile-co-itaconic acid). Journal of Applied Polymer Science 2006; 100(4): 3055-62.
[20] Fochler HS, Mooney JR, Ball LE, Boyer RD, Grasselli JG. Infrared and NMR spectroscopic studies of the thermal-degradation of polyacrylonitrile. Spectrochimica Acta Part A Molecular and Biomolecular Spectroscopy 1985; 41(1-2):271-8.
[21] Shimada I, Takahagi T, Fukuhara M, Morita K, Ishitani A. FT-IR study of the stabilization reaction of polyacrylonitrile in the production of carbon-fibers. Journal of Polymer Science Part A: Polymer Chemistry 1986; 24(8):1989-95.
[22] Usami T, Itoh T, Ohtani H, Tsuge S. Structural study of polyacrylonitrile fibers during oxidative thermal degradation by pyrolysis-gas chromatography, solid state C-13 nuclear magnetic resonance, and fourier transform infrared spectroscopy. Macromolecules 1990; 23(9): 2460-5.
[23] Zhu Y, Wilding MA, Mukhopadhyay SK. Estimation, using infrared spectroscopy, of the cyclization of poly(acrylonitrile) during the stabilization stage of carbon fibre production . Journal of Materials Science 1996; 31(14): 3831-7.
[24] Devasia R, Reghunadhan CP, Sivadasan NP, Katherine BK, Ninan KN. Cyclization reaction in poly(acrylonitrile/itaconic acid) copolymer: An isothermal differential scanning calorimetry kinetic study. Journal of Applied Polymer Science 2003; 88(4): 915-20.
[25] Gallaher KL, Lukco D, Grasselli JG. Investigation of the assignment of the 2190 cm^{-1} infrared band in polyfumaronitrile. Canada Journal of Chemistry. 1985; 63(7):1960-6.
[26] Yu MJ, Bai YJ, Wang CG, Xu Y, Guo PZ. A new method for the evaluation of stabilization index of polyacrylonitrile fibers. Materials Letter 2007; 61(11-12): 2292-4.
[27] Gupta A, Harrison IR. New aspects in the oxidative stabilization of pan-based carbon fibers. Carbon. 1996; 34(11):1427-45.
[28] Hou YP, Sun TQ, Wang HJ, Wu D. Thermal-shrinkage investigation of the chemical reaction during the stabilization of Polyacrylonitrile fibers. Journal of Applied Polymer Science. 2009; 114: 3668-72.
[29] Yu MJ, Wang CG, Bai YJ, Wang YX, Xu Y. Influence of precursor properties on the thermal stabilization of polyacrylonitrile fibers. Polymer Bulletin. 2006; 57(5):757-63.
[30] Kim DY, Kim YC, and Kim CY. Thermal analysis of PAN precursor of carbon fibers. Polymer (Korea) 1985; 9: 518-524.
[31] Bahl OP, Manocha LM. Shrinkage behavior of polyacrylonitrile during thermal treatment. Angewandte Makromolekulare Chemie 1975; 48: 145-59.
[32] Warner SB, Uhlmann DR, Peebles LH. Oxidative stabilization of acrylic fibers 3. Morphology of polyacrylonitrile. Journal of Material Science 1979; 14(8): 1893-8.
[33] Gupta AK, Singhal RP. Effects of co-polymerization and heat-treatment on the structure and x-ray diffraction of polyacrylonitrile. Journal of Polymer Physics Edition 1983; 21(11): 2243-62.

Table. 1 - Tensile properties and structural parameters of precursor PAN and PAN/CNT composite fibers.

	Control PAN	PAN/CNT1	PAN/CNT2	PAN/CNT3
Effective diameter (μm)	10.4	9.6	11.1	10.2
Tensile modulus (N/tex)	15.0±1.5	17.5±2.7	16.9±2.9	16.9±2.3
Tensile strength (N/tex)	0.73±0.11	0.92±0.07	0.75±0.04	0.81±0.06
Strain to failure (%)	9.5 ± 1.0	8.6±0.6	7.7±0.3	8.3±0.6
Crystallinity (%)	53	57	54	54
XS (nm)	9.2	11.4	9.3	9.1
$2\theta_{\text{Meridional scan}}$	39.2	38.9	39.1	39.2
f_{PAN}	0.89	0.90	0.89	0.89
f_{CNT}	/	0.93	0.90	0.94
Reinforcement efficiency of CNT (N/tex)	/	250	190	190

XS: PAN crystal size is calculated by the width of PAN (200,110) peak using Scherrer Equation. *f*: Herman's orientation factor, for PAN molecule, it is calculated from Azimuthal scan of PAN (200,110) planes; for CNT, it is calculated from G band intensity [14] of Raman spectra. The reinforcement efficiency of CNT is calculated by $\frac{YM_{Composite} - YM_{Control} \cdot f_w(PAN)}{f_w(CNT)}$ (YM: Young's modulus (N/tex), f_w: Weight fraction (%)).

Table. 2 – Fraction of conjugated nitrile and β-amino nitrile in PAN and PAN/CNT composite fibers stabilized under a stress of 20 MPa at 267 ^{o}C for various times.

Stabilization Time (hr)	PAN			PAN/CNT1			PAN/CNT2			PAN/CNT3		
	ϕ_c (%)	ϕ_a (%)	ϕ_c/ϕ_a	ϕ_c (%)	ϕ_a (%)	ϕ_c/ϕ_a	ϕ_c (%)	ϕ_a (%)	ϕ_c/ϕ_a	ϕ_c (%)	ϕ_a (%)	ϕ_c/ϕ_a
1	17	6	2.9	19	5	3.8	21	6	3.5	15	4	3.7
2	39	8	4.9	36	6	6.0	46	8	5.8	30	5	6.0
4	57	10	5.7	62	8	7.7	68	9	7.4	63	9	7.0
6	66	10	6.6	66	8	8.2	72	9	8.0	71	9	7.9
8	74	11	6.8	70	8	8.8	73	10	7.3	70	10	7.0
10	72	12	6.0	71	10	7.1	71	10	7.1	71	12	5.9

ϕ_c: Mole fraction of conjugated nitrile. ϕ_a *:* Mole fraction of β-amino nitrile. Fractions are calculated from nitrile peak fitting curves as shown in Figure 4.

Table. 3 – Crystal size and orientation factors of PAN and PAN/CNT composite fibers stabilized under a stress of 20 MPa at different temperature as shown in Figure 1.

Stabilization Time (hr)	Control PAN				PAN/CNT1			
	234 °C	at 267 °C			234 °C	267 °C		
	XS* (nm)	XS (nm)	f_{PAN}	$f_{ladder-polymer}$	XS (nm)	XS (nm)	f_{PAN}	$f_{ladder-polymer}$
0	9.2	9.2	0.89		11.4	11.4	0.90	
1	15.0	17.5	0.88	\	15.5	14.7	0.87	\
2	14.8	13.2	0.84	0.46	16.9	13.7	0.84	0.48
4	16.8	11.5	0.80	0.51	15.7	13.6	0.81	0.56
6	14.9	4.0	0.67	0.61	14.6	5.7	0.74	0.64
8		1.2	0.53	0.64		1.9	0.57	0.67
10		\	\	0.62		\	\	0.63

Stabilize Time (hr)	PAN/CNT2				PAN/CNT3			
	234 °C	267 °C			234 °C	267 °C		
	XS (nm)	XS (nm)	f_{PAN}	$f_{ladder-polymer}$	XS (nm)	XS (nm)	f_{PAN}	$f_{ladder-polymer}$
0	9.3	9.3	0.89		9.1	9.1	0.89	
1	14.5	13.6	0.85	\	14.8	17.4	0.88	\
2	14.9	10.8	0.83	0.51	15.4	11.7	0.85	0.50
4	15.3	4.25	0.65	0.62	14.7	6.1	0.65	0.62
6	12.1	1.6	0.54	0.66	13.2	2.9	0.63	0.66
8		1.3	\	0.65		1.7	\	0.65
10		\	\	0.64		\	\	0.65

Note: * XS: PAN crystallite size, calculated by the width of PAN (200, 110) peak using Scherrer equation. *f*: Herman's orientation factor, for PAN crystal, it is calculated from Azimuthal scan of PAN (200,110) planes; for ladder polymer, it is calculated from Azimuthal scan at $2\theta=25.7^{o}$.

Table. 4 - Tensile properties of PAN and PAN/CNT composite fibers stabilized under a stress of 20 MPa at 267 ^{o}C for various times.

Stabilization Time (hr)	Control PAN			PAN/CNT1 (99/1)		
	S* (N/tex)	M** (N/tex)	ε_b***	S (N/tex)	M (N/tex)	ε_b
0	0.73±0.11	15.0±1.5	9.5±1.0	0.92±0.07	17.5±2.7	8.6±0.6
1	0.44±0.09	13.5±1.7	9.1±2.0	0.44±0.06	15.2±1.6	7.7±1.0
2	0.38±0.05	12.3±1.4	9.2±1.4	0.40±0.04	15.1±1.9	10.0±1.0
4	0.19±0.03	8.6±1.1	6.4±1.9	0.35±0.05	12.9±1.9	9.3±0.7
6	0.22±0.03	9.0±1.0	8.1±2.3	0.22±0.04	11.4±1.9	6.1±1.8
8	0.19±0.02	8.7±0.9	6.1±1.2	0.19±0.02	11.7±2.1	4.4±0.9
10	0.18±0.01	8.4±0.8	6.4±1.6	0.18±0.02	11.5±2.4	3.2±1.4

Stabilization Time (hr)	PAN/CNT2 (99/1)			PAN/CNT3 (99/1)		
	S (N/tex)	M (N/tex)	ε_b	S (N/tex)	M (N/tex)	ε_b
0	0.75±0.04	16.9±2.9	7.7±0.3	0.81±0.06	16.9±2.3	8.3±0.6
1	0.48±0.09	14.9±1.8	8.3±1.0	0.54±0.10	15.5±1.8	8.7±0.8
2	0.42±0.06	14.3±2.1	9.8±1.3	0.43±0.10	14.0±2.6	9.0±1.3
4	0.29±0.05	11.2±2.3	9.0±1.2	0.34±0.07	11.4±2.8	9.8±1.3
6	0.25±0.04	11.4±2.8	6.0±1.2	0.26±0.04	11.0±1.4	8.0±1.2
8	0.22±0.03	11.2±1.9	4.6±0.9	0.24±0.05	10.8±2.4	6.9±1.2
10	0.21±0.03	10.8±3.0	4.3±1.0	0.20±0.03	10.3±2.2	5.7±1.0

Note: * Specific strength, ** specific young's modulus, and *** elongation at break.
tex: mass of 1000 meters length of fiber in grams.

Table.5 - Tensile properties of PAN and PAN/CNT1 fibers stabilized at 267 ^{o}C for 8 hr under various stresses.

Applied Stress (MPa)	PAN			PAN/CNT1		
	S* (N/tex)	ε_b** (%)	M*** (N/tex)	S (N/tex)	ε_b (%)	M (N/tex)
2.1	0.14±0.02	6.0±2.2	5.0±1.1	0.17±0.01	6.6±1.6	7.6±0.8
10	0.15±0.01	5.8±1.4	6.4±1.6	0.16±0.02	4.7±1.2	9.0±0.8
15	0.15±0.02	5.0±1.4	7.2±1.2	0.17±0.03	5.0±0.9	9.9±1.5
22	0.20±0.03	8.2±1.5	8.6±1.2	0.21±0.02	7.5±1.4	10.5±1.4

* Specific strength. ** Elongation at break. *** Specific young's modulus.

Table.6 - Nitrile band fitting data of PAN and PAN/CNT1 fibers stabilized at 267 ^{o}C for 8 hr under various stresses.

Applied Stress (MPa)	PAN			PAN/CNT1		
	ϕ_a (%)	ϕ_c (%)	Ratio*	ϕ_a (%)	ϕ_c (%)	Ratio
2.1	18	60	3.3	12	67	5.4
10	14	70	5.0	12	68	5.6
15	13	66	5.1	10	67	6.5
22	10	74	7.3	8	71	9.0

ϕ_c: Mole fraction of conjugated nitrile. ϕ_a: Mole fraction of β-amino nitrile. *Ratio=Mole fraction of conjugated nitrile (ϕ_c) over β-amino (ϕ_a) nitrile

Table. 7 - Herman's orientation factors calculated from azimuthal scans shown in Figure 10.

Applied Stress (MPa)	PAN	PAN/CNT1		
		Overall curve	Curve 1	Curve 2
2.1	0.54	0.60	0.97	0.59
10	0.58	0.61	0.96	0.61
15	0.61	0.62	0.91	0.62
22	0.63	0.66	0.99	0.65

* For PAN/CNT1 fibers, Azimuthal scan is deconvoluted into a highly ordered region (Fitting curve 1) and surrounding matrix (Fitting curve 2).

Table. 8 – Shrinkage values from shrinkage curves shown in Figure 11.

Applied Stress (MPa)	PAN			PAN/CNT1		
	$S_{Entropic}$ (%)	$S_{Stretch}$ (%)	$S_{Chemical}$ (%)	$S_{Entropic}$ (%)	$S_{Stretch}$ (%)	$S_{Chemical}$ (%)
2.1	13.6	0	18.8	9.9	0	17.0
10	8.5	-1.1	15.4	7.4	0	13.5
15	5.9	-1.2	12.7	6.7	-0.4	11.0
22	2.8	-4.1	8.2	4.1	-1.2	6.8
24		Break		3.3	-2.5	5.0
26		/			Break	

* S: Strain. Positive value means shrinking (Fiber length is reduced), and negative value means stretching (Fiber length is increased).

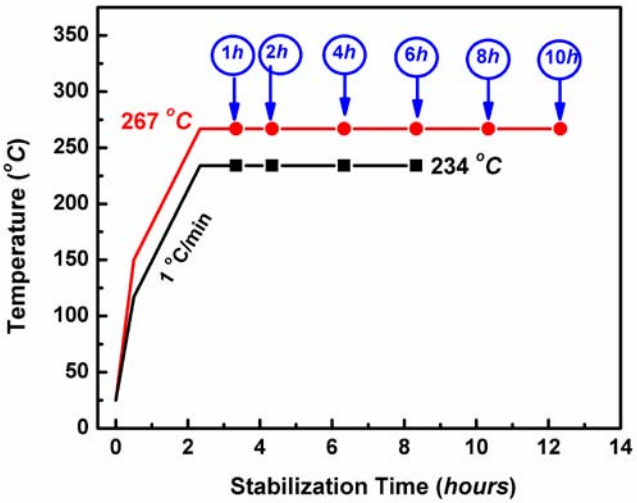

Figure. 1 - Stabilization process and samples collection points. Air flow rate is 20 standard cubic feet per hour (SCFH).

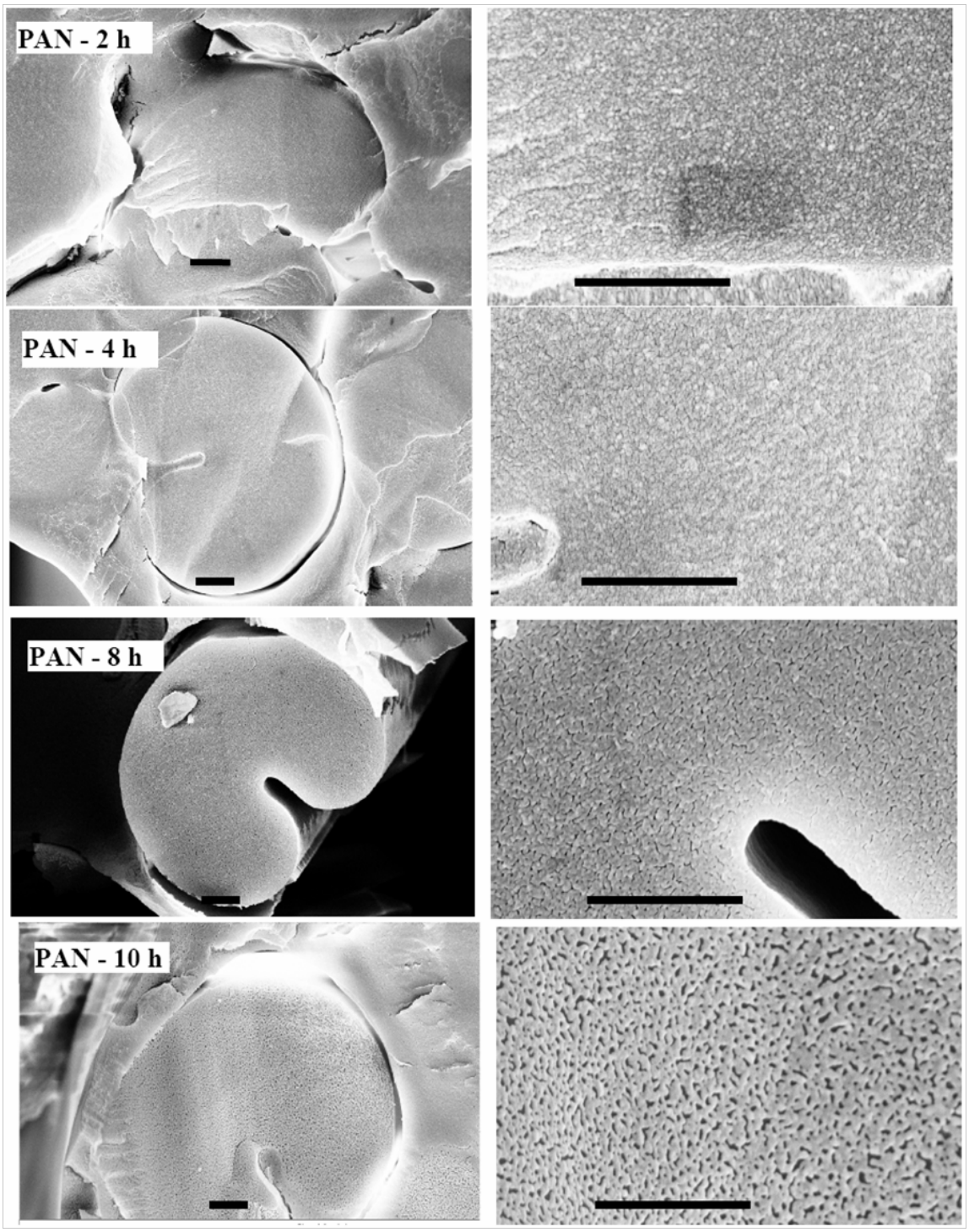

Figure. 2 - SEM images of cross sections of stabilized PAN fibers after boiling in DMF for 6 hr. Top to bottom: fibers stabilized at 267 ^{o}C for 2, 4, 8 and 10 hr. All scale bars: 2 μm. Matrix surrounding fibers is dried glue.

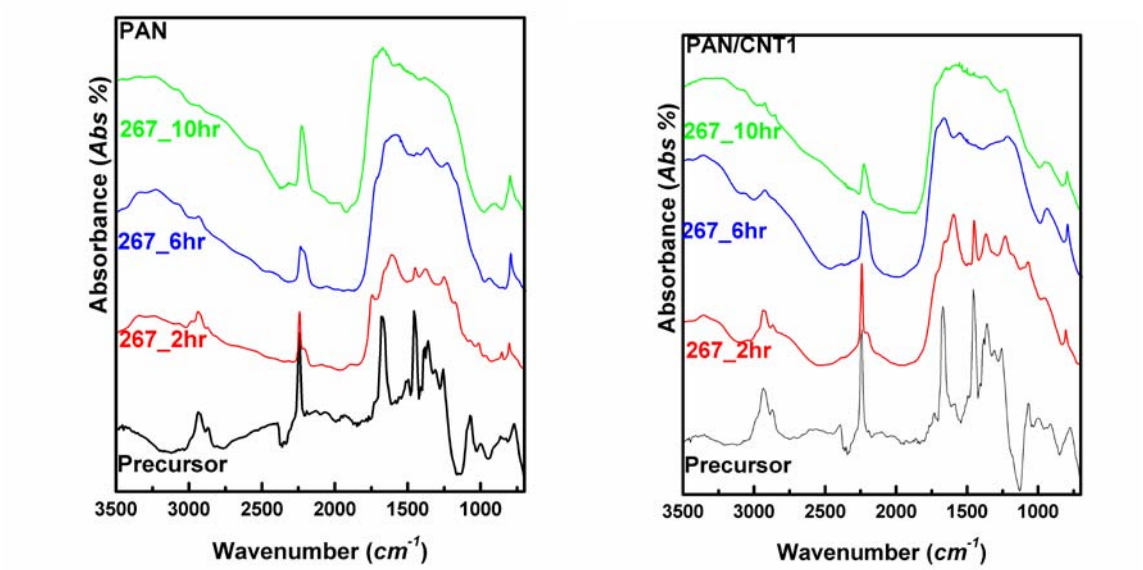

Figure. 3 - FT-IR spectra of control PAN and PAN/CNT1 (99/1) precursor and stabilized fibers. Stabilization is carried out at 267 ^{o}C for 2, 6 and 10 hr under a stress of 20 MPa (Temperature profile is shown in Figure 1).

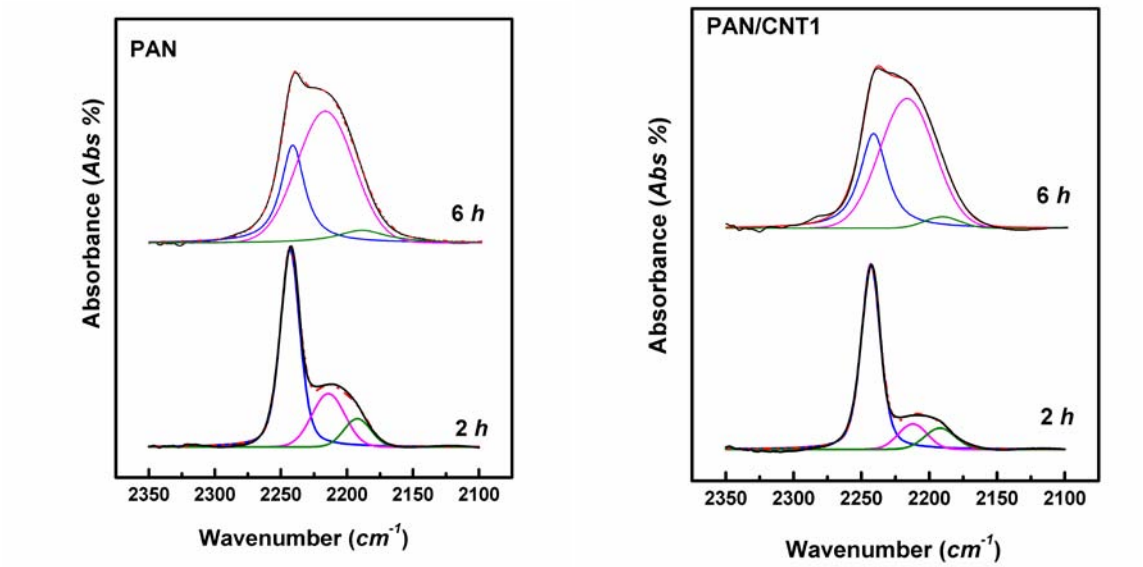

Figure. 4 - Nitrile band peak fitting of IR spectra of PAN and PAN/CNT1 fibers. Stabilization was carried out at 267 ^{o}C under a stress of 20 MPa for 2 and 6 hrs respectively.

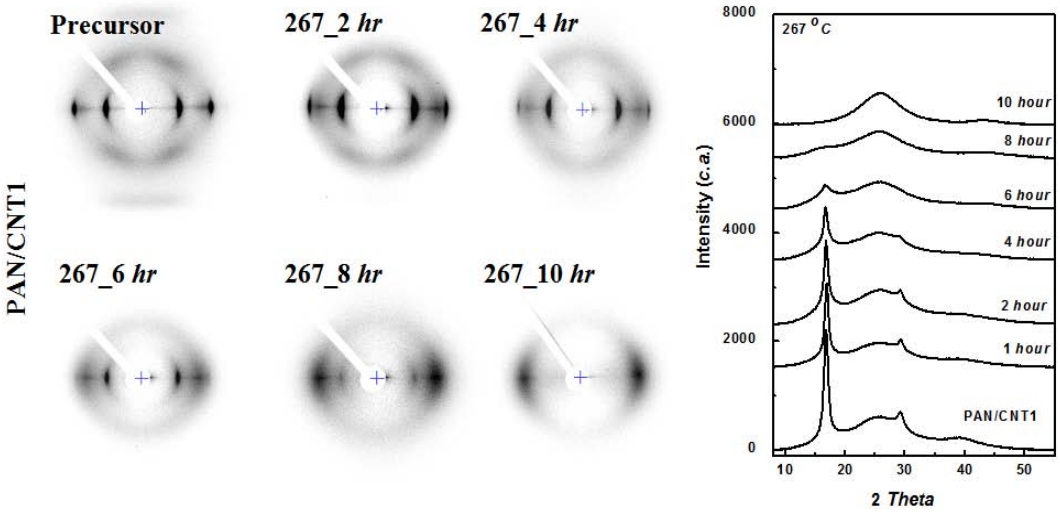

Figure. 5 – 2D X-ray diffraction patterns and integrated scans of PAN/CNT1 composite fibers stabilized at 267 ^{o}C for various times under a stress of 20 MPa.

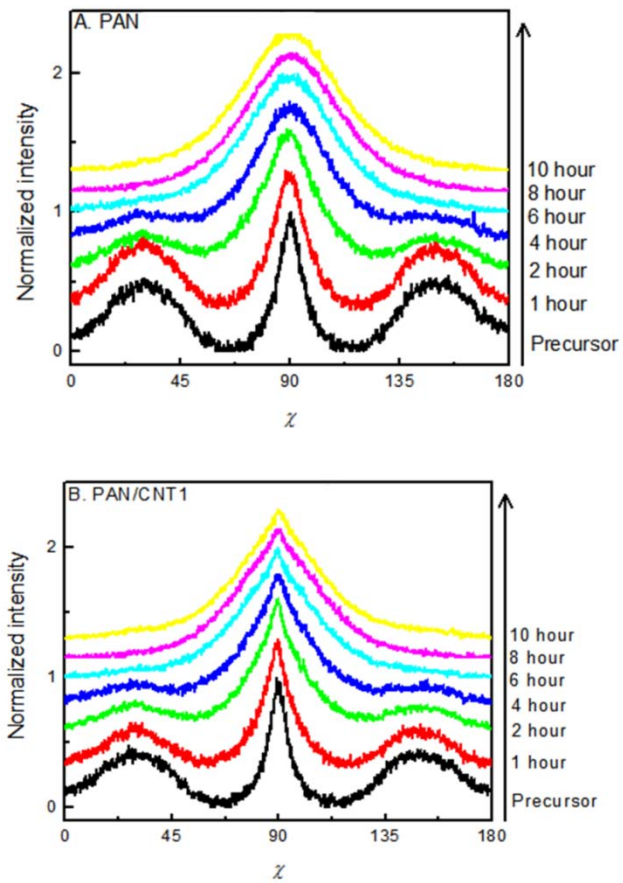

Figure. 6 - Azimuthal scans of PAN (A) and PAN/CNT1 composite fibers (B) at $2\theta=25.7^{o}$. Fibers were stabilized at 267 ^{o}C for various times under a stress of 20 MPa.

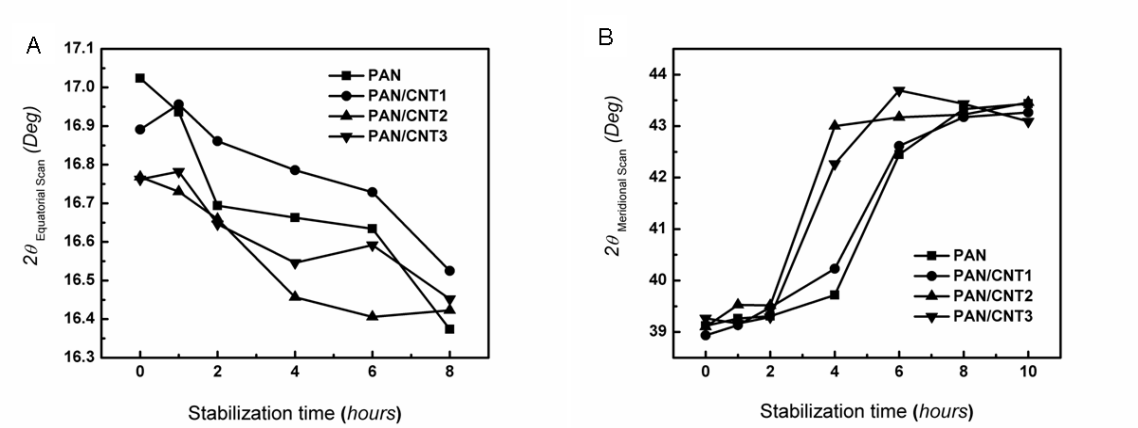

Figure. 7 – Changes of XRD Peak positions during stabilization at 267 ^{o}C under a stress of 20 MPa. A. PAN (200,110) peak in Equatorial scan; B. Meridional scan peak.

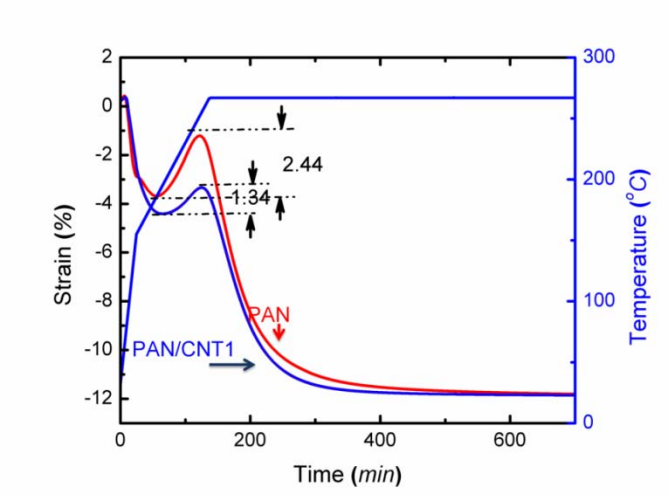

Figure. 8 - Shrinkage curves of PAN and PAN/CNT1 fibers under a stress of 20 MPa. Stabilization temperature followed the profile shown in figure 1, and shrinkage behaviors were monitored by TMA. Negative means shrinking, and positive means stretching.

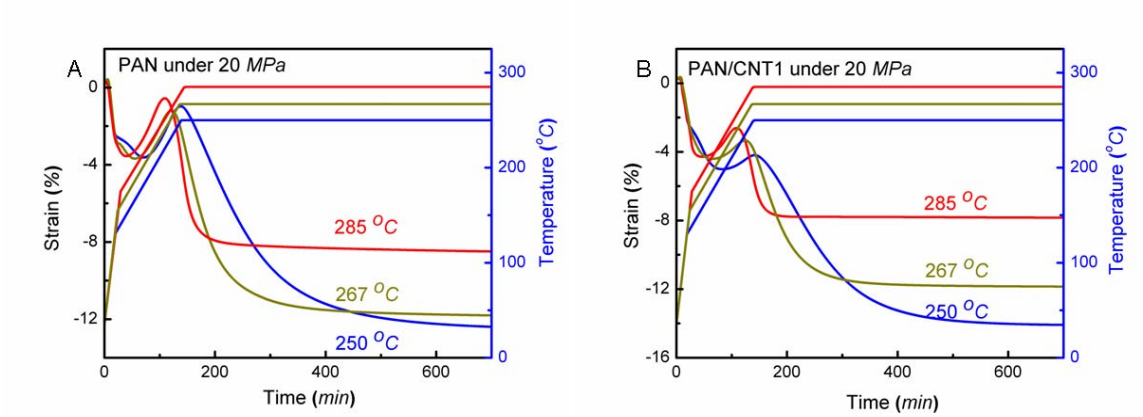

Figure. 9 - Shrinkage curves of PAN and PAN/CNT1 fibers stabilized at various temperatures under a stress of 20 MPa. A: PAN fibers; B: PAN/CNT1 composite fibers.

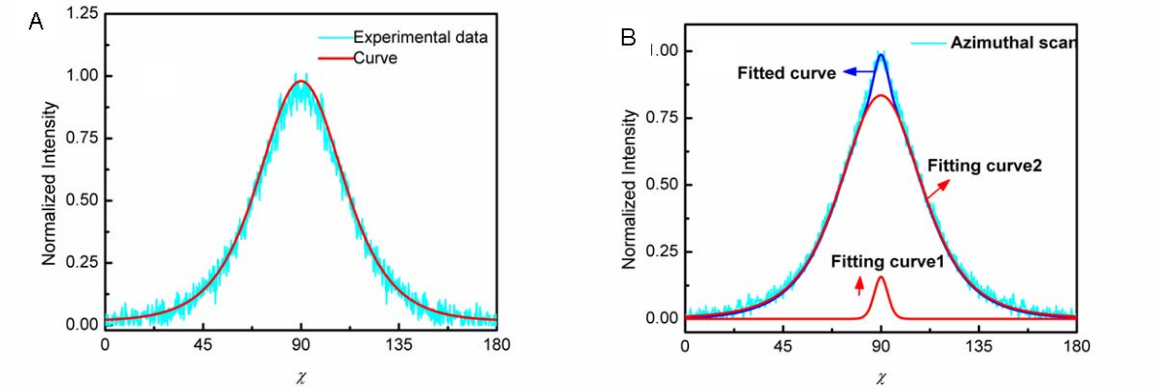

Figure. 10 - Azimuthal scans of formed ladder polymer at 2θ=25.7^{o} for fibers stabilized at 267 ^{o}C for 8 hr under a stress of 22 MPa. A: Stabilized PAN fibers; B: Stabilized PAN/CNT1 composite fiber. Azimuthal scan of stabilized composite fibers was deconvoluted into a highly ordered region (Fitting curve 1) and surrounding matrix (Fitting curve 2).

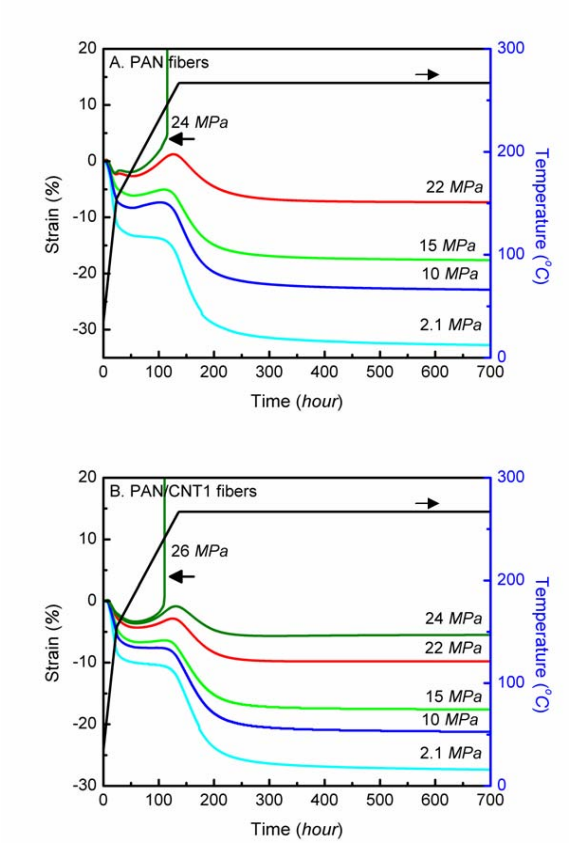

Figure. 11 – Shrinkage curves of PAN and PAN/CNT1 fibers stabilized under various stresses. A. PAN fibers; B. PAN/CNT1 composite fibers. The arrows toward left point breakage of fibers.

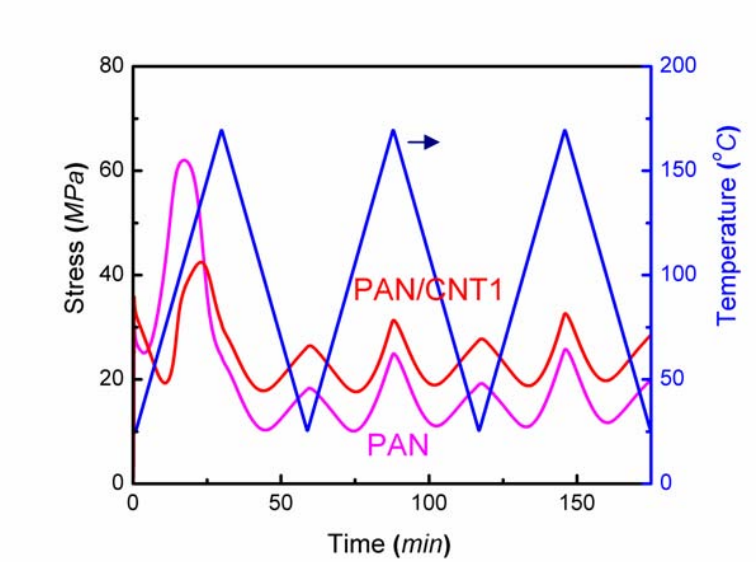

Figure. 12 - Stress curves of PAN and PAN/CNT1 fibers during thermal cycling under iso-strain condition.

Supporting information

Stabilization of Gel-spun Polyacrylonitrile/Carbon Nanotubes Composite Fibers. Part I: Effects of Carbon Nanotubes

Yaodong Liu, Han Gi Chae, Satish Kumar
School of Polymer, Textile and Fiber Engineering, Georgia Institute of Technology, 801 Ferst Dr. NW, Atlanta, GA 30332, USA

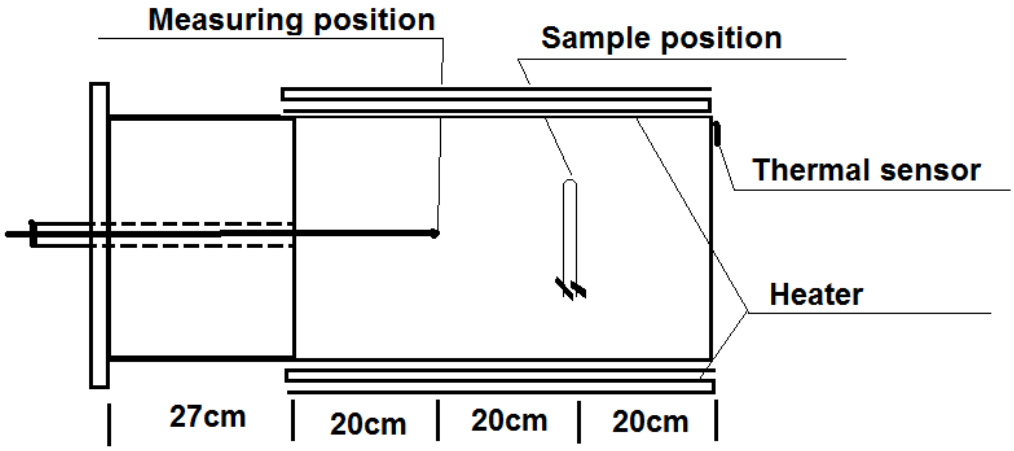

Cartoon of the position of thermal sensor and samples in the furnace (Top view)

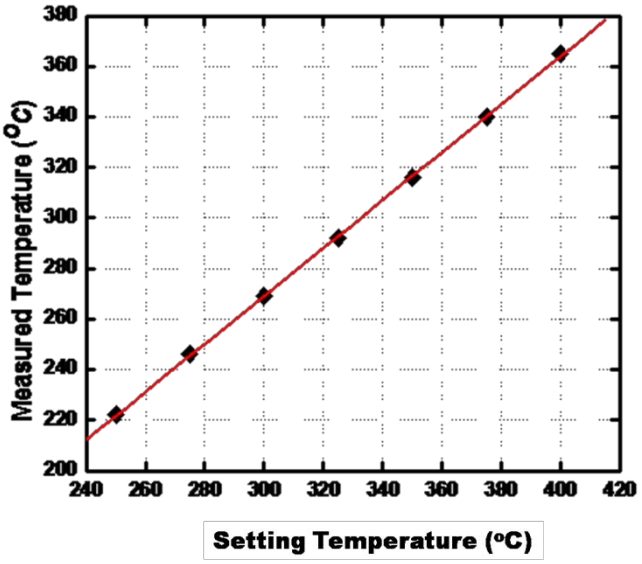

The calibration equation is :

$$T_{Measure} = 0.94857 \cdot T_{Setting} - 15.42857$$

S.Figure 1 – Temperature calibration curve for the furnace.

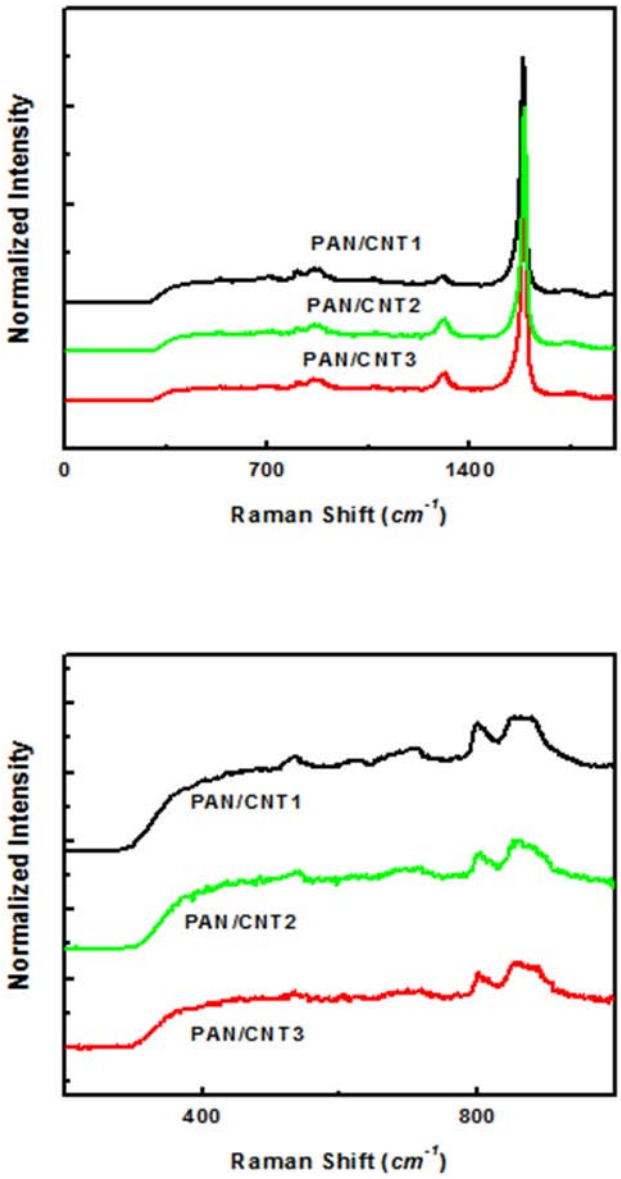

S.Figure 2 - Raman spectra of precursor PAN/CNT composite fiber.

S.Table 1 - Surface area test results of different kinds of CNTs used in experiments.

CNT	Batch#	BET SA (m^2/g)
CNT1	X0122UA	659 ± 9
CNT2	X0437UA	560 ± 3
CNT3	XB928	546 ± 3

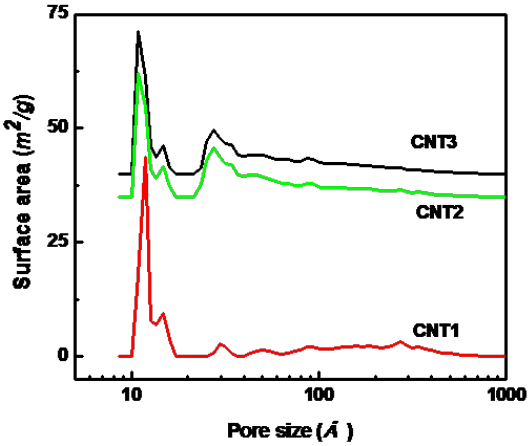

S.Figure 3 - Pore size distribution of different kinds of CNTs used in experiments.

Surface area was tested on Micromeretics Porosimeter.

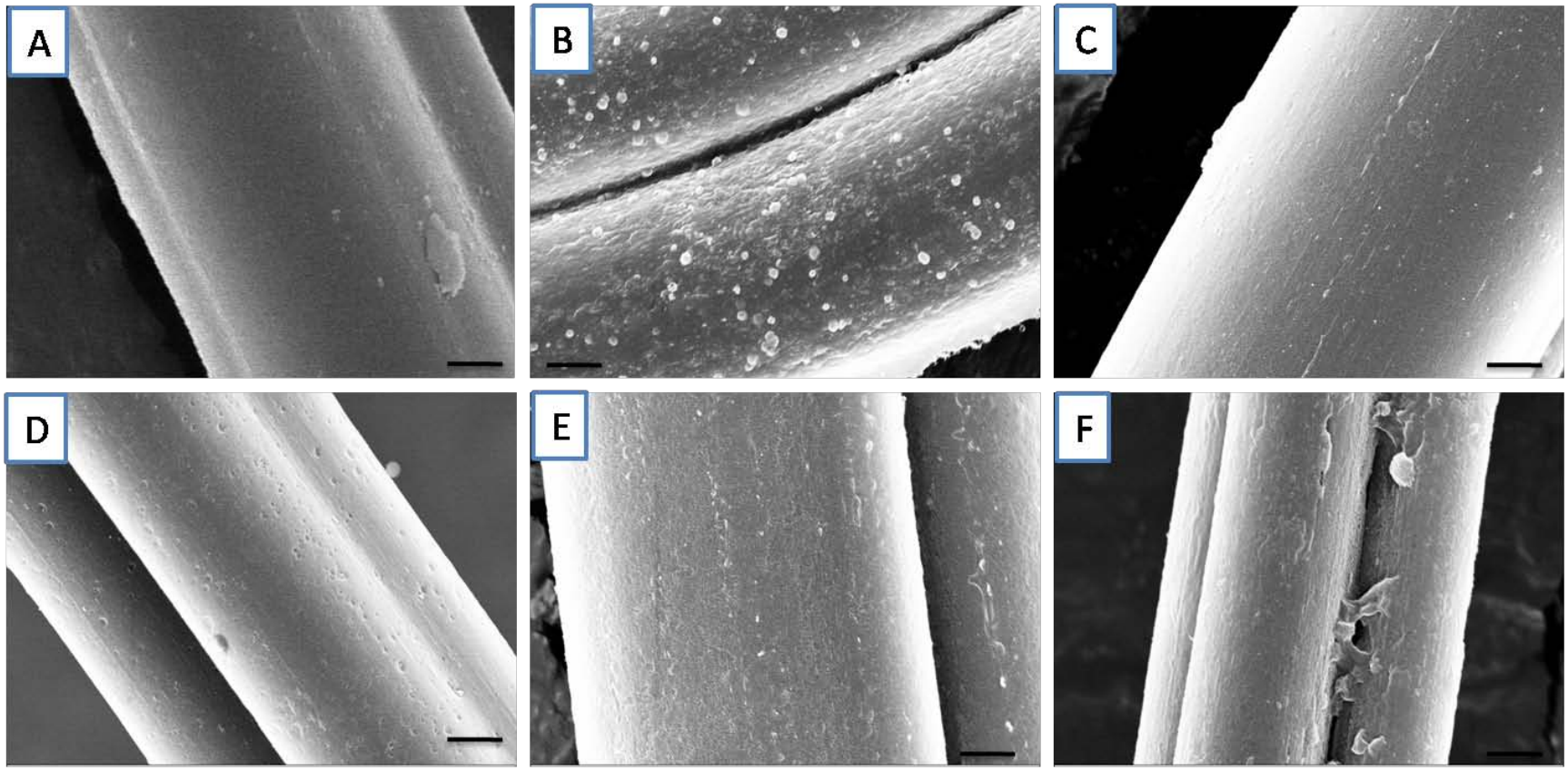

S.Figure 4 - SEM images of PAN/CNT1 precursor fiber and stabilized fibers after boiling in DMF.
A: Precursory fiber; B: stabilized at 267 ^{o}C for 2h; C: for 4hours; D: for 6 hours; E: for 8 hours, F: for 10 hours.
Scale Bar: 1 µm.

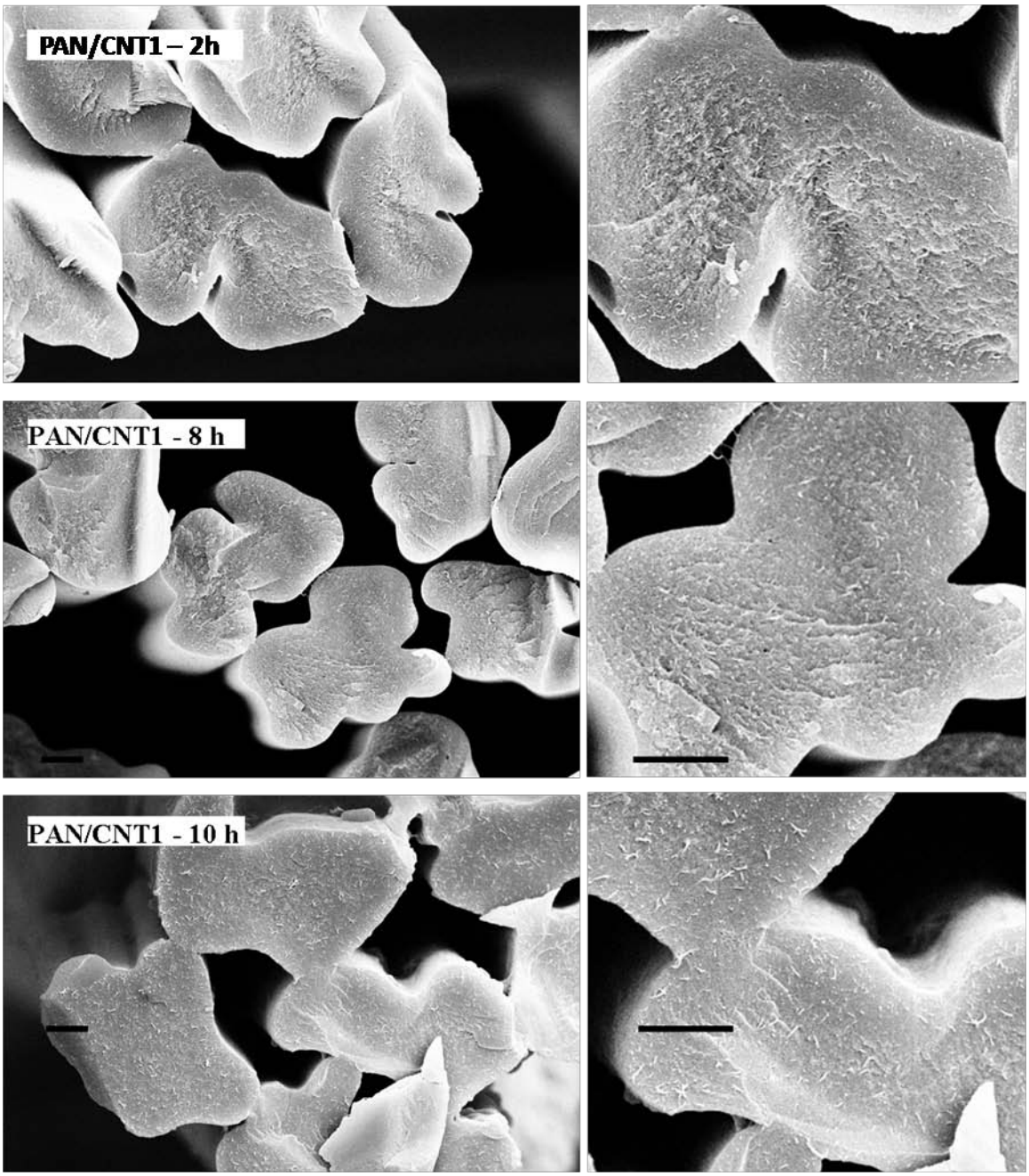

S.Figure 5 - SEM images of cross sections of stabilized PAN/CNT1 fibers after boiling in DMF for 6 hr. Top to bottom: fibers stabilized at 267 ^{o}C for 2, 8 and 10 hours, all scale bars: 2 μm.

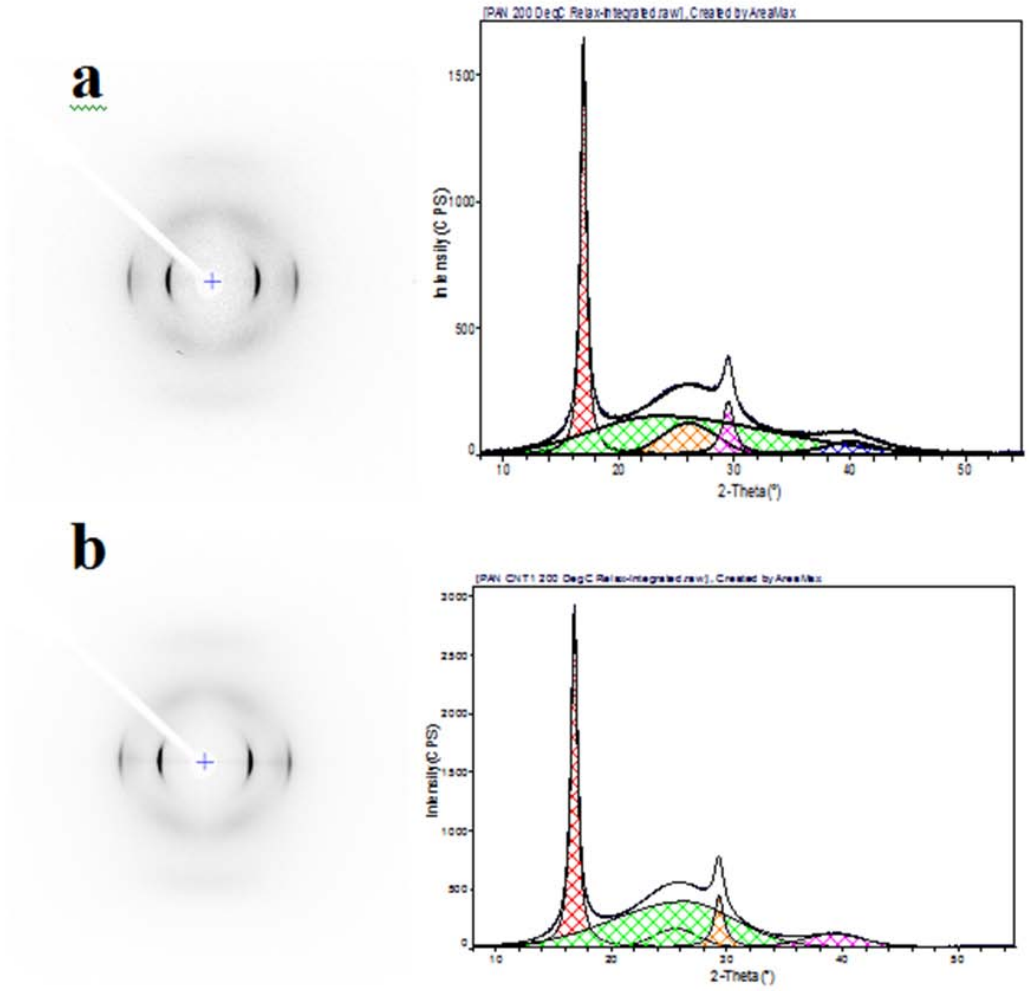

S.Figure 6 - WAXD pattern and integrated curves of fibers after thermal treatment*.
a. PAN; b. PAN/CNT1.
*Note: Thermal treatment – Fibers are held at constant length; temperature is raised from room temperature to 200 ^{o}C, then quenched to room temperature.

S.Table 2 - XRD data of PAN and PAN/CNT1 fibers after thermal treatment*.

Treatment	Sample	Crystallinity (%)	XS (*nm*)	f_c	$2\theta_{(100)}$	Ratio
Before	**PAN**	53	9.2	0.89	16.98	1.718
	PAN/CNT1	57	11.4	0.89	16.87	1.725
After	**PAN**	49	13.6	0.88	16.94	1.727
	PAN/CNT1	50	14.7	0.87	16.78	1.733

* XS: crystal size; f_c: Herman's orientation factor; Ratio=*d(~17^{o})/ d(~29^{o}).*

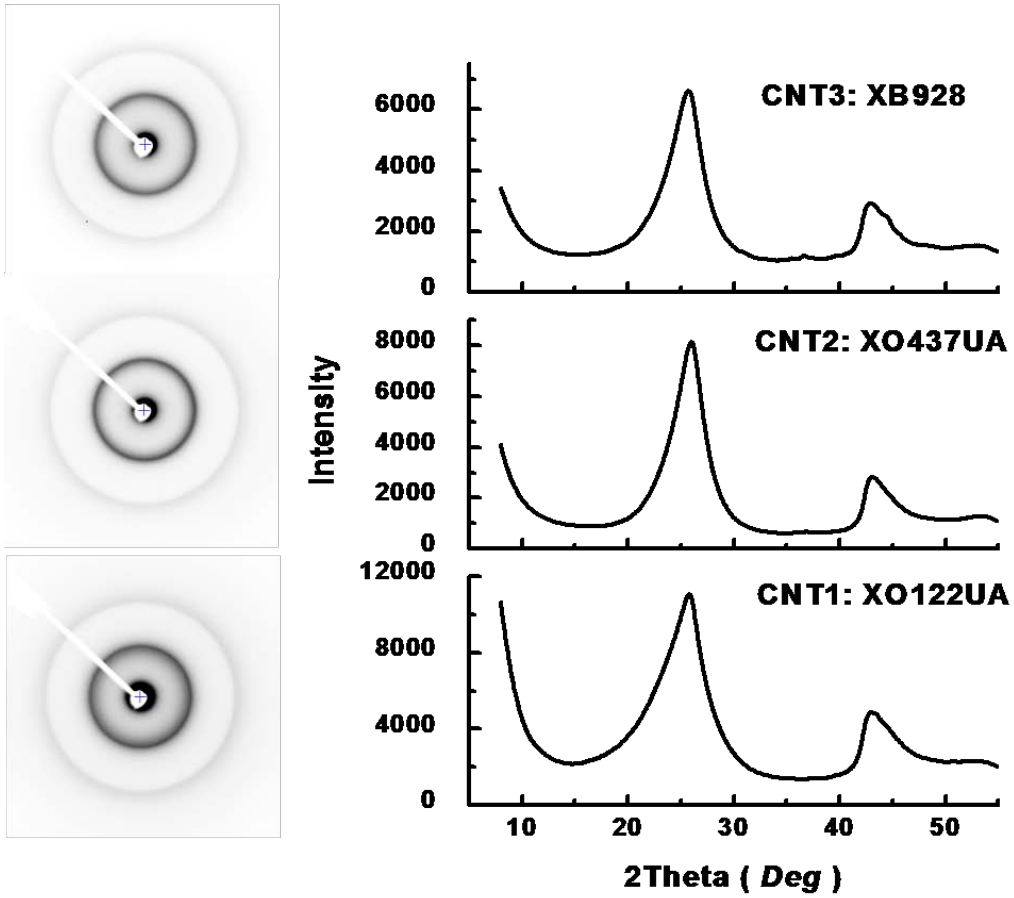

S.Figure 7 - Integrated XRD patterns of as received CNT powders.

S.Table 3 – Structural parameters of different kinds of CNTs obtained from XRD patterns.

CNT	**Batch#**	**FWHM (*d~0.345 nm*)**	**XS (*nm*)**	**Average Wall Number**
CNT1	X0122UA	5.92±0.03	1.4±0.1	4.1±0.3
CNT2	X0437UA	3.88±0.01	2.1±0.1	6.1±0.3
CNT3	XB928	4.07±0.01	2.0±0.1	5.8±0.3

* XS: Calculated crystal size.

The CNT2 and CNT3 were prepared using same method and processing parameters, the only difference between them was the purification. After purification, the contents of residual catalyst were 1 wt. % and 4 wt. % for CNT2 and CNT3 respectively. The surface area test using gas absorbance method showed no significant difference between CNT2 and CNT3; also, the calculated wall number from XRD powder diffraction showed comparable values.

SECTION III

Stabilization of Gel-spun Polyacrylonitrile/Carbon Nanotubes Composite Fibers. Part II: Stabilization Kinetics and Effects of Various Chemical Reactions.

Yaodong Liu, Han Gi Chae, Satish Kumar

School of Polymer, Textile & Fiber Engineering, Georgia Institute of Technology
801 Ferst Dr. NW, Atlanta, GA 30332-0295

Abstract

Gel-spun polyacrylonitrile (PAN) and PAN/carbon nanotube (CNT) composite fibers have been stabilized using various processing conditions to study the stabilization kinetics. Differential scanning calorimetry (DSC), infrared spectroscopy (IR), wide angle x-ray diffraction (WAXD) and thermo-gravimetric analysis (TGA) studies suggest that individual reactions such as cyclization, oxidation, dehydrogenation, and cross-linking can be distinguished at different stabilization stages. It is shown that the overall stabilization reaction is limited by cyclization reaction and oxygen diffusion because the oxidation preferably occurs with cyclized structure. The addition of CNT results in reduced activation energy as compared to control PAN fiber. Shrinkage behavior under different gas environments was also studied, suggesting that more inter-molecular cyclization happens in air than in nitrogen. Shrinkage behavior of PAN/CNT composite fiber exhibited that CNT significantly reduces overall shrinkage and increases the maximum stress that can be applied to fiber, indicating good interaction with PAN matrix.

1. Introduction

During the preparation of carbon fiber (CF) from polyacrylonitrile (PAN) precursor fibers [1], stabilization process is one of the most important steps [2-4], which strongly affects the carbon yield and the ultimate mechanical properties of resulting CFs. Usually, stabilization process is carried out in the temperature range of 200 to 400 ^{o}C in the presence of oxidative gas, typically air environment. During stabilization, PAN fibers undergo complex physical and chemical changes [5-7]. It is known that the chemical reactions include cyclization [8, 9], oxidation[10, 11], dehydrogenation[12] and cross-linking [8]. It is however, difficult to distinguish because all the reactions take place concurrently. The stabilization reactions of PAN-based fibers have been studied for over 40 years, although there are some points of consensus, no direct evidence and definitive mechanism have been reported. If one can better understand the kinetics [12, 13] and effects of different chemical reactions, then it would help in optimizing the stabilization process.

Stabilization reactions are exothermic. Based on the heat evolution that can be monitored by differential scanning calorimetry (DSC), reaction peak temperature can be obtained and reaction activation energy can also be calculated [14, 15]. There are literature reports on the existence of two DSC exothermic peaks during heat treatment in air, and these peaks were ascribed to different reactions [13, 16]. However, the problems are: 1. not all reactions show distinguishable individual peaks; 2. reactions may be inter-dependent, for example, Watt[10] observed that cyclization reaction strongly affected oxidation and concluded that the primary

reaction caused by heating was cyclization, and cyclized ladder polymer was the prerequisite of oxidation. Cyclization reaction can occur in inert or oxidative gas environment [17]; thus, it is possible to separate reactions by using different gas environments at different stabilization stages.

In this paper, stabilization kinetics of gel-spun PAN and PAN/carbon nanotube (CNT) composite fibers were studied. As reported previously [18], gel-spun PAN/CNT composite fibers result in carbon fibers with significantly improved mechanical properties as compared to the comparably processed PAN fibers. The CNT containing gel-spun PAN fibers are considered to be a candidate for the next generation carbon fiber. The detailed stabilization study of the gel-spun fibers was carried out as follows. The stabilization reactions are divided into cyclization, oxidation and additional cross-linking by changing environmental gas during heat treatment. The same method by changing atmosphere has been used by Fitzer [12] to study the influence of oxygen on stabilization, but no relationship between DSC exothermic peaks and stabilization reactions was investigated. In the current work, the activation energy of individual reaction was calculated from DSC data. The effects of different reactions on the structural changes, dynamic mechanical properties, and shrinkage of PAN and PAN/CNT composite fibers are investigated.

2. Experimental

Homopolymer PAN (Average Mw=250,000 g/mol, Japan Exlan Co., Japan) and CNT (lot# XO122UA, 1 wt% catalytic impurity Unidym Inc., Houston, TX) were used in this study. Precursor composite fibers contain 1 wt % CNTs. Detailed fiber spinning process and mechanical properties were reported elsewhere [19]. Infrared spectra were examined using infrared spectrometer (Spectrum One, Perkin Elmer Corp.) by collecting 256 scans at a resolution of 2 cm^{-1}. Wide angle X-ray diffraction (WAXD) patterns were obtained by Rigaku micromax-002 using CuK_α (λ=0.1542 nm) radiation and Rigaku R-axis IV++ detector. Weight loss during stabilization was recorded by thermo-gravimetric analysis (TGA, Q5000, TA Instruments). The shrinkage and stress variations were monitored by thermo-mechanical analyzer (TMA, Q-400, TA Instruments). Heat flow curves were collected by differential scanning calorimetry (DSC, Q-100, TA Instruments). Dynamic mechanical analysis (DMA) experiments were performed on RSA III (TA Instruments). A fiber bundle containing 100 filaments was tested under three frequencies (0.1, 1, and 10 Hz) at a heating rate of 1 ^oC/min.

3. Results and discussion

3.1 Separating different stabilization reactions

PAN fibers were first stabilized in nitrogen, and cooled to room temperature. Then, the pre-treated fibers were further stabilized in air. The heating profile is shown in Figure 1. Sample_1, Sample_2, and Sample_3 were collected at different stabilization stages after DMA tests for further characterizations; for control sample, it was only stabilized in air from room temperature to 380 ^oC at a heating rate of 1 ^oC/min.

Figure 2 shows DSC curves of PAN fiber heated in different gas environments. The heat flow curve of control PAN fiber (Figure 2C) exhibited a broad exothermic peak due to the multiple and complex stabilization reactions. If stabilization is carried out in nitrogen, a sharp and narrow peak only caused by cyclization reaction is observed (Figure 2A). Similar result was previously reported by Fitzer et al. [20]. Further heat-treatment of this sample (Figure 2A) in air

resulted in two broad exothermic peaks (Figure 2B), indicating that different reactions happens at different temperature (one at around 170 ^{o}C and the other at around 300 ^{o}C).

IR spectra of stabilized fibers were compared to understand the changes of chemical structures, and reactions related to the heat evolution at different temperature stages. Figure 3 shows the IR spectra of stabilized PAN fibers at different stages. For PAN precursor fibers, the peak at ~2931 cm^{-1} can be assigned to C-H vibration in PAN backbone, ~2242 cm^{-1} is assigned to the stretching of C≡N groups, ~1462 cm^{-1} is from C-C chain vibration. After fibers were heat treated in nitrogen up to 310 ^{o}C (Sample_1), the peak intensity of C≡N group decreases as compared with peaks of C-H and C-C vibration. A new peak appears at ~ 1617 cm^{-1} caused by the formation of C=N groups formed during cyclization reaction. When the same fibers were further treated in air up to 210 ^{o}C (Sample_2), peak at ~ 804 cm^{-1} due to formation of C=C-H after dehydrogenation reaction and a deep shoulder at ~ 1725 cm^{-1} due to ketonic structure [16] were evolved by oxidation reaction. Both peaks at ~ 804 cm^{-1} and ~ 1725 cm^{-1} are observed simultaneously, suggesting that oxidation and dehydrogenation reactions take place concurrently. Considering DSC results of sample B and C in Figure 2, oxidation temperature is greatly reduced if cyclization occurs prior to oxidation, which also suggests that oxidation takes place preferably to the cyclized structure. After the treatment temperature was raised to 380 ^{o}C (Sample_3), intensities of C-H peak at ~ 2931 cm^{-1}, C=C peak at ~ 1617 cm^{-1} and C=C-H peak at ~ 804 cm^{-1} decrease, indicating that hydrogen atoms are eliminated from the cyclized structure, and that inter-molecular cross-linking may happen at this stage [16].

Figure 4 shows weight loss curves of PAN fibers. The initial weight loss at around 150 ^{o}C (~ 4 wt %) may be due to the residual DMF and absorbed moisture. Obvious weight loss occurred above 250 ^{o}C. It was observed that HCN groups were eliminated during stabilization reaction, which may lead to major weight loss [20, 21]. Also, it can be found that heating rate affects the final weight loss (Figure 4A); higher heating rate leads to more weight loss. The higher heating rate will cause faster exothermic reaction (Figure 7), since PAN is not a good thermal conductive medium, it may cause localized over-heating, leading to decomposition of PAN. Stabilization in air has less weight loss than in nitrogen, since oxygen participated into reactions. For PAN fibers stabilized in air after being cyclizd in nitrogen, an increase of weight could be found when temperature was higher than 100 ^{o}C. The increase was caused by oxygen up-take due to the oxidation reaction, and confirmed by IR spectra as discussed earlier. Further weight reduction can be observed when temperature was higher than 330 ^{o}C, which may be caused by cross-linking or partial decomposition.

The integrated WAXD patterns of stabilized samples in each stage are shown in Figure 5. The characteristic PAN crystals peaks (2θ ~ 17^{o} and 30^{o}) diminishes as stabilization progresses. The peak evolved at ~ 26 ^{o} is due to the cyclic structure formation. It can be also noted that the peak intensity increases with the progress of stabilization reaction, indicating that the content of cyclic structure increases during stabilization. WAXD curves of Sample_3 and control sample show comparable pattern. This suggests that these fibers have similar structure even though they underwent different stabilization processes.

The dynamic mechanical property changes during heat treatment were monitored and shown in Figure 6. In Figure 6A and 6B, the first tan δ peak at around 80 ^{o}C, glass transition behavior of PAN molecules, was observed. Different gas environments show little effect on glass transition temperature, since it is a physical change. The second tan δ peak in Figure 6A appears at around 280 ^{o}C, which is caused by chemical reactions during stabilization. Tan δ peak of PAN fibers stabilized in air (Figure 6A) appeared at higher temperature (~ 15 ^{o}C higher) compared

with fibers stabilized in nitrogen. The stabilization in air involved much more complex reactions compared with in nitrogen and showed much broader tan δ peak. The tan δ peak positions of stabilization reactions show very little frequency dependence, suggesting very high activation energy. For fibers stabilized just in air, the storage modulus increases monotonically with increasing temperature. This is because stabilization reaction in air includes oxidation, dehydrogenation, and cross-linking as well as cyclization. Among them, cross-linking can lead to the improvement in storage modulus. On the other hand, fibers heat treated in nitrogen, the storage modulus decreases after initial increase. As discussed earlier, when the fiber treated in nitrogen, only cyclization reaction occurs without having oxidation and cross-linking reaction. Further heat treatment at higher temperature would result both cross-linking and thermal decomposition, which is confirmed by TGA experiment in nitrogen shown in Figure 4. Considering sudden decrease in storage modulus, however, suggests that thermal decomposition is dominant in this stage.

For PAN sample treated in air after cyclized in nitrogen (Figure 6C), the storage modulus slightly decreases below 210 ^{o}C, then increases with increasing temperature. The storage modulus increases rapidly and loss modulus decreases when temperature was raised to over 300 ^{o}C. This confirms that the cross-linking reaction occurs at this stage. Suresh et al. [22] reported changes in visco-elastic properties during oxidative stabilization reactions that were affected by co-monomer acid type and content using DMA. Here, using the same method, the effects of different stabilization reaction on dynamic mechanical properties could be compared. Both the DSC curves in Figure 2 and tan δ curves in Figure 6A show transitions in the same temperature range.

3.2 Reaction activation energy

Based on above proposed method, using nitrogen and air in sequence, the effects of additives, such as carbon nanotubes, co-monomers, on different stabilization chemical reactions can be compared. In this part, the activation energies of PAN and PAN/CNT composite fibers were determined, and the effect of addition of CNTs was studied. Figure 7 presents DSC curves of PAN and PAN/CNTs fibers heated in air at different ramping rates: 1, 2.5, 5, 10, and 20 ^{o}C/min. Figure 8 shows DSC curves of PAN and PAN/CNTs in nitrogen and run again in air at different heating rates from 1 to 15 ^{o}C/min. The exothermic peaks shift to higher temperature and become stronger at higher heating rate. Comparing the exothermic peak of PAN fibers heated in different gas environments, the reactions in air happen in a much broader temperature range and exothermic peak appears at much higher temperature (> 15 ^{o}C) than that in nitrogen. It can also be noted that the addition of CNTs elevates peak position to higher temperature (~ 5 ^{o}C) and broaden the exothermic peak of PAN fibers stabilized in nitrogen (inset figure in Figure 8B). The FWHMs of DSC exothermic peaks in air and in nitrogen are listed in Table 1. It can be found that exothermic peak becomes sharper if heating rate is higher. For stabilization in air, no straight effect on FWHM can be found after the addition of CNTs, since the stabilization in air involves complex chemical reactions and may be affected by many factors. For stabilization in nitrogen, only cyclization reaction happens, it can be found that the addition of CNTs significantly broaden the reaction exothermic peak. It has been found [23] that the PAN showed more ordered structure in the vicinity of CNT as compared to the bulk PAN matrix farther away from CNTs. It is conceivable that this highly ordered structure may undergo different stabilization reaction and will have distinct properties. In previous study [19, 24], a small amount of highly ordered structure was found both in the stabilized and carbonized PAN/CNT composite fibers. The

structural differences after the addition of CNTs lead to different reaction activities, and causes broad exothermic peak.

When heating rate is faster than 10 ^{o}C/min, an endothermic peak appears right after the strong exothermic peak for fibers heated in nitrogen. The endothermic peak was ascribed to the melting of PAN crystals [25]. If the heating rate is fast enough, melting would occur before stabilization reaction. The DSC curves of PAN and PAN/CNTs fibers at a heating rate of 60 ^{o}C/min are shown in Figure 9. Similar effects of CNTs addition on stabilization reactions can be also found on melting behavior. The CNTs incorporation shifted it to higher temperature and also made it broader.

DSC peak positions with different heating rates were summarized in Table 1. The activation energy could be obtained by fitting Kissinger's equation [15] and Ozawa's equation [14] as shown below:

Kissinger's Method $$-\frac{E_a}{R}=\frac{d\left[\ln\left(\phi/T_S^2\right)\right]}{d\left(1/T_S\right)}$$

Ozawa's Method $$-\frac{E_a}{R}=2.15\frac{d\left(\log\left(\phi\right)\right)}{d\left(1/T_S\right)}$$

where E_a is activation energy, Φ is heating rate (^{o}C/min), and T_S is peak temperature (K).

Above two equations are used to estimate the activation energy irrespective of the detailed reaction mechanism. By plotting $\ln(\Phi/T_S^2)$ versus $1/T_S$ according to Kissinger's equation, and $\log(\Phi)$ versus $1/T_S$ according to Ozawa's equation, the slope of linear fitting line is equal to $-E_a/R$. The plots are shown in Figure 10. The activation energies related to different reactions were named cyclization reaction activation energy ($E_{a\text{-Cyclization}}$), Oxidation reaction activation energy ($E_{a\text{-Oxidation}}$), and cross-linking reaction activation energy ($E_{a\text{-Cross-linking}}$). Based on calculated activation energy, the pre-exponential factor A in Arrhenius equation, $\kappa = Ae^{-E_a/RT}$, could be calculated using the following equation [26] :

$$A=\frac{\phi E_a}{RT_m^2}e^{E_a/RT_m}$$

The exponential factor A was calculated from the DSC data at the heating rate of 1 ^{o}C/min, and the calculated results are listed in Table 2. Among all kinds of reactions, oxidation reaction exhibits the minimum activation energy. Other researchers [13, 17, 27] reported multi-peaks in DSC curves. By deconvolution, cyclization and oxidation peak were separated. The reported value of oxidation activation energy, 118 kJ/mol [13], is much higher than the value calculated here. The reason is that oxidation reaction is limited by cyclization reaction. Since oxidation reactions happens at much lower temperature (< 200 ^{o}C) for cyclized PAN fibers than that for control PAN fibers (> 250 ^{o}C), it suggests that the oxidation reaction prefers to react with cyclized ladder polymer, not directly with PAN molecules. For stabilization of PAN only in air (control sample), the oxidation exothermic peak will be delayed till temperature is high enough

to form cyclized structure. In this study, cyclized polymer was formed before oxidation reaction, and oxidation exothermic peak can be observed. This would be main reason why we obtain different activation energy as compared to the reported results. Based on data in Table 2, the rate coefficients of cyclization and oxidation reaction of PAN stabilized in air at 281.6 ^{o}C are calculated to be 0.13 and 9.2 sec^{-1}, respectively, suggesting that oxidation is much faster than cyclization at this temperature. Since oxygen preferably reacts with cyclized PAN, by comparing rates of cyclization and oxygen diffusion, one can determine whether the stabilization is limited by reaction or oxygen diffusion.

The activation energy as a function of exothermic peak position is plotted in Figure 11, and shows a linear relationship with peak temperature. Reaction with higher activation energy requires higher temperature to initiate. Comparing PAN and PAN/CNT composite fiber, addition of CNTs decreases the activation energies of oxidation and cross-linking reactions, while it only slightly lowers the activation energy of cyclization reaction. For composite fibers, it has been found that the addition of CNTs improves the content of planar zigzag structure in PAN fibers, improves crystallinity, increases crystal size and induces highly ordered ladder polymer around CNTs after stabilization [19]. Since there is almost no difference for the cyclization activation energies of PAN and PAN/CNT composite fibers, it is suggested that the above structural changes don't affect the mechanism of cyclization reaction. From FTIR studies [19] of nitrile band in stabilized fibers, addition of CNTs improves the segment length of conjugated nitrile in stabilized fibers, and makes cyclized polymer easier to react with oxygen and further cross-link together.

3.3 Effect of reactions on shrinkage

The PAN/CNT composite fibers were stabilized in TMA by following the procedure in Figure 1. The strain variation curve of PAN/CNT fiber stabilized in air after stabilized in nitrogen is shown in Figure 12 (sample_3 in Figure 1). Cyclization is an important reaction for stabilization because it constructs the main structural frame of the resulting carbon fiber. Shrinkage behavior is mainly caused by cyclization reactions. Once cyclization reaction was completed in nitrogen, fiber length almost does not change during further oxidation and cross-linking reactions (about 0.2% shrinkage at about 380 ^{o}C in Figure 12). Figure 13 shows shrinkage curves of PAN/CNT fiber stabilized under a stress of 4 MPa in air and nitrogen respectively. Entropic shrinkages happen at the temperature below 200 ^{o}C, and are not affected by gas environment, either oxidative or inert; however, reaction shrinkages show significant difference as fibers are stabilized in air or in nitrogen. It can be found that the reaction shrinkage in air is much larger than that in nitrogen. Wang [28] reported that no difference was found for the shrinkage of PAN fibers stabilized in air or argon, but more results [17, 29, 30] showed that shrinkage of PAN fibers stabilized in air was much larger than that in inert gas. As for intra-molecular cyclization, the length of polymer should remain unchanged; inter-molecular cyclization will contribute more to the reaction shrinkage [20]. Since reaction shrinkage in air (Figure 13) is much larger than in nitrogen, which indicates that cyclization in air involved more inter-molecular cyclization reaction as compared to in nitrogen. For copolymer PAN fibers containing acid which can initiate cyclization reaction, it was found that higher content of copolymer led to larger reaction shrinkage [20]. When fibers are stabilized in air, the oxidative structure can initiate cyclization reaction [12], which may lead to larger shrinkage.

To better understand the effects of oxygen on shrinkage, stress and strain changes of PAN and PAN/CNT composite fibers under various conditions were investigated. Higher stress

reduces both entropic and reaction shrinkages during stabilization both in nitrogen (Figure 14) and in air [19]. For PAN fiber stabilized in nitrogen, if stress increases from 0.4 to 4 MPa, chemical shrinkage can be reduced from 20% to 5%, while entropic shrinkage is reduced from 16% to 12%. If stress is increased to 20 MPa, a stretching process happens, and fiber length even increases. In comparison, if fibers are stabilized in air under the same stress of 20 MPa, large final shrinkage ~ 10 % occurs. For stabilized fibers, if more inter-molecular cyclization happens, fibers will be much stiffer and show betters resistance to external force [31]. On the other hand, if more intra-molecular cyclization occurs, the polymer chains will lose their cohesive energy and are easy to slip. For fiber stabilized in nitrogen, a stress as low as 8 MPa can reduce reaction shrinkage to almost zero. The stress evolution during stabilization under constant length mode is also shown at Figure 14A. For fibers stabilized in air, reaction stress significantly increases along with stabilization, whereas in nitrogen, stress decreases during stabilization reaction. Shrinkage curves under different stresses in nitrogen are shown in Figure 14B. With increasing stress, the reaction shrinkage was reduced or even be stretched when stress was higher than 8 MPa. In comparison, PAN fibers stabilized under a constant stress of 20 MPa in air (Figure 14C), reaction shrinkage is more than 5 %. The formed ladder polymer stabilized in nitrogen is much easier to slip than that stabilized in air, which also indicates that cyclization reaction in nitrogen prefers intra-molecular propagation that has relatively poor inter-chain adhesion. For the stress change of fibers in nitrogen at constant length mode in Figure 14A, before cyclization started (~ 270 ^{o}C), the residual stress were 17 and 15 MPa for PAN and PAN/CNT composite fibers respectively, which were higher than 8 MPa. Under this high tension, polymer began to slip and fibers were stretched, which led to decrease of stress during stabilization.

In order to obtain high modulus carbon fiber, orientation of stabilized PAN and final carbon fibers must be maintained during processing. Therefore, shrinkage should be minimized and the maximum stress should be applied [19]. The addition of CNT reduces shrinkage in two ways: 1. Comparing shrinkage curves of PAN/CNT composite fibers with PAN fibers (Figure 14B and 14C), addition of CNTs slightly reduced entropic shrinkage, but greatly reduced chemical shrinkage either in nitrogen or in air, especially for fibers stabilized under low stress. 2. For stabilization in nitrogen (Figure 14B), addition of CNTs improves the maximum stress from 20 MPa to 22 MPa.

4. Conclusions

In summary, this study shows the effect of different chemical reactions and CNT addition on the stabilization behavior of PAN fiber. To clearly investigate these effects, precursor fibers were stabilized using nitrogen and air in sequence. It has been shown that the complex chemical reactions could be separated into cyclization stage, oxidation and dehydrogenation, and additional cross-linking. Separating reactions was helpful to better understand the effects of different reactions on the structure changes during stabilization. It is also found that the additional cross-linking reaction has the highest activation energy followed by cyclization and oxidation reaction. Addition of CNTs in PAN fibers showed marginally reduced the activation energy of cyclization reaction, whereas it lowered the activation energy of oxidation and cross-linking reactions. It would be better to understand the limitation of reactions if one can compare the rate of different reactions with gas (oxygen) diffusion coefficient, and optimize the stabilization reaction. The cyclization occurred in air involved more inter-molecular cyclization, and leads to larger shrinkage as compared to that of the stabilized fiber in nitrogen. For

PAN/CNTs composite fibers, addition of CNTs reduced both entropic and reaction shrinkages; also, it can improve the maximum applied stress during stabilization.

References

[1] Minus ML, Kumar S. The processing, properties, and structure of carbon fibers. Jom. 2005 Feb;57(2):52-8.

[2] Dalton S, Heatley F, Budd PM. Thermal stabilization of polyacrylonitrile fibres. Polymer. 1999;40(20):5531-43.

[3] Deurbergue A, Oberlin A. Stabilization and carbonization of pan-based carbon fibers as related to mechanical properties. Carbon. 1991;29(4-5):621-8.

[4] Rahaman MSA, Ismail AF, Mustafa A. A review of heat treatment on polyacrylonitrile fiber. Polymer Degradation and Stability. 2007 Aug;92(8):1421-32.

[5] Bashir Z. A critical review of the stabilisation of polyacrylonitrile. Carbon. 1991;29(8):1081-90.

[6] Gupta A, Harrison IR. New aspects in the oxidative stabilization of PAN-based carbon fibers: II. Carbon. 1997;35(6):809-18.

[7] He D-X, Wang C-G, Bai Y-J, Lun N, Zhu B, Wang Y-X. Microstructural evolution during thermal stabilization of PAN fibers. Journal of Materials Science. 2007;42(17):7402-7.

[8] Josef S. Discoloration effects in acrylonitrile polymers. Journal of Polymer Science. 1958;28(117):438-9.

[9] Coleman MM, Sivy GT. Fourier transform ir studies of the degradation of polyacrylonitrile copolymers--I: Introduction and comparative rates of the degradation of three copolymers below 200°c and under reduced pressure. Carbon. 1981;19(2):123-6.

[10] Watt W, Johnson W. Mechanism of oxidization of polyacrylonitrile fibers. Nature. 1975;257(5523):210-2.

[11] Rangarajan P, Bhanu VA, Godshall D, Wilkes GL, McGrath JE, Baird DG. Dynamic oscillatory shear properties of potentially melt processable high acrylonitrile terpolymers. Polymer. 2002;43(9):2699-709.

[12] Fitzer E, Müller DJ. The influence of oxygen on the chemical reactions during stabilization of pan as carbon fiber precursor. Carbon. 1975;13(1):63-9.

[13] Ouyang Q, Cheng L, Wang H, Li K. Mechanism and kinetics of the stabilization reactions of itaconic acid-modified polyacrylonitrile. Polymer Degradation and Stability. 2008;93(8):1415-21.

[14] Ozawa T. A new method of analyzing thermogravimeteric data. Bull Chem Soc Jpn. 1965;38(11):1881-&.

[15] Kissinger HE. Reaction Kinetics in Differential Thermal Analysis. Analytical Chemistry. 1957;29(11):1702-6.

[16] Mittal J, Bahl OP, Mathur RB, Sandle NK. IR studies of PAN fibres thermally stabilized at elevated temperatures. Carbon. 1994;32(6):1133-6.

[17] Gupta A, Harrison IR. New aspects in the oxidative stabilization of pan-based carbon fibers. Carbon. 1996;34(11):1427-45.

[18] Chae HG, Minus ML, Rasheed A, Kumar S. Stabilization and carbonization of gel spun polyacrylonitrile/single wall carbon nanotube composite fibers. Polymer. 2007 Jun;48(13):3781-9.

[19] Liu Y, Chae HG, Kumar S. Stabilization of gel-spun polyacrylonitrile/carbon nanotubes composite fibers. Part I: Effects of carbon nanotubes. Submitted. 2010.
[20] Fitzer E, Frohs W, Heine M. Optimization of stabilization and carbonization treatment of PAN fibres and structural characterization of the resulting carbon fibres. Carbon. 1986;24(4):387-95.
[21] Sivy GT, Gordon Iii B, Coleman MM. Studies of the degradation of copolymers of acrylonitrile and acrylamide in air at 200°C. Speculations on the role of the preoxidation step in carbon fiber formation. Carbon. 1983;21(6):573-8.
[22] K. I. Suresh KSTBSRCPRN. Viscoelastic properties of polyacrylonitrile terpolymers during thermo-oxidative stabilization (cyclization). Polymers for Advanced Technologies. 2008;19(7):831-7.
[23] Chae HG, Minus ML, Kumar S. Oriented and exfoliated single wall carbon nanotubes in polyacrylonitrile. Polymer. 2006;47(10):3494-504.
[24] Chae HG, Choi YH, Minus ML, Kumar S. Carbon nanotube reinforced small diameter polyacrylonitrile based carbon fiber. Composites Science and Technology. 2009;69(3-4):406-13.
[25] Dunn P, Ennis BC. Thermal analysis of polyacrylonitrle. 1. Melting of polyacrylonitrle. Journal of Applied Polymer Science. 1970;14(7):1795-&.
[26] Reghunadhan Nair CP, Krishnan K, Ninan KN. Differential scanning calorimetric study on the Claisen rearrangement and thermal polymerisation of diallyl ether of bisphenols. Thermochimica Acta. 2000;359(1):61-7.
[27] Ouyang Q, Cheng L, Wang HJ, Li KX. DSC study of stabilization reactions in poly(acrylonitrile-co-itaconic acid) with peak resolving method. J Therm Anal Calorim. 2008 Oct;94(1):85-8.
[28] Wang PH. Aspects on prestretching of PAN precursor: Shrinkage and thermal behavior. Journal of Applied Polymer Science. 1998 Feb;67(7):1185-90.
[29] Om Parkash Bahl LMM. Shrinkage behaviour of polyacrylonitrile during thermal treatment. Angewandte Makromolekulare Chemie. 1975;48(1):145-59.
[30] Kim DY, Kim YC, Kim CY. Thermal Analysis of PAN Precursors of Carbon Fibers. Polymer (Korea). 1985;9(6):7.
[31] Hou YP, Sun TQ, Wang HJ, Wu D. Effect of heating rate on the chemical reaction during stabilization of polyacrylonitrile fibers. Text Res J. 2008 Sep;78(9):806-11.

Table 1. DSC data for PAN and PAN/CNT fibers

Heating rate (°C/min)	In air		In nitrogen		Rerun in air after running in nitrogen			
	PAN	PAN/CNT	PAN	PAN/CNT	PAN		PAN/CNT	
	T_s (°C)	T_s (°C)	T_s (°C)	T_s (°C)	T_{s1} (°C)*	T_{s2} (°C)*	T_{s1} (°C)*	T_{s2} (°C)*
1	281.6	286.0	265.9	271.4	173.8	308.5	172.5	309.8
2.5	301.0	303.2	280.7	285.9	182.9	315.3	185.1	316.5
5	315.0	317.1	293.0	298.0	193.3	330.7	197.0	333.3
10	326.4	329.7	305.7	311.7	209.2	NA	211.8	NA
15	/	/	313.3	320.6	219.0	NA	222.6	NA
20	340.4	340.4	/	/	/	/	/	/

Heating rate (°C/min)	In air		In nitrogen	
	PAN	PAN/CNT	PAN	PAN/CNT
	FWHM (°C)			
1	78.0	57.5	3.3	9.2
2.5	66.2	55.9	2.2	7.0
5	42.9	50.5	2.1	5.8
10	33.4	36.0	2.3	5.3
15	/	/	2.4	5.0
20	34.4	31.8	/	/

* 1 and 2 represent the first and second exothermic peaks, respectively. FWHM: Full width at half maximum of DSC exothermic peaks.

Table 2. Calculated kinetic parameters for PAN and PAN/CNTs fibers

		From Kissinger's Equation		From Ozawa's Equation	
		E_a (kJ/mol)*	A (s^{-1})*	E_a (kJ/mol)*	A (s^{-1})*
PAN	In air	135.4	3.0E+11	135.9	3.3E+11
	Cyclization	140.2	2.2E+12	140.1	2.2E+12
	Oxidation	98.1	1.7E+10	99.2	2.3E+10
	Cross-linking	188.6	5.8E+15	186.0	3.3E+15
PAN/CNT	In air	145.0	2.0E+12	145.0	2.0E+12
	Cyclization	138.5	1.1E+12	138.7	1.1E+12
	Oxidation	91.1	2.6E+09	92.7	4.1E+09
	Cross-linking	176.8	4.4E+14	175.0	3.0E+14

* E_a is activation energy and A is exponential factor in Arrhenius equation.

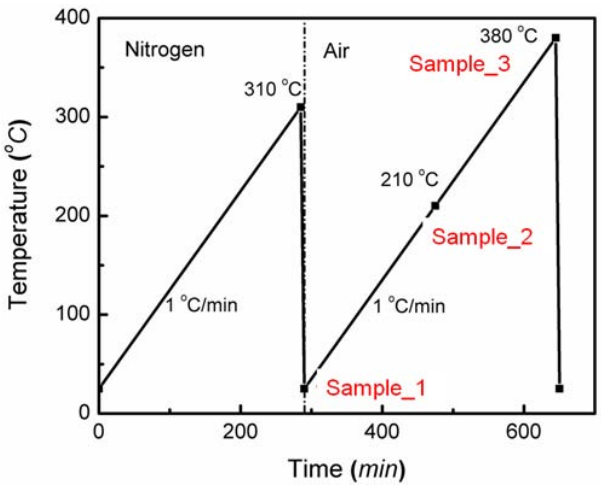

Figure 1. Heating profile for step-wise stabilization of PAN and PAN/CNT precursor fiber conducted in RSA III.

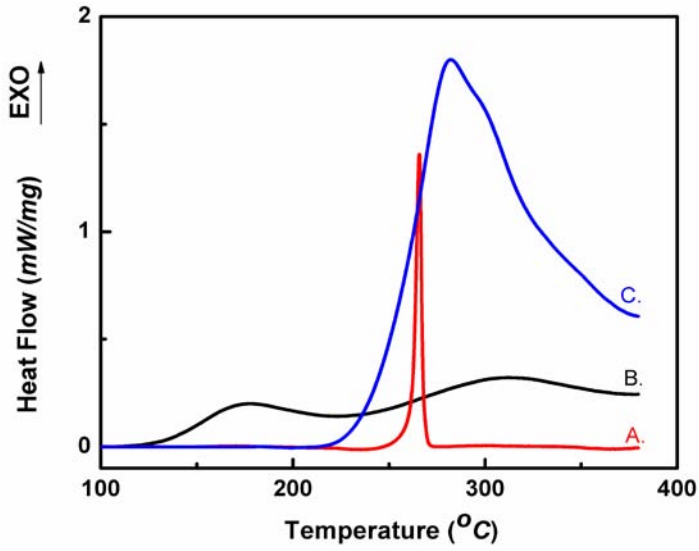

Figure 2. DSC heat flow curves of PAN precursor fibers at a heating rate of 1 °C/min. (A) in nitrogen (B) rerun in air after running in nitrogen, and (C) heat flow in air only.

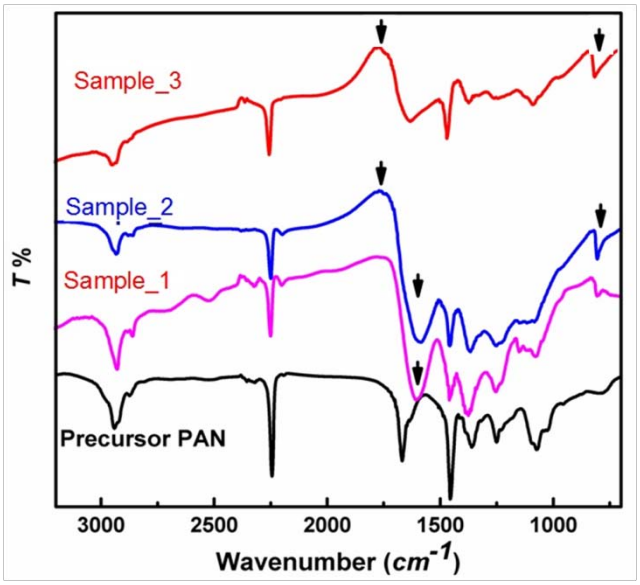

Figure 3. IR spectra of Sample_1, Sample_2, Sample_3, and PAN precursor fibers. IR spectra are shifted upward for clear comparison. Peak at ~804 cm^{-1} (pointed by far right arrow) is due to the formation of C=C-H after dehydrogenation. Peak at ~1617 cm^{-1} (pointed by middle arrow) in Sample_1 and Sample_2 is ascribed to the formation of C=N group due to the cyclization reaction. The deep shoulder appeared at ~1725 cm^{-1} (pointed by far left arrow) is known to be due to the ketonic structure [16].

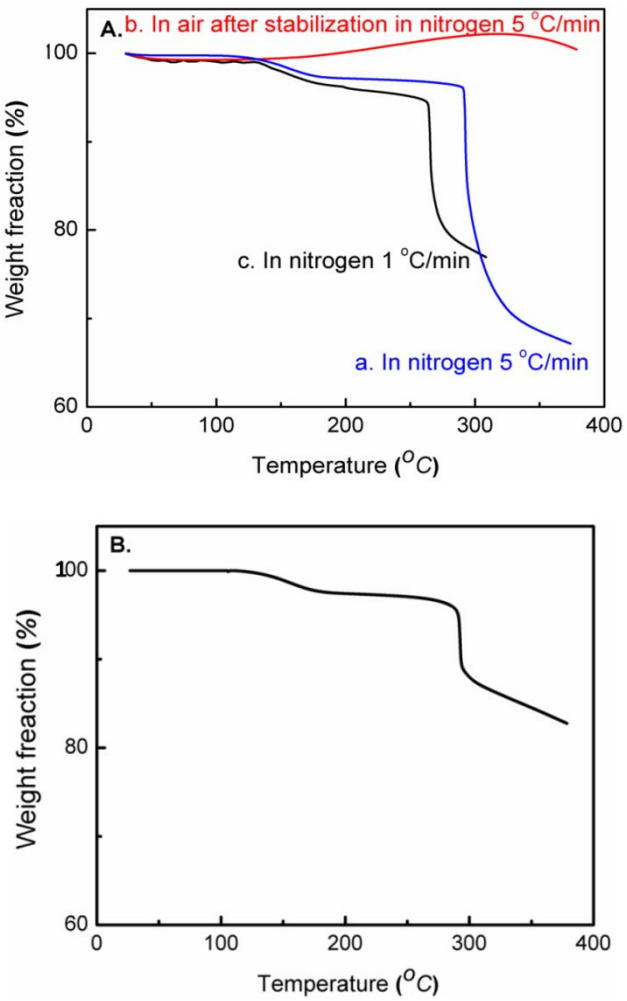

Figure 4. Weight loss curves of PAN precursor fibers. (A) a. in nitrogen at a heating rate of 5 °C/min, b. rerun in air after running in nitrogen at a heating rate of 5 °C/min, and c. in nitrogen at a heating rate of 1 °C/min, and (B) in air only at a heating rate of 5 °C/min.

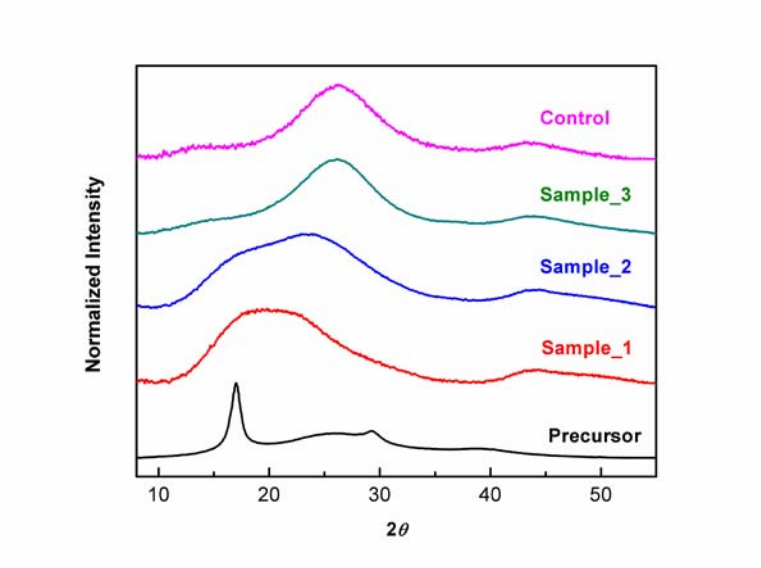

Figure 5. Integrated WAXD patterns of PAN fibers. Precursor is PAN/CNT precursor fiber. Control sample represents PAN fiber stabilized in air from room temperature to 380 ^{o}C at a heating rate of 1 ^{o}C/min. Sample_1, Sample_2, and Sample_3 are the specimen designated in Figure 1.

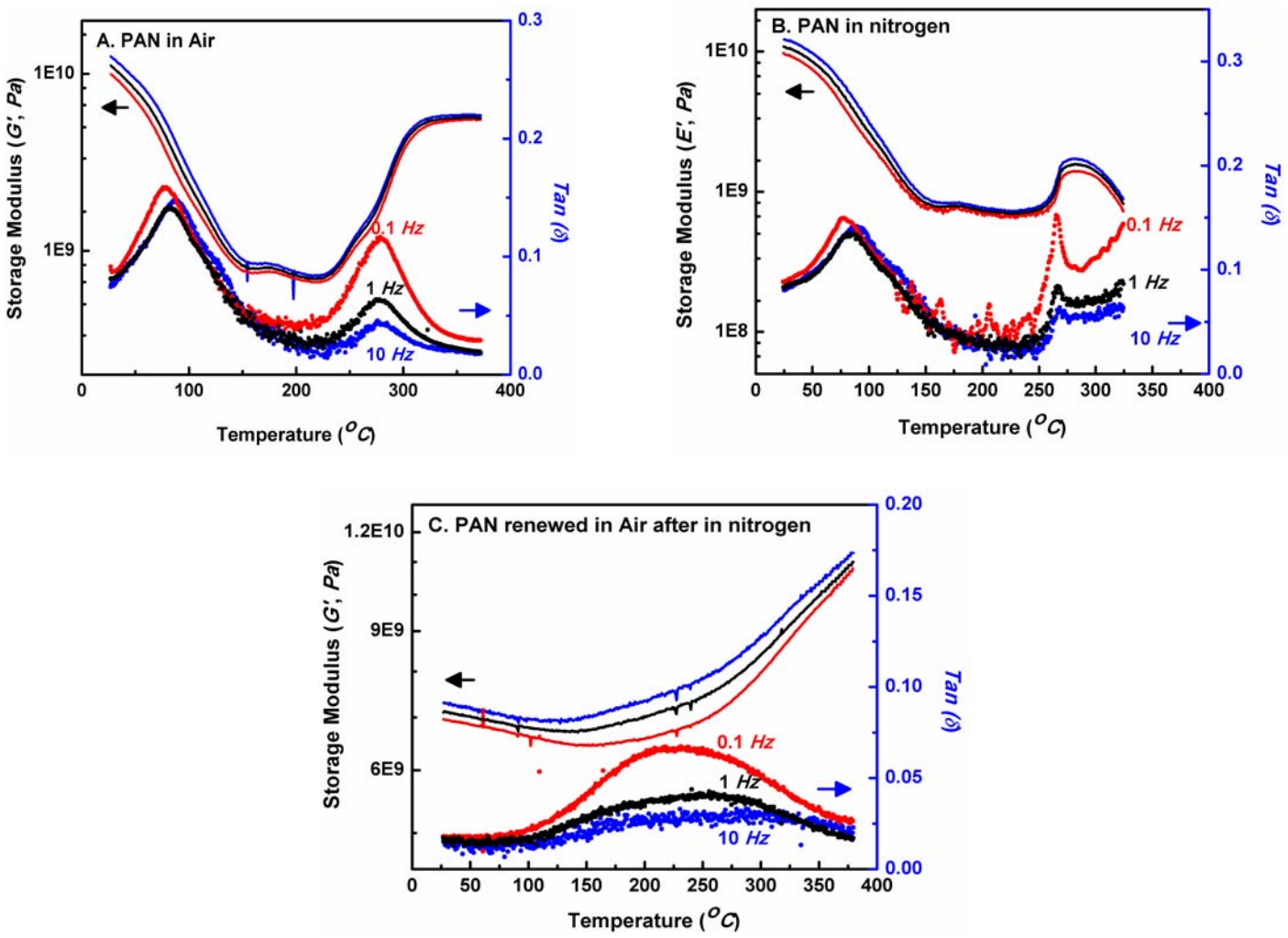

Figure 6. DMA curves of PAN precursor fibers during different heating treatment process. (A) In air, (B) in nitrogen, and (C) rerun in air after running in nitrogen.

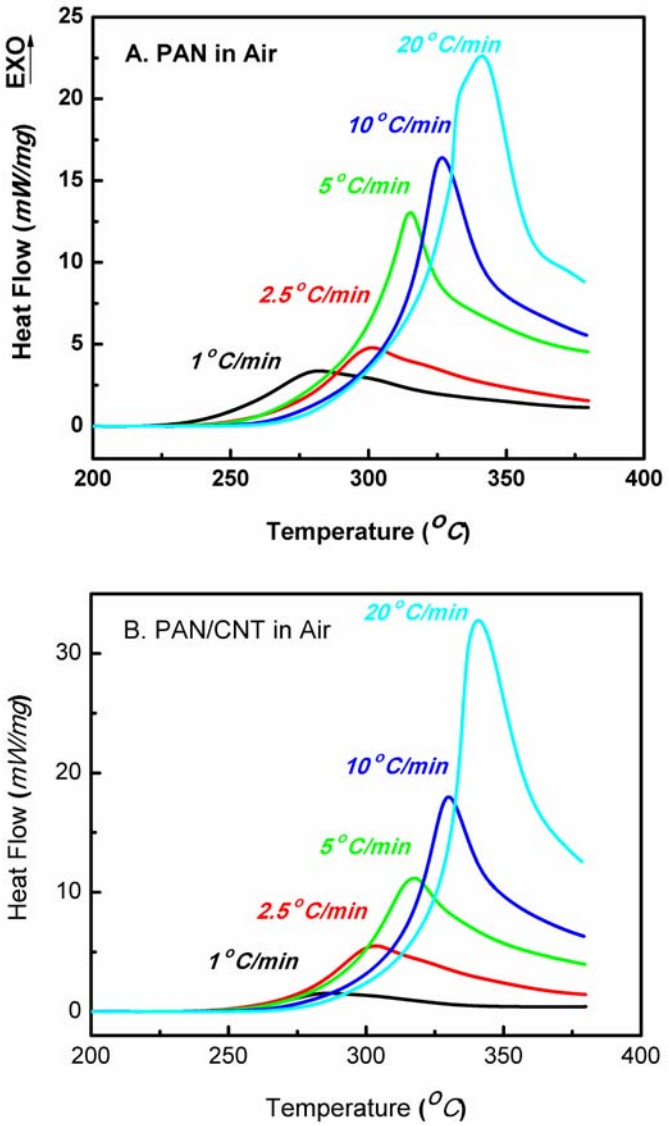

Figure 7. DSC heat flow curves of (A) PAN and (B) PAN/CNT composite precursor fibers at different heating rates in air.

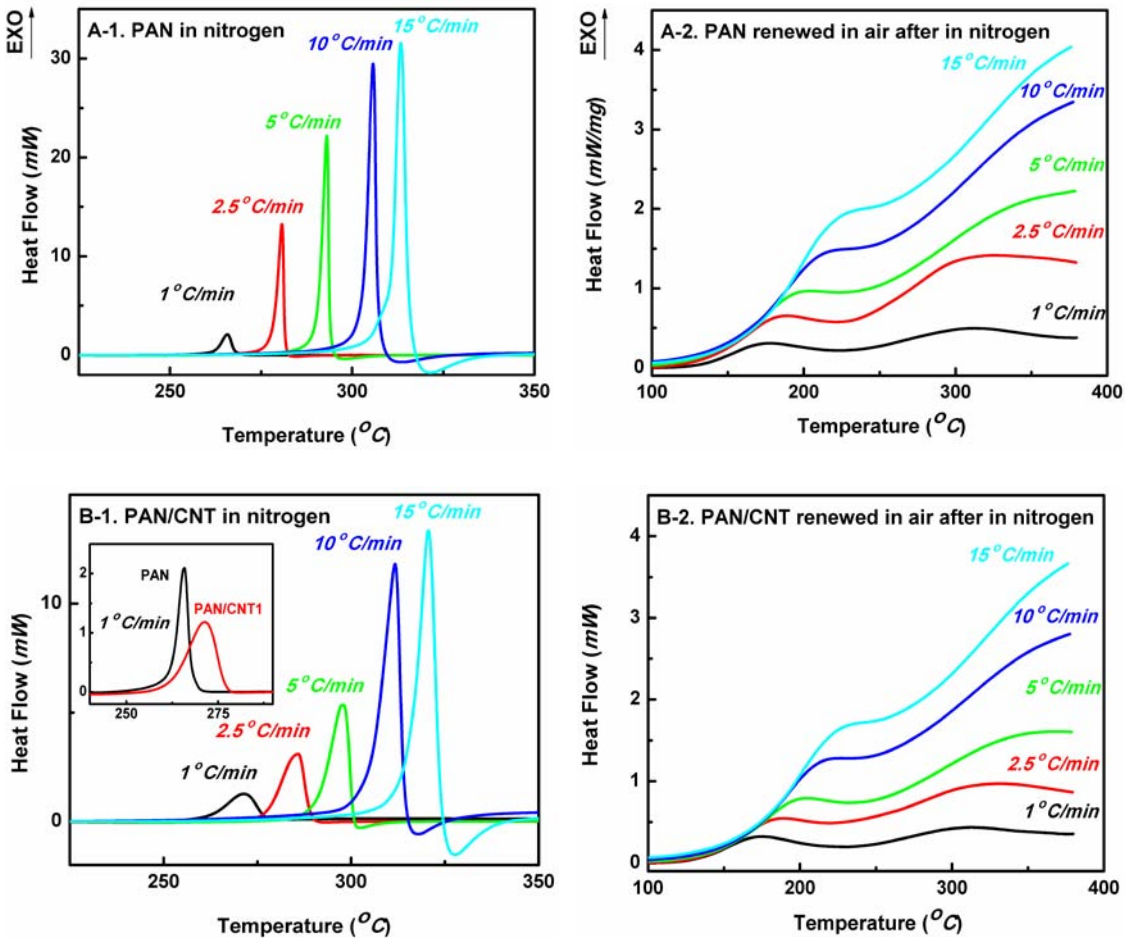

Figure 8. DSC curves of PAN and PAN/CNT precursor fibers stabilized at different heating rates. (A-1) PAN precursor fibers in nitrogen, (A-2) PAN fibers rerun in air after running in nitrogen, (B-1) PAN/CNT precursor fibers in nitrogen, and (B-2) PAN/CNT fibers rerun in air after running in nitrogen.

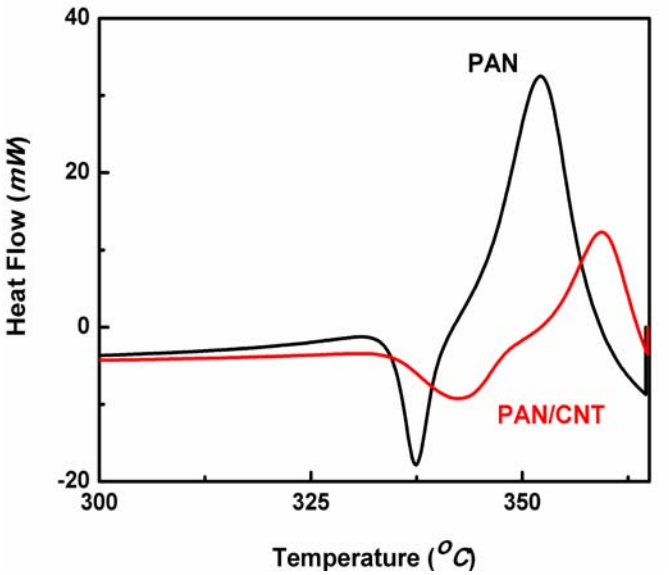

Figure 9. DSC curves of PAN and PAN/CNT precursor fibers heat treated in nitrogen at a heating rate of 60 ^{o}C/min.

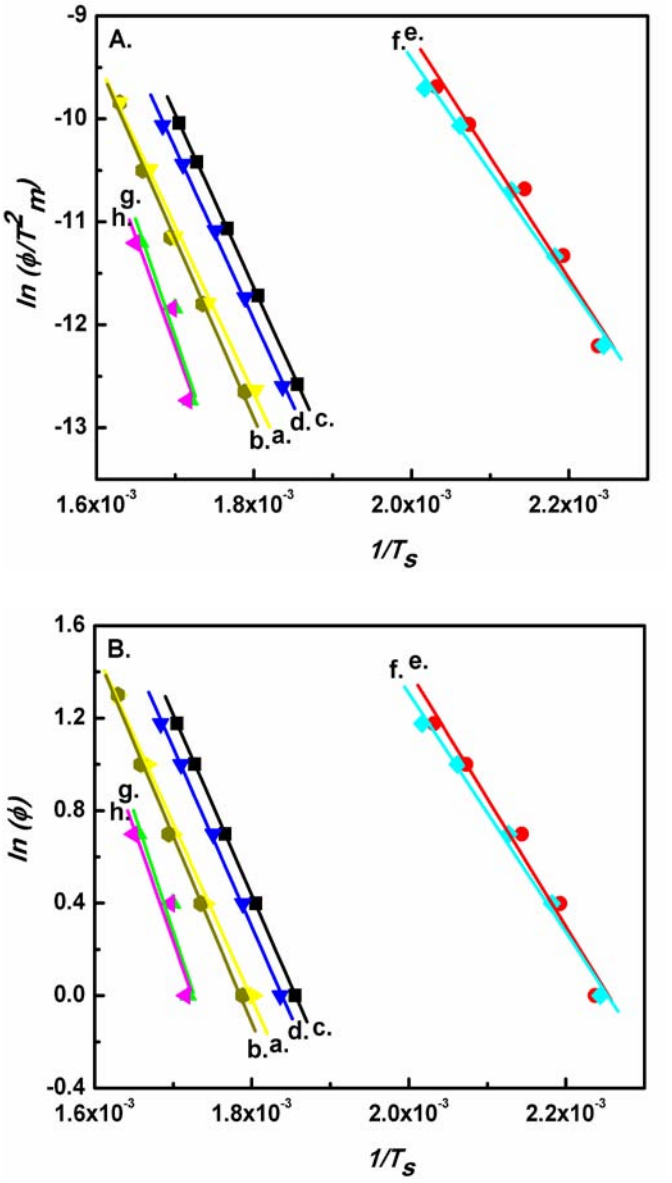

Figure 10. Plots according to (A) Kissinger's equation and (B) Ozawa's equation for a. PAN fibers in air, b. PAN/CNT fibers in air, c. cyclization peak of PAN fibers in nitrogen, d. cyclization peak of PAN/CNT fibers in nitrogen, e. oxidation peak of PAN fibers rerun in air after running in nitrogen, f. oxidation peak of PAN/CNT fibers rerun in air after running in nitrogen g, additional cross-linking peak of PAN fibers rerun in air after running in nitrogen, and h. additional cross-linking peak of PAN/CNT fibers rerun in air after running in nitrogen.

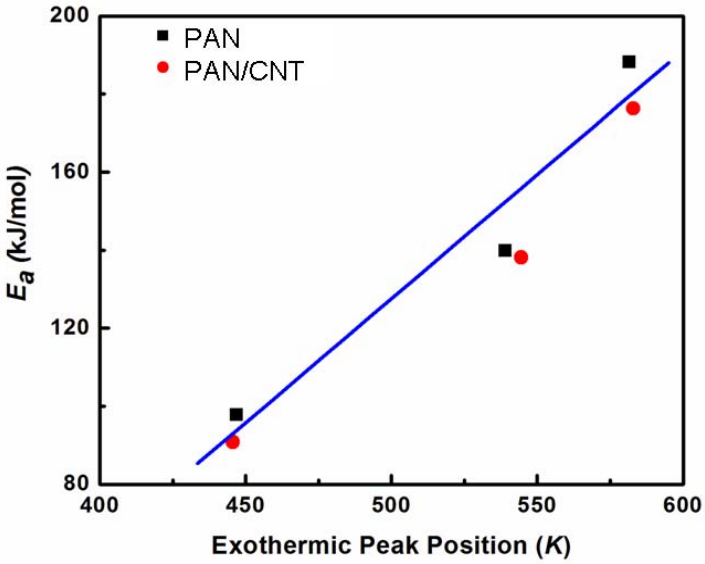

Figure 11. Plot of reaction activation energies versus DSC exothermic peak positions.

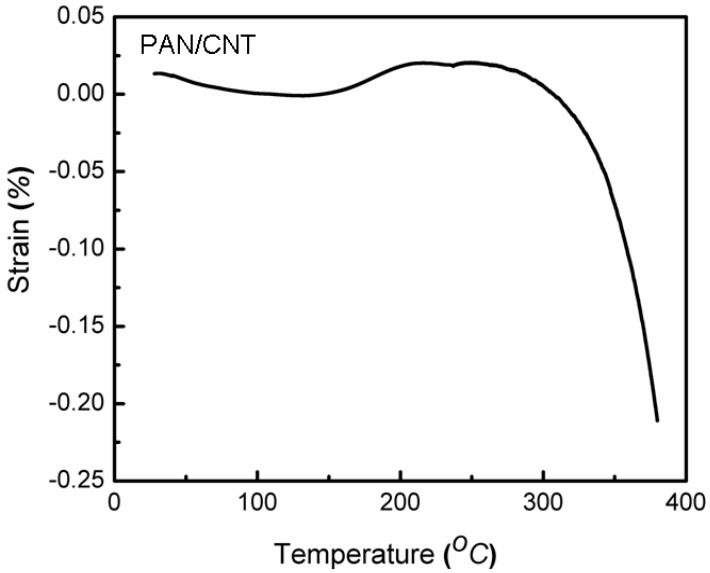

Figure 12. Strain variation curve of PAN/CNT composite fibers in air under 20 MPa at a heating rate of 1 ^{o}C/min. Before the experiment, fiber was pre-stabilized in nitrogen to 320 ^{o}C at a heating rate of 1 ^{o}C/min. Negative strain represents fiber shrinkage.

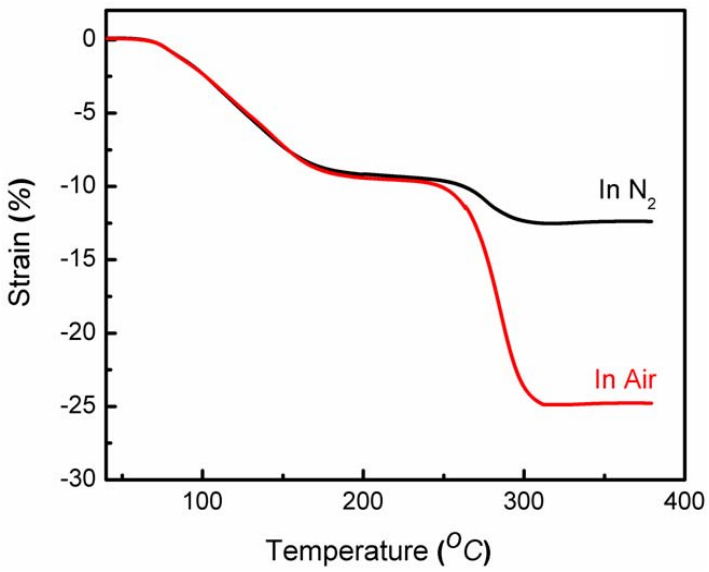

Figure 13. Strain variation curves of PAN/CNT precursor fibers under 4 MPa in air and in nitrogen respectively at a heating rate of 1 ^{o}C/min.

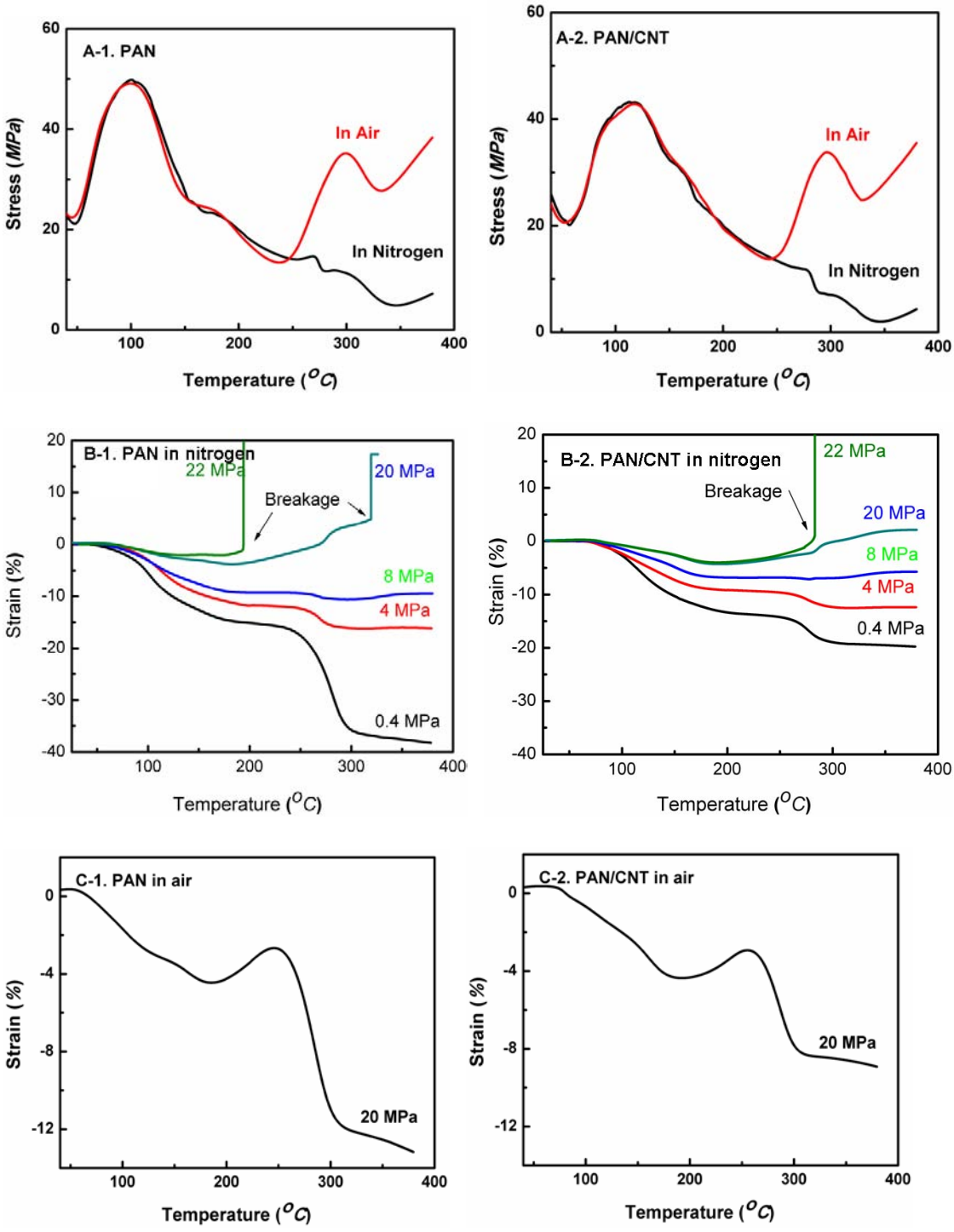

Figure 14. (A-1) and (A-2) are stress variation curves of PAN and PAN/CNT precursor fibers stabilized in air and nitrogen at a constant length mode, respectively, (B-1) and (B-2) are strain variation curves of PAN and PAN/CNT precursor fibers stabilized in nitrogen under various constant pretensions, respectively, and (C-1) and (C-2) are strain variation curves of PAN and PAN/CNT precursor fibers stabilized in air under a constant stress of 20 MPa, respectively.

SECTION IV

Stabilization of Gel-spun Polyacrylonitrile/Carbon Nanotubes Composite Fibers. Part III: Effects of Stabilization Conditions.

Yaodong Liu, Han Gi Chae, Young Ho Choi, Satish Kumar

School of Polymer, Textile & Fiber Engineering, Georgia Institute of Technology
801 Ferst Dr. NW, Atlanta, GA 30324

Abstract

Oxidative stabilization of gel-spun polyacrylonitrile (PAN)/carbon nanotube (CNT) composite fiber has been studied and optimized in batch process. In order to produce the ultimate carbon fibers, the highest tension without breaking fiber during heat treatment should be applied; also, the fiber needs to be further treated at a stabilization temperature over 300 ^{o}C which promotes the additional cross-linking reaction and improves the strength and modulus of resulting carbon fibers. Optimal stabilization time depends on both applied tension and temperature. Various characterization methods such as thermal shrinkage, dynamic mechanical analysis, infrared spectroscopy, and wide angle X-ray diffraction are used to monitor the chemical and structural evolution during stabilization and carbonization. By optimizing stabilization, carbon fiber with strength of 4 GPa and modulus of 286 GPa was obtained at the carbonization temperature of 1100 ^{o}C.

1. Introduction

High strength carbon fiber is an important reinforcement material for high-performance composites [1, 2]. To produce high strength carbon fibers, polyacrylonitrile (PAN) is widely used as a precursor [3]. Previous studies [4, 5] show that addition of carbon nanotubes (CNTs) in PAN precursor fiber significantly improves the strength and modulus of resulting carbon fibers as compared to the carbon fibers prepared from neat PAN precursor fiber. It has been discussed that the addition of CNTs can induce highly ordered graphite structure in its vicinity when fiber is carbonized at a relatively low temperature, 1100 ^{o}C. Thus, PAN/CNT composite precursor fiber is considered to be a promising candidate for the next generation carbon fibers.

In the process of conversion from PAN precursor fiber to carbon fiber, oxidative stabilization which involves complex physical and chemical changes is important for obtaining high-performance carbon fibers [6-8], and needs to be carefully optimized because degradation of PAN may occur during high temperature stabilization. A number of researches have been done on the thermal treatment process of PAN in the last 50 years; however, no consensus exists for the best process conditions of stabilization and carbonization because the stabilization is strongly dependent on the precursor fiber properties, diameter, co-monomer type, and co-monomer content, etc.

For stabilization of PAN fibers in batch process, there are three controllable processing parameters including applied tension, temperature, and residence time. Based on the relationship of temperature and time, there are three possible heat treatment profiles [9] including slow

ramping, isothermal, and stepwise. In the present work, isothermal and stepwise temperature profiles are adopted. Based on the properties of resulting carbon fibers, the effects of different stabilization processing parameters are compared and the best conditions are proposed for composite fiber used in this study. In addition, the relationship between processing parameters and resulting carbon fibers properties will be discussed. Furthermore, for methodological study of stabilization, different characterization methods including shrinkage behavior, dynamic mechanical properties, infrared spectra and X-ray diffraction pattern, are compared to obtain the best processing parameters. Characterization of stabilized fibers can be done in two ways: 1. Real-time monitoring of properties variation during stabilization and 2. Post session characterization - characterization is performed after stabilization. In this study, the relationships between various characterization methods and optimal stabilization time were studied. A new method by monitoring dynamic mechanical properties was used in this study, which can narrow down the optimal stabilization time range.

2. Experimental

Homo-polymer PAN (molecular weight ~ 250,000 g/mol) used in this study was produced by Japan Exlan Co. (Japan). CNT (lot no. XO122UA) containing ~ 1 wt % catalyst was obtained from Unidym Inc. (Houston, TX). Composite fiber contains 1 wt% CNTs with respect to polymer. Spinning solutions preparation and fiber spinning procedures are described elsewhere [10]. For spinning solution, solid content was 150 g/L. 7 holes spinneret was used, and total draw ratio was 13.2. Drawn fibers were dried in vacuum oven at 50 ^{o}C for 2 days to remove residual solvent. The stabilization was carried out in a tube furnace manufactured by Micropyretics Heaters International (Cincinnati, OH). The temperature inside the furnace was measured by a calibrated temperature probe, and is used for the experiment.

Fourier Transformed Infrared spectra were collected using infrared spectrometer (FT IR, Spectrum One, Perkin Elmer Corp.). 128 scans were collected with a resolution of 4 cm^{-1}. Wide angle X-ray diffraction (WAXD) patterns were obtained by Rigaku micromax-002 using CuK_{α} (λ=0.1542 nm) radiation and Rigaku R-axis IV++ detector. Shrinkage behavior and dynamic mechanical properties were obtained by thermo-mechanical analyzer (TMA, TA Q-400) manufactured by TA Instruments-Waters LLC. For dynamic mechanical test, a constant tension of 25 MPa (Stress calculation is based on the diameter of the precursor fiber) was applied, and force amplitude was set to be 4 MPa and frequency was 1 Hz. Mechanical properties of single carbon fiber were tested on RSA III solid analyzer (Rheometric Scientific Co.) at a crosshead speed of 0.1 %/s with a gauge length of 6 mm. Microstructure of carbon fibers was observed on S-800 scanning electron microscope (SEM, Hitachi Com.) at an operating voltage of 10 kV, and cross-section area was calculated using ImageJ image analysis software (NIH).

3. Results and discussion

Table 1 lists the mechanical and structural properties of precursor PAN/CNT fiber. Shrinkage behavior during stabilization was measured by TMA. As reported previously, shrinkage of PAN fiber can be divided into entropic shrinkage and reaction shrinkage. In this study, entropic relaxation was allowed by heating the fiber from room temperature to 200 ^{o}C under 4 MPa of tension at a heating rate of 5 ^{o}C/min; then, sample was quickly raised to desired temperature (typically in less than 40 sec), and reaction shrinkage was monitored. Figure 1

shows the isothermal reaction shrinkage curves obtained both in nitrogen and air at various temperatures. As can be seen from Figure 1(A_1) and (B_1), stabilization temperature has little effects on the final reaction shrinkages for the fiber stabilized in nitrogen; whereas, in air, lower temperature results in larger reaction shrinkage. Regardless of stabilization temperature, reaction shrinkage occurring in air is larger than that in nitrogen, and this is consistent with previous literature reports [11, 12]. The different shrinkage behaviors in different gas environments are caused by different cyclization mechanisms [13]. The cyclization reaction in air involves more inter-molecular reactions such as oxidation and cross-linking as compared to that in nitrogen. Figure 1(B_2) shows derivatives of reaction shrinkage-time curves obtained in air and nitrogen at 255 ^{o}C. While the shrinkage in nitrogen slowed down with time, there was an acceleration period (~ 5 min) for reaction shrinkage in air, and shrinkage rate became much faster in air as compared with sample in nitrogen. After ~ 60 min, shrinkage in nitrogen was completed; however, shrinkage in air required longer time to be completed.

The reaction shrinkage was found [14, 15] to be correlated with cyclization reaction, and could be used to calculate the reaction activation energy. Reaction shrinkage was fitted by the equation shown below and one example of fitting curve is shown in Figure 1(A_2).

$$CS = L(1 - e^{-bt})$$ L: Final shrinkage; b: Exponential parameter; t: time.

The exponential parameter b has an Arrhenius-type of dependence with absolute reaction temperature, and can be used to calculate the reaction activation energy which is listed in Table 2. The calculated values are very close to the cyclization reaction activation energy calculated from DSC data [13], 138.5 kJ/mol. Also, it should be noted that the shrinkage curve fitting for samples stabilized in air has a R^2~0.96, worse than that for the samples stabilized in nitrogen, R^2>0.99. The reason is probably that stabilization in air involves more complex reactions than that in nitrogen. Since reaction shrinkage has direct relationship with stabilization reaction, it is possible to be used as criteria to find optimal residence time. The stabilization times that fibers reached the maximum reaction shrinkage and when no more reaction shrinkage occurred are listed in Table 2. From the Table 2, it can be noted that fibers stabilized in air needs longer time than that in nitrogen to complete reactions. For stabilization reactions in air, oxidative reaction happens after cyclization reaction [13]. Oxidation reaction can be limited either by cyclization reaction or oxygen diffusion. Since the stabilization reactions in air lasted longer than in nitrogen, it suggests that the stabilization in air is limited by oxygen diffusion. In the late stage of stabilization, reaction shrinkage in air changes slowly along with the stabilization time, which makes it difficult to get the accurate time for the end of reactions.

The curing process of thermosetting materials has been widely studied by investigating dynamic mechanical properties [16, 17]. By comparing the transition of storage modulus and loss tangent, gelation time can be obtained and chemical conversion can be calculated. During the oxidative stabilization of PAN, cyclization and other reactions make fiber molecules cyclized and cross-linked. Changes of visco-elastic properties during oxidative stabilization have been reported and were used to compare the influence of precursor polymer [18]. Storage and loss modulus were recorded by TMA as a function of stabilization time (Figure 2). Same temperature profile as the shrinkage experiments was used to monitor the variation of dynamic mechanical properties. During the isothermal stabilization, the storage modulus continuously increased and then reached a plateau; whereas, loss modulus reached its maximum value and then slowly decreased. From previous study [13], the sequence of stabilization reactions for homopolymer

PAN is known to be in the order of cyclization, oxidation, and additional cross-linking. Different stabilization reactions showed different effects on the dynamic mechanical properties. The cyclization reaction increased storage modulus, and destruction of PAN crystals leads to increase of loss modulus. The additional cross-linking reaction led to further improvement in storage modulus and decrease in loss modulus. The transition times defined as the time that either storage or loss modulus reaches the maximum value are listed in Table 3. The transition time of storage modulus indicates all stabilization reactions are completed; however, it may lead to over-stabilization since reaction will continue happen during the heating stage of carbonization process, including thermal degradation. The transition time of loss modulus indicates that oxidative reaction is almost completed and cross-linking reaction becomes dominant. Therefore, the optimal stabilization time may be between the above two transition times.

Based on the reaction shrinkage behavior and dynamic mechanical properties, PAN/CNT composite fibers were first stabilized in air, and then carbonized in argon to produce carbon fiber. In this study, 255 ^{o}C was used as stabilization temperature, since the optimal stabilization time determined by shrinkage and dynamic mechanical property experiments lies in the range of 240 ~ 420 minutes, and the storage modulus stabilized at 255 ^{o}C was the highest among all the other stabilized fibers at different temperatures. For carbonization, temperature was raised from room temperature to 1100 ^{o}C at a heating rate of 5 ^{o}C/min, and then sample was isothermally carbonized for 10 min. During stabilization and carbonization, constant stresses of 35 MPa and 4 MPa were applied respectively on fiber bundle by a pair of graphite clamps.

The chemical and physical structure changes of stabilized fiber were characterized by FTIR and WAXD. Figure 3 shows the infrared spectra of stabilized fibers. Along increasing stabilization time, the peak intensity of nitrile band (at 2243 cm^{-1}) continuously decreases and becomes broad, and a broad peak appeared and increased at around 1595 cm^{-1} which is caused by the formation of ladder polymer. The stabilization index (E_s) [19] is defined as the ratio of peak height of 1595 cm^{-1} over peak height of 2243 cm^{-1}, which is proportional to the ratio of ladder polymer over residual nitrile group (Figure 3B). It can be found that E_s continuously increases with stabilization time. As mentioned earlier [5, 20-22], nitrile band becomes broad during stabilization, which is caused by the formation of β-amino nitril at 2194 cm^{-1} and conjugated nitrile at 2218 cm^{-1}. Along with the stabilization, unreacted nitrile reduces, and β-amino nitrile and conjugated nitrile increases, which leads to the changes of nitrile band shape and position. The dependence of peak position of nitrile band on time is shown in Figure 3B. After fiber was stabilized for over 200 minutes, a transition of the peak position of nitrile band can be found. Very low fraction of unreacted nitrile still remained even after fiber was stabilized for 300 minutes, since these nitrile groups are isolated and hard to form ladder polymer.

The ladder polymer formation of stabilized fibers was characterized by WAXD. In the integrated WAXD patterns shown in Figure 4A, the diffraction peak at $2\theta=16.7^{o}$ corresponding to the (200, 110) planes of PAN crystal decreases during stabilization, and almost disappears after thermal treatment for 260 minutes at 255 ^{o}C. Based on the change of intensity of PAN (200, 110) peak, stabilization index (I_s) is calculated [23] and shown in Figure 4B.

$I_s = \frac{I_0 - I}{I_0}$ I_0: Intensity of precursor fiber; I: Intensity of stabilized fiber.

The stabilization index I_s increases fast at first, then slows down. After fiber was stabilized at 255 ^{o}C for 260 minutes, I_s is more than 0.9. The increase of peak intensity at $2\theta \sim 25.5^{o}$ is due to the formation of cyclized ladder structure. The orientation of ladder polymer is also calculated from the azimuthal scan and is shown in Figure 4B. The Herman's orientation

factor of ladder polymer increases during stabilization, reaches the maximum value at 260 minutes, and then decreases that could be because of the degradation by over-stabilization.

The mechanical properties of resulting carbon fibers are listed in Table 4. The stabilization time has significant effects on the final properties of resulting carbon fiber. The best stabilization time is 260 minutes at 255 ^{o}C. Either longer or shorter stabilization time reduces the strength of resulting carbon fibers. The modulus of resulting carbon fiber increases with increasing stabilization time, and then becomes stable. The variations of mechanical properties of ultimate carbon fiber are in agreement with the structural analysis results of the stabilized fibers.

It has been reported that the tension applied during thermal treatment of carbon fibers is very important for the mechanical properties of resulting carbon fibers [3, 6, 24, 25]. In the current experiment, the applied tension during stabilization and carbonization was kept constant at 35 MPa. The mechanical properties of resulting carbon fiber are listed in Table 5. The average fiber diameter was calculated from the fiber cross-section images observed under SEM. The applied tension during carbonization shows strong effects on the final properties of resulting carbon fibers. While the tension was increased from 4 MPa to 35 MPa, the strength of the resulting carbon fiber increased from 1.6 GPa to 3.6 GPa. Stabilization time is very important for the final properties of carbon fibers. In addition, it should also be noted that the residence time during stabilization is very important to the resulting carbon fiber properties. As listed in Table 5, we changed stabilization time in 15 min steps from 230 min to 290 min. 15 min difference in stabilization time, reduced the tensile strength by up to 10% as compared to that of the best sample stabilized for 260 min. Figure 5 shows the images of cross-sectional area of stabilized fibers and resulting carbon fibers cut by a sharp razor blade. Fibrous structure can be found and it shows very uniform distribution through the whole cross-section, which indicates that carbon nanotubes are well dispersed in PAN matrix.

To further explore the effects of applied tension, the constant stress during stabilization and carbonization was increased from 35 MPa to 46 MPa. The mechanical properties of resulting carbon fibers are listed in Table 6. Comparing the best stabilization time under different tensions in Table 5 and Table 6, it can be found that higher stress reduce the optimal stabilization time. The shrinkage curves of fibers under different tensions during thermal stabilization detected by TMA are shown in Figure 6. Higher stress leads to less shrinkage, or even stretches the fiber. In case of stabilized fiber using 35 MPa, the fiber is stretched to ~ 4 %, and the fiber is even stretched to over 20 % after stabilization at the pretension of 46 MPa. Assuming poisson's ratio is 0.5, the diameter of stabilized fiber under 46 MPa will be ~ 8 % smaller than that of the stabilized fiber under 35 MPa. The smaller diameter fiber reduces oxygen diffusion distance to the center of fiber, and ultimately reduces diffusion time. Since the stabilization reaction is limited by oxygen diffusion, the higher applied stress may expedite the stabilization reaction.

Herman's orientation factors of stabilized fibers and carbonized fibers were calculated from azimuthal scans, and they were found to slightly increase from 0.69 to 0.70 and 0.88 to 0.90 respectively, when the applied stress is increased from 35 MPa to 46 MPa. The modulus of resulting carbon fiber with optimal stabilization time is improved from 245 GPa to 289 GPa. The higher orientation of carbon structure leads to higher modulus of resulting carbon fibers. The strength of resulting carbon fibers is also improved from 3.60 GPa to 4.03 GPa. For precursor fiber used in this study, the 46 MPa is the highest pretension that can be applied during thermal treatment without breaking the fiber. Thus, to obtain the best properties of resulting carbon fibers, the maximum tension should be applied during heating treatment. Literature [26] reported that not the highest tension but a suitable tension showed the best effects on the mechanical

properties of resulting carbon fibers, while a contradict conclusion is drawn in this study. The reason is that the stabilization time which is affected by applied tension was not considered in the previous literature, and a fixed stabilization time was used. As shown in Table 5 and Table 6, if the stabilization time is fixed at 260 minutes, the tensile properties of resulting carbon fiber will be worse when applied stress is improved from 35 MPa to 46 MPa; however, the optimal stabilization time depends on both applied tension and temperature, and must be considered.

In our previous study, the different stabilization reactions were separated by using nitrogen and air as gas environments subsequently [13]. Same method is used here and the DSC curves are shown in Figure 7. When the fiber is re-heated in air after in nitrogen, two exothermic peaks related to oxidation reaction and additional cross-linking reaction respectively appear. It has been found that additional cross-linking reaction happens at a temperature over 300 ^{o}C [27, 28] although reactions were not clearly separated. If the additional cross-linking reaction is enhanced, will it improve the final mechanical properties of resulting carbon fiber? To answer this question, after fiber was isothermally stabilized at 255 ^{o}C for 120 minutes, then temperature was raised to 320 ^{o}C at a rate of 5 ^{o}C/min, and fiber was isothermally stabilized for various times. 320 ^{o}C is the exothermic peak temperature of additional cross-linking reaction in DSC curve (Figure 7, curve B). Stabilized fibers were subsequently carbonized at 1100 ^{o}C. The dynamic mechanical properties measured during stabilization are shown in Figure 8. When temperature was raised to 320 ^{o}C, the transition times of loss modulus and storage modulus are 10 min and 45 min respectively for stabilization at 320 ^{o}C. The residence time at 320 ^{o}C was changed from 15 min to 35 min. The mechanical properties of resulting carbon fibers are listed in Table 7. Comparing the data in Table 4 and Table 6, total stabilization time is reduced while stabilization temperature is increased. Final properties of resulting carbon fibers become much more sensitive to stabilization time when stabilization temperature is higher. Comparing the fibers further stabilized at 320 ^{o}C with the fiber stabilized just at 255 ^{o}C, the best tensile strength is improved from 3.60 GPa to 3.97 GPa, and tensile modulus is improved from 245 GPa to 286 GPa. When the fibers are further stabilized at a high temperature, the additional cross-linking reaction is enhanced, which significantly improves the tensile modulus of resulting carbon fibers while the elongation at break remained at the same level.

The Integrated XRD curves of stabilized fibers are shown in Figure 9. PAN (200, 110) diffraction peak completely disappeared. It was found that the peak from aromatic structure slightly shift its peak position from 26.05 to 26.12 when stabilization temperature was raised from 255 ^{o}C to 320 ^{o}C, indicating that additional cross-linking reaction makes stabilized fiber more compact. Azimuthal scans of stabilized fibers are also shown in Figure 10. Very sharp peaks can be found for both azimuthal curves, which come from highly ordered ladder polymer induced by addition of CNTs [4]. Using the same curve fitting method described elsewhere [4], the contributions from highly ordered regions and matrix can be deconvoluted and fitting data is listed in Table 8. The Herman's orientation factor for fiber further stabilized at 320 ^{o}C is even slightly lower than fibers stabilized at 255 ^{o}C only; however, fraction of highly ordered region is improved from 2.5 % to 3.3 %. The Herman's orientation factors for carbonized fibers are 0.88 and 0.87 for fiber stabilized at 255 ^{o}C only and fibers further stabilized at 320 ^{o}C, respectively. The improvement of modulus of resulting carbon fibers with elevated stabilization temperature at 320 ^{o}C is not from better orientation of resulting carbon structure, but may be from the higher volume fraction of highly ordered phase caused by additional cross-linking reactions. Raman spectra of stabilized fiber and carbonized fibers are shown in Figure 11. For stabilized fibers, the intensity of peak at 1585 cm^{-1} increased when fibers were further stabilized at 320 ^{o}C. This peak

comes from tangential vibration of graphitic structure (G-band) [4], and indicates that additional cross-linking reaction at 320 ^{o}C leads to the formation of 2-dimentional graphite-like structure, which is not found for fibers stabilized at a relatively low temperature at 255 ^{o}C. Raman spectra of carbonized fibers show similar result. If fibers are further stabilized at 320 ^{o}C to facilitate additional cross-linking, the resulting carbon fibers contain more graphite-like regions, leading to the improvement in tensile modulus.

Fiber further stabilized at 320 ^{o}C for 22.5 minutes under a stress of 35 MPa, carbonization was carried out at various temperatures (1100, 1300, and 1500 ^{o}C). Mechanical properties of resulting carbon fibers are listed in Table 9. While carbonization temperature was increased, fiber diameter and elongation at break were reduced whereas modulus was improved. The higher carbonization temperature (1300 ^{o}C) marginally improves the strength of resulting carbon fibers. Then a sudden decline of tensile strength and strain to failure can be found at 1500 ^{o}C. The images of carbon fiber surfaces observed by SEM are shown in Figure 12. For fiber carbonized at 1100 ^{o}C, fiber surface is very smooth. When carbonization temperature is increased to 1300 ^{o}C, surface of carbon fiber becomes rough; particle-like structure with a diameter of tens of nanometers begins to appear. When carbonization temperature is increased to 1500 ^{o}C, porous structure can be found on the fiber surface with dimensions of about 50 nm. These surface defects would strongly affect the mechanical properties of the resulting carbon fiber. Since all the processing done in this study was based on batch processing, the exposure time for carbonization is typically more than 4 hr at above 1000 ^{o}C. As compared to the industrial carbon fiber, this exposure time is very long and it is conceivable that possible thermal degradation may occur during carbonization. Additionally, as pointed out by Watt [29], the decrease in strength at 1500 ^{o}C is caused by impurities such as foreign particles coming from environment during fiber spinning and heat treatment, which results in defects during carbonization process.

4. Conclusion

To produce carbon fibers with ultimate mechanical properties, the three controllable batch process parameters including temperature, applied tension and stabilization time were optimized and carefully controlled. The highest tension without breaking the fiber should be applied during stabilization and carbonization. To obtain the optimal stabilization time, a new method by monitoring changes in dynamic mechanical properties is suitable to narrow down stabilization time range. Additionally, further stabilization above 300 ^{o}C improves ultimate carbon fiber properties. The optimal stabilization time depends on both applied tension and temperature. Higher applied stress will reduce stabilization time. By optimizing thermal treatment, carbon fibers with an average strength of as high as 4 GPa were obtained at the carbonization temperature of 1100 ^{o}C.

References

[1] Chand S. Carbon fibers for composites. Journal of Materials Science. 2000;35(6):1303-13.

[2] Minus ML, Kumar S. The processing, properties, and structure of carbon fibers. Jom. 2005 Feb;57(2):52-8.

[3] Deurbergue A, Oberlin A. Stabilization and carbonization of pan-based carbon fibers as related to mechanical properties. Carbon. 1991;29(4-5):621-8.

[4] Chae HG, Choi YH, Minus ML, Kumar S. Carbon nanotube reinforced small diameter polyacrylonitrile based carbon fiber. Composites Science and Technology. 2009;69(3-4):406-13.

[5] Chae HG, Minus ML, Rasheed A, Kumar S. Stabilization and carbonization of gel spun polyacrylonitrile/single wall carbon nanotube composite fibers. Polymer. 2007 Jun;48(13):3781-9.

[6] Dalton S, Heatley F, Budd PM. Thermal stabilization of polyacrylonitrile fibres. Polymer. 1999;40(20):5531-43.

[7] Tse-Hao Ko H-YTC-HL. Thermal stabilization of polyacrylonitrile fibers. Journal of Applied Polymer Science. 1988;35(3):631-40.

[8] Rahaman MSA, Ismail AF, Mustafa A. A review of heat treatment on polyacrylonitrile fiber. Polymer Degradation and Stability. 2007 Aug;92(8):1421-32.

[9] Fitzer E, Frohs W, Heine M. Optimization of stabilization and carbonization treatment of PAN fibres and structural characterization of the resulting carbon fibres. Carbon. 1986;24(4):387-95.

[10] Chae HG, Minus ML, Kumar S. Oriented and exfoliated single wall carbon nanotubes in polyacrylonitrile. Polymer. 2006;47(10):3494-504.

[11] Gupta A, Harrison IR. New aspects in the oxidative stabilization of pan-based carbon fibers. Carbon. 1996;34(11):1427-45.

[12] Bahl OP, Manocha LM. Shrinkage behaviour of polyacrylonitrile during thermal treatment. Angewandte Makromolekulare Chemie. 1975;48(1):145-59.

[13] Liu Y, Chae HG, Kumar S. Kinetics and effects of different chemical reactions in stabilization of polyacrylonitrile fibers. Submitted. 2009.

[14] Johannis Simitzis SS. Correlation of chemical shrinkage of polyacrylonitrile fibres with kinetics of cyclization. Polymer International. 2008;57(1):99-105.

[15] Hou Y, Sun T, Wang H, Wu D. A new method for the kinetic study of cyclization reaction during stabilization of polyacrylonitrile fibers. Journal of Materials Science. 2008;43(14):4910-4.

[16] Ramis X, Cadenato A, Morancho JM, Salla JM. Curing of a thermosetting powder coating by means of DMTA, TMA and DSC. Polymer. 2003;44(7):2067-79.

[17] Cadenato A, Salla JM, Ramis X, Morancho JM, Marroyo LM, Martin JL. Determination of gel and vitrification times of thermoset curing process by means of TMA, DMTA and DSC techniques - TTT diagram. 1997: John Wiley & Sons Ltd; 1997. p. 269-79.

[18] Suresh KI, Thomas KS, Rao BS, Nair CPR. Viscoelastic properties of polyacrylonitrile terpolymers during thermo-oxidative stabilization (cyclization). Polymers for Advanced Technologies. 2008;19(7):831-7.

[19] Ouyang Q, Cheng L, Wang H, Li K. Mechanism and kinetics of the stabilization reactions of itaconic acid-modified polyacrylonitrile. Polymer Degradation and Stability. 2008;93(8):1415-21.

[20] Fochler HS, Mooney JR, Ball LE, Boyer RD, Grasselli JG. Infrared and NMR spectroscopic studies of the thermal degradation of polyacrylonitrile. Spectrochimica Acta Part A: Molecular Spectroscopy. 1985;41(1-2):271-8.
[21] Sivy GT, Gordon IB, Coleman MM. Studies of the degradation of copolymers of acrylonitrile and acrylamide in air at 200°C. Speculations on the role of the preoxidation step in carbon fiber formation. Carbon. 1983;21(6):573-8.
[22] Shimada I, Takahagi T, Fukuhara M, Morita K, Ishitani A. FT-IR study of the stabilization reaction of polyacrylonitrile in the production of carbon fibers. Journal of Polymer Science Part A: Polymer Chemistry. 1986;24(8):1989-95.
[23] Yu M-J, Bai Y-J, Wang C-G, Xu Y, Guo P-Z. A new method for the evaluation of stabilization index of polyacrylonitrile fibers. Materials Letters. 2007;61(11-12):2292-4.
[24] Yu MJ, Wang CG, Bai YJ, Wang YX, Zhu B. Evolution of tension during the thermal stabilization of polyacrylonitrile fibers under different parameters. Journal of Applied Polymer Science. 2006;102(6):5500-6.
[25] Wu GP, Lu CX, Ling LC, Hao AM, He F. Influence of tension on the oxidative stabilization process of polyacrylonitrile fibers. Journal of Applied Polymer Science. 2005;96(4):1029-34.
[26] Bahl OP, Mathur RB. Effect of load on the mechanical-properties of carbon-fibers from PAN precursor. Fibre Science & Technology. 1979;12(1):31-9.
[27] Gupta A, Harrison IR. New aspects in the oxidative stabilization of PAN-based carbon fibers: II. Carbon. 1997;35(6):809-18.
[28] Mittal J, Bahl OP, Mathur RB, Sandle NK. IR studies of PAN fibres thermally stabilized at elevated temperatures. Carbon. 1994;32(6):1133-6.
[29] Moreton R, Watt W. Tensile strengths of carbon-fibers. Nature. 1974;247(5440):360-1.

Table 1. Mechanical and structural properties of PAN/CNT precursor fiber.

	PAN/CNT fiber
Tensile strength (GPa)	0.83 ± 0.09
Tensile modulus (GPa)	23.8 ± 2.4
Strain to failure (%)	6.6 ± 0.6
Diameter (μm)	7.4
f_{PAN} *	0.86
PAN crystallinity (%)	60
PAN crystal size (nm)**	9.5

* *f*: Herman's orientation factor is calculated from azimuthal scan of PAN (110, 200) diffraction peak. **PAN crystal size is determined from (110,200) reflection, using Scherrer's equation.

Table 2. Residence time and reaction activation energy from reaction shrinkage data.

Environment	Transition time (min)*					Activation energy (kJ/mol)
	225 °C†	240 °C†	255 °C†	270 °C†	285 °C†	
Nitrogen	600	240	130	30	10	151
Air	800	420	240	120	30	142

* Transition time is defined as the time when reaction shrinkage reaches the maximum value.
† Fibers are isothermally stabilized at each temperature.

Table 3. Transition times obtained from dynamic mechanical properties during stabilization in air.

	Transition time (min)*				
	225 °C	240 °C	255 °C	270 °C	285 °C
Loss modulus	820	510	260	120	70
Storage modulus	>900	700	420	270	190

* Transition time is defined as the time that either storage or loss modulus reached the maximum value.

Table 4. Mechanical properties of resulting carbon fibers after stabilized at 255 ^{o}C under 35 MPa with various stabilization times. Carbonization was carried out at 1100 ^{o}C using 4 MPa of pretenstion. Fiber diameter was about 4.7 μm.

Stabilization time (min)	Tensile strength (GPa)	Tensile modulus (GPa)	Strain to failure (%)
19	0.79 ± 0.10	134 ± 11	0.60 ± 0.09
57	0.85 ± 0.08	173 ± 16	0.49 ± 0.13
130	1.05 ± 0.11	188 ± 12	0.57 ± 0.08
200	1.34 ± 0.12	197 ± 23	0.67 ± 0.11
260	1.58 ± 0.14	204 ± 16	0.80 ± 0.09
320	1.48 ± 0.09	207 ± 12	0.75 ± 0.12

Table 5. Mechanical properties of resulting carbon fibers after stabilized at 255 ^{o}C with various stabilization times. Carbonization was carried out at 1100 ^{o}C using 35 MPa of pretenstion. Fiber diameter was about 4.5 μm.

Stabilization time (min)	Tensile strength (GPa)	Tensile modulus (GPa)	Strain to failure (%)
230	2.55 ± 0.53	214 ± 34	1.16 ± 0.13
245	3.24 ± 0.43	246 ± 22	1.20 ± 0.13
260	3.60 ± 0.40	245 ± 19	1.47 ± 0.25
275	3.17 ± 0.50	246 ± 24	1.24 ± 0.16
290	2.74 ± 0.42	225 ± 34	1.17 ± 0.24

Table 6. Mechanical properties of resulting carbon fibers after stabilized at 255 ^{o}C with various stabilization time. Carbonization was carried out at 1100 ^{o}C using 46 MPa of pretenstion. Fiber diameter was about 4.4 μm.

Stabilization time (min)	Tensile strength (GPa)	Tensile modulus (GPa)	Strain to failure (%)
200	3.10 ± 0.42	266 ± 16	1.17 ± 0.12
215	3.78 ± 0.51	271 ± 35	1.33 ± 0.14
230	4.03 ± 0.46	289 ± 32	1.40 ± 0.13
245	3.83 ± 0.47	291 ± 32	1.34 ± 0.16
260	3.02 ± 0.57	256 ± 42	1.20 ± 0.13

Table 7. Mechanical properties of resulting carbon fibers after stabilized at 255 ^{o}C for 120 minutes, then at 320 ^{o} for various stabilization times. Carbonization was carried out at 1100 ^{o}C using 35 MPa of pretenstion. Fiber diameter was about 4.4 μm.

Stabilization time (min)	Tensile strength (GPa)	Tensile modulus (GPa)	Strain to failure (%)
15	3.17 ± 0.63	282 ± 29	1.14 ± 0.20
20	3.24 ± 0.43	294 ± 23	1.24 ± 0.14
22.5	3.97 ± 0.42	286 ± 31	1.42 ± 0.15
25	3.74 ± 0.50	267 ± 32	1.34 ± 0.14
35	2.86 ± 0.62	262 ± 30	1.08 ± 0.10

Table 8. WAXD analysis results of azimuthal scans for the stabilized fibers.

Stabilization conditions	$f_{Overall}$	Highly ordered region		Matrix	
		f	Area (%)	f	Area (%)
At 255 ^{o}C for 260 min	0.69	0.95	2.5	0.68	97.5
At 255 ^{o}C for 120 min, then 320 ^{o}C for 22.5 min	0.68	0.94	3.3	0.67	96.7

Table 9. Mechanical properties of resulting carbon fibers after stabilized at 255 ^{o}C for 120 minutes, then at 320 ^{o} for 2.25 minutes and carbonized at various temperatures using 35 MPa of pretension.

Temp.$_{Carbonization}$ (^{o}C)	Diameter (μm)	Tensile strength (GPa)	Tensile modulus (GPa)	Strain to failure (%)
1100	4.4	3.97 ± 0.42	286 ± 31	1.42 ± 0.15
1300	4.1	4.09 ± 0.53	324 ± 32	1.25 ± 0.15
1500	3.7	2.78 ± 0.41	352 ± 38	0.86 ± 0.14

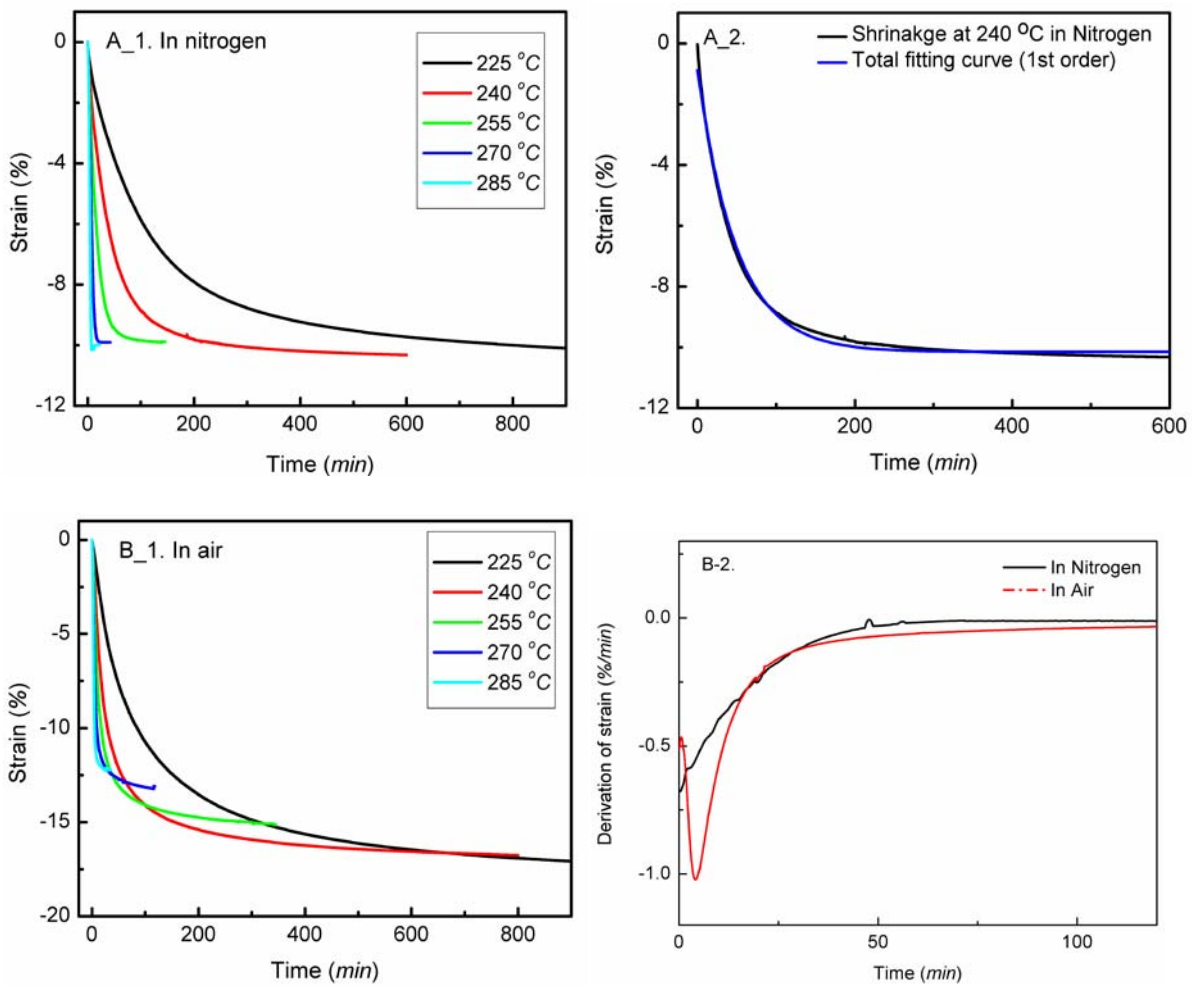

Figure 1. Chemical reaction shrinkage behavior of PAN/CNT composite fiber isothermally stabilized at various temperatures under a constant stress of 4 MPa. (A_1) in nitrogen, (A_2) comparison of experimental and fitting results. Curve fitting conducted using exponentially decaying function as described in the text, (B_1) in air, and (B_2) derivatives of strain with time for stabilizations at 255 ^{o}C in air and nitrogen.

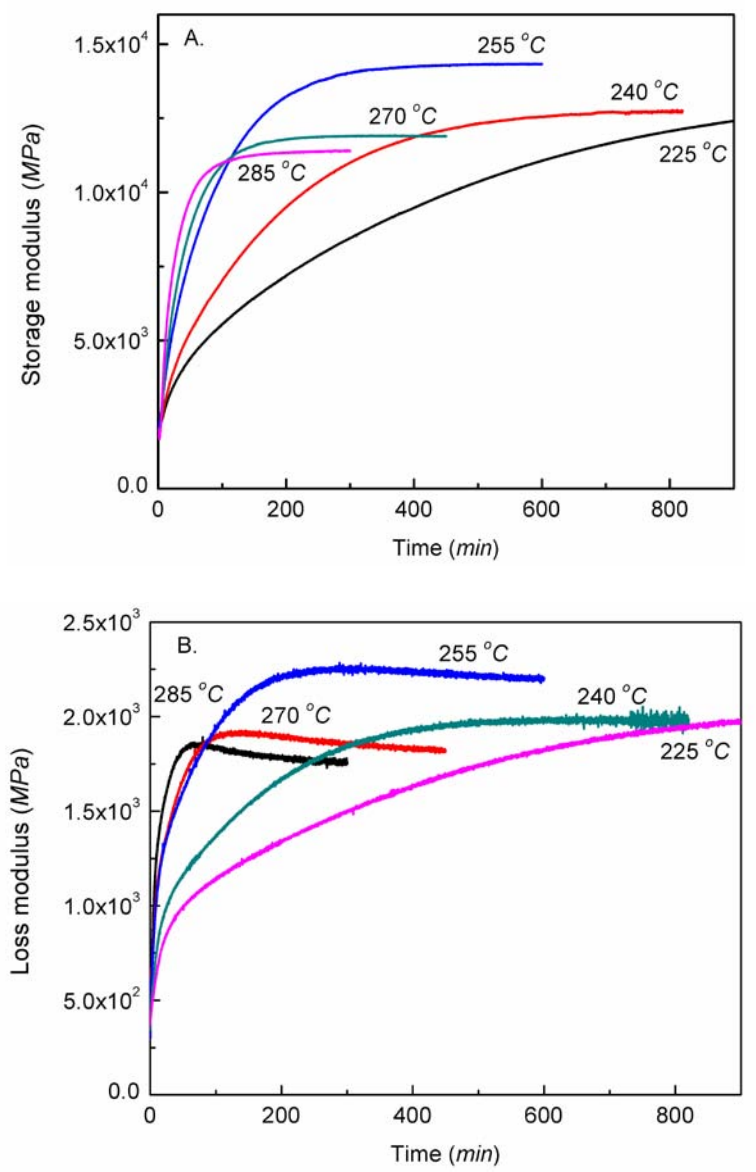

Figure 2. Dynamic mechanical behavior of fiber isothermally stabilized at different temperatures under air. (A) Storage modulus and (B) loss modulus.

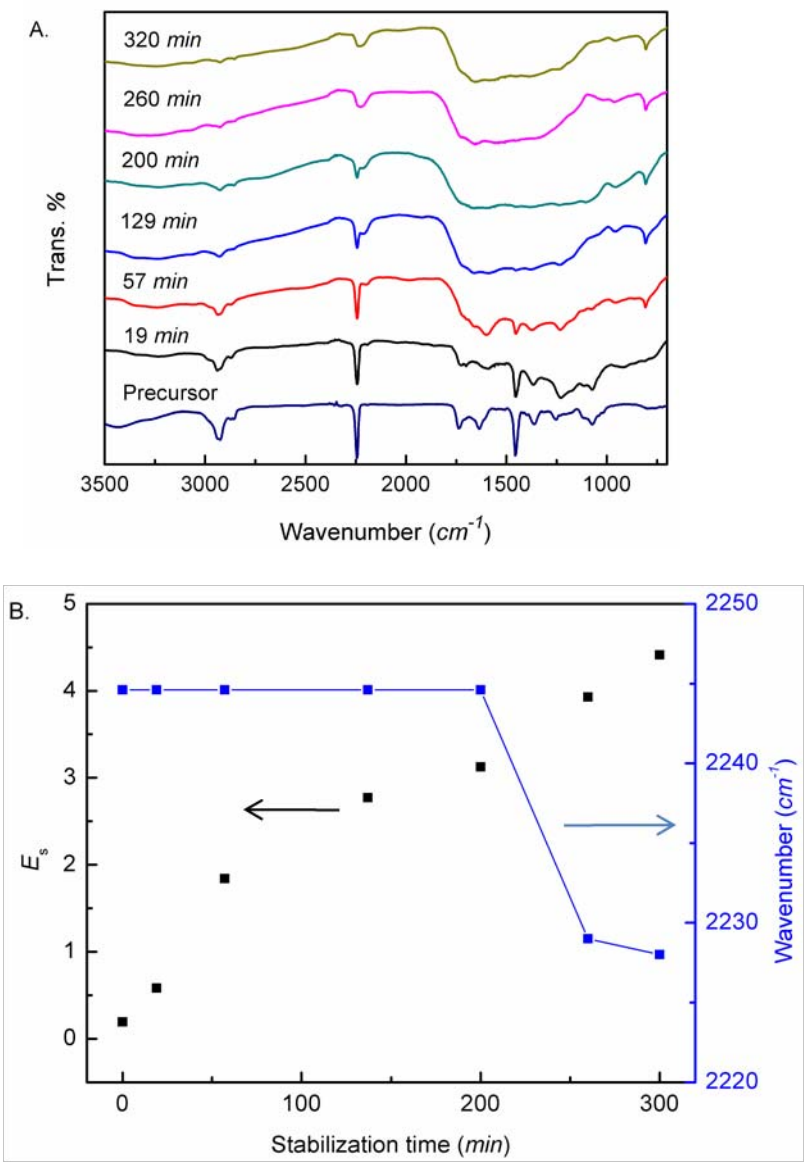

Figure 3. FTIR results of fibers stabilized at 255 ^{o}C for various times under air. (A) FTIR spectra and (B) Stabilization index E_s and peak position of nitrile band. FTIR spectra in (A) are shifted upward for clear comparison.

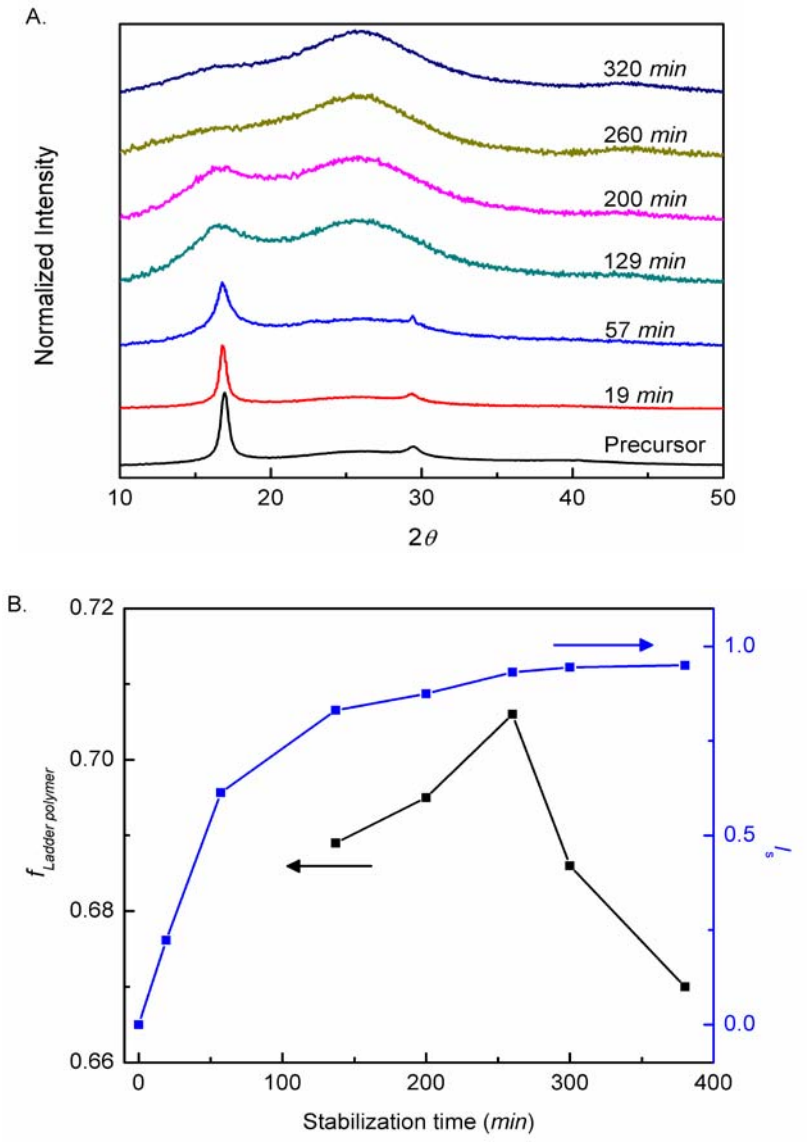

Figure 4. WAXD results of fibers stabilized at 255 ^{o}C for various times. (A) Integrated scans and (B) variation of f_{Ladder} (Herman's orientation factor of stabilized ladder polymer) and I_s (stabilization index) as a function of stabilization time. Intensity profiles of integrated scans in (A) are shifted upward for clear comparison.

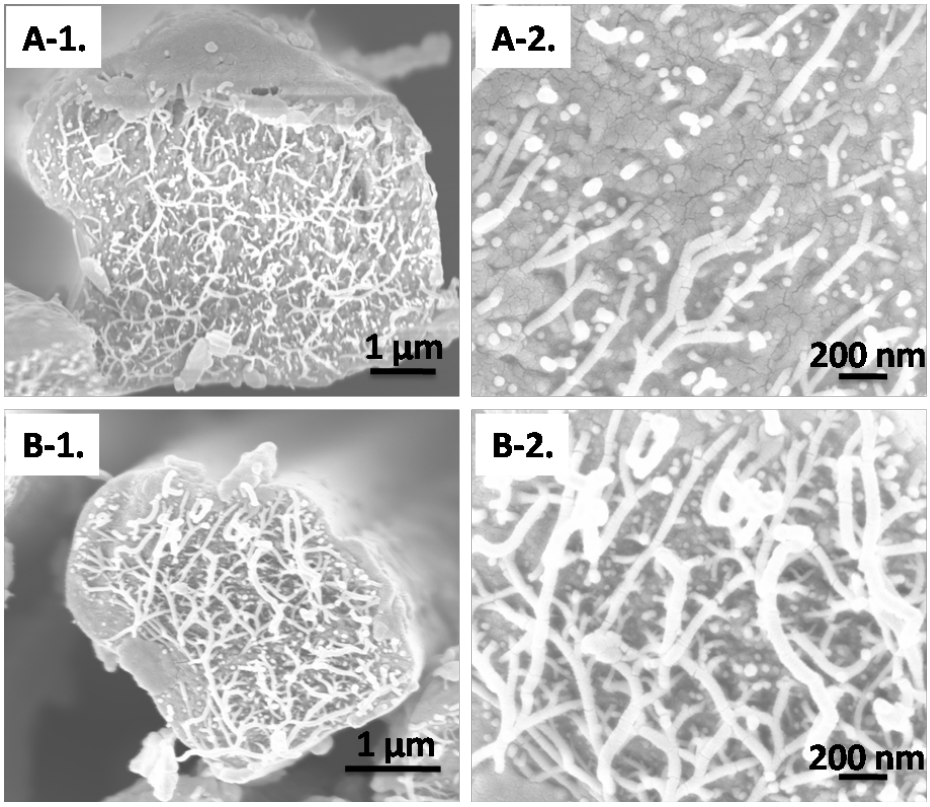

Figure 5. Cross-sectional SEM images. (A-1) (A-2) The precursor fiber was stabilized at 255 ^{o}C for 260 minutes under a constant stress of 35 MPa. (B-1) (B-2) Stabilized fibers were further carbonized at 1100 ^{o}C under a constant stress of 35 MPa. Fibrillar structure exhibits that CNTs are uniformly distributed throughout the fiber cross-section.

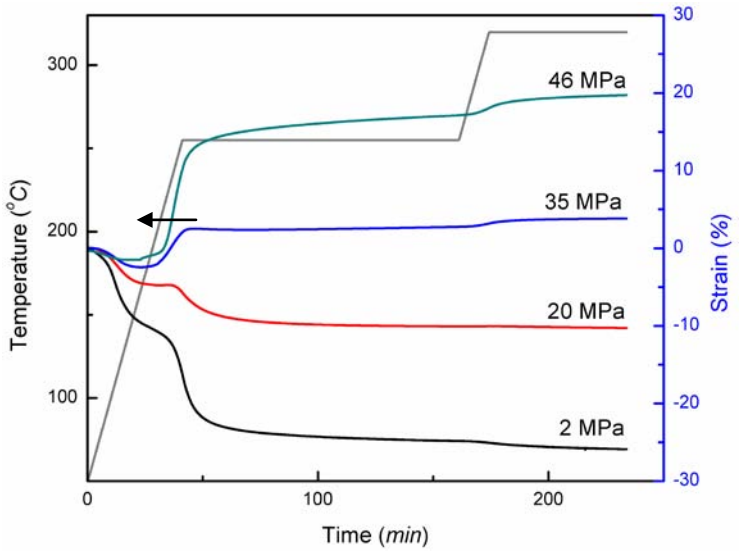

Figure 6. Shrinkage behavior of fibers stabilized under various stresses, showing the significant effect of stress on the shrinkage by chemical reaction. This suggests that the higher stress can minimize fiber shrinkage or even stretch the fiber (46 MPa). Heating profile for these experiments is also shown in the figure.

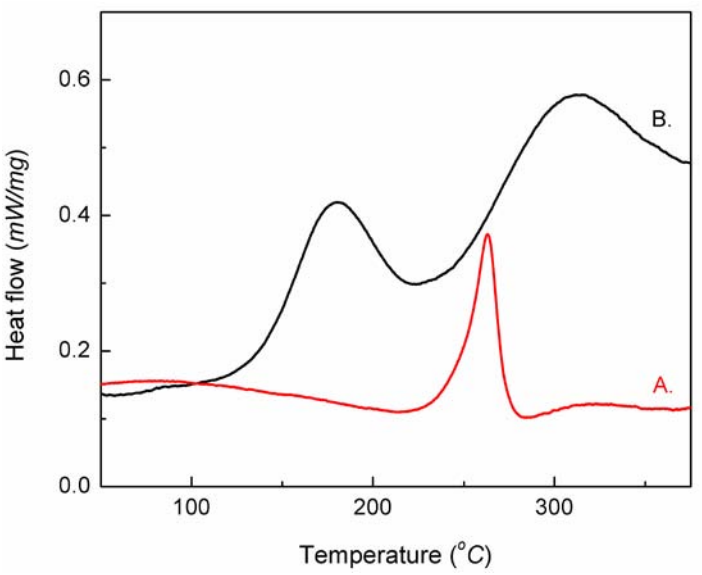

Figure 7. DSC curves of PAN/CNT composite precursor fiber at a heating rate of 1 ^{o}C/min. (A) in nitrogen and (B) Sample of run A re-run in air.

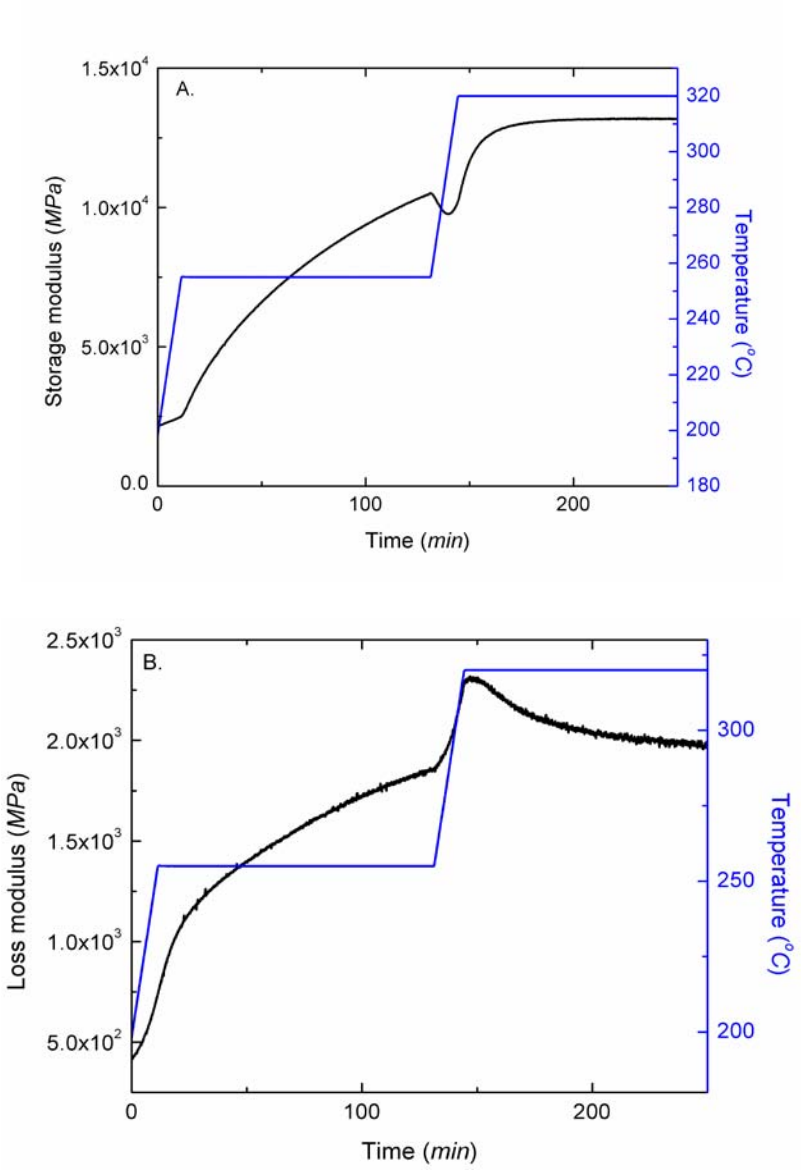

Figure 8. Dynamic mechanical behaviors of PAN/CNT precursor fibers during stepwise stabilization in air. Heating profile is also given in the plot. Stabilization temperatures are 255 and 320 ^{o}C, and heating rate was 5 ^{o}C/min. (A) Storage modulus and (B) loss modulus.

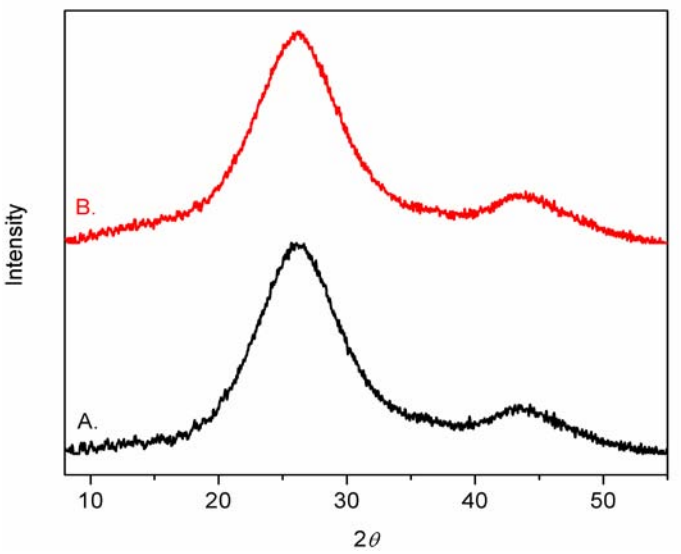

Figure 9. Integrated WAXD scans of stabilized PAN/CNT composite fibers. (A) Stabilized at 255 ^{o}C for 120 min then 320 ^{o}C for 22.5 min and (B) stabilized at 255 ^{o}C for 260 min. Both fibers exhibit comparable structure. Intensity profile of sample B is shifted upward for clear comparison.

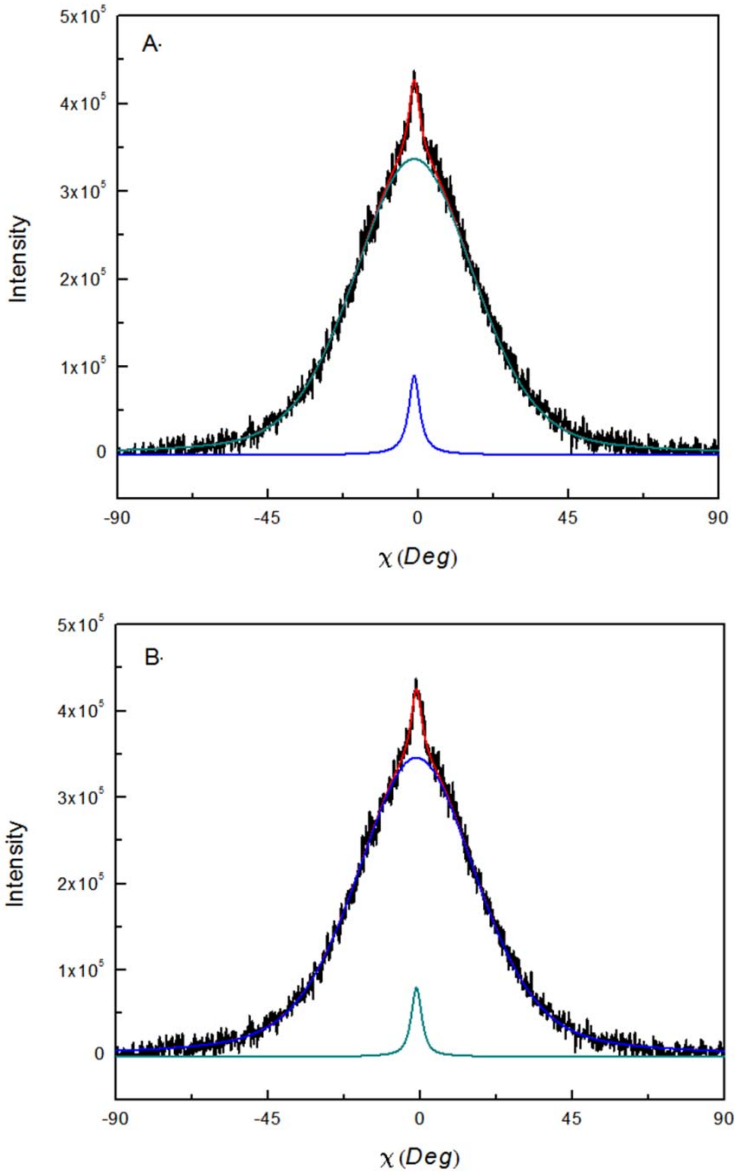

Figure 10. Azimuthal WAXD scans of stabilized PAN/CNT composite fibers. (A) Stabilized at 255 ^{o}C for 120 min then 320 ^{o}C for 22.5 min and (B) stabilized at 255 ^{o}C for 260 min. Both fibers exhibit comparable orientational order as listed in Table 8. However, curve fitting results reveal that the volume fraction of highly ordered phase in sample (A) is slightly higher than that in sample (B). Further carbonization from above fibers show that the carbon fiber from sample (A) has higher tensile modulus than that of the carbon fiber obtained from sample (B). This indicates that the higher volume fraction of highly ordered phase in the vicinity of CNT is preferable to obtain high modulus in resulting carbon fiber.

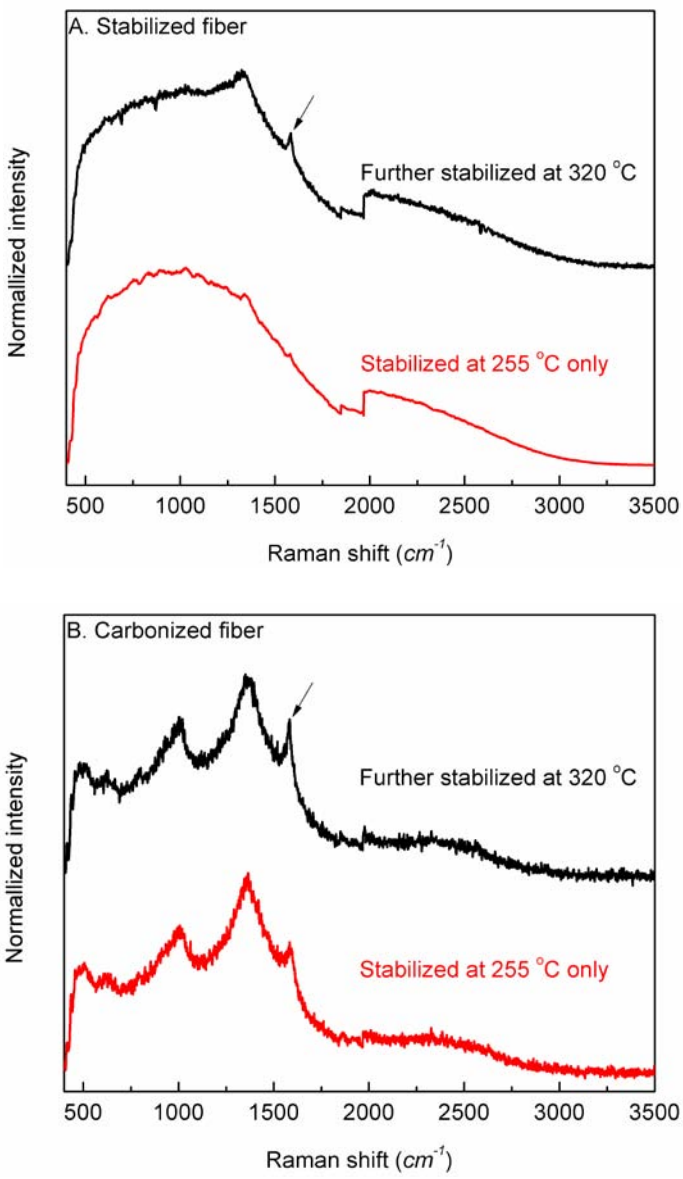

Figure 11. (A) Raman spectra of stabilized PAN/CNT composite fibers at different stabilization conditions. Top spectrum is from the fiber stabilized at 255 ^{o}C for 120 min, then at 320 ^{o}C for 22.5 min. Bottom spectrum is from the fiber stabilized at 255 ^{o}C for 260 min. Both stabilization was carried out under air environment. (B) Raman spectra of carbonized fibers from (A) at 1100 ^{o}C. G-band evolution at about 1585 cm^{-1} suggests that graphitic structure is developed. It should be noted that the graphitic feature can be observed even after stabilization at higher temperature (320 ^{o}C), while the other stabilized fiber barely shows G-band evolution. Top Raman spectra both in (A) and (B) are shifted upward for clear comparison. The discontinuity in (A) is instrumental artifact.

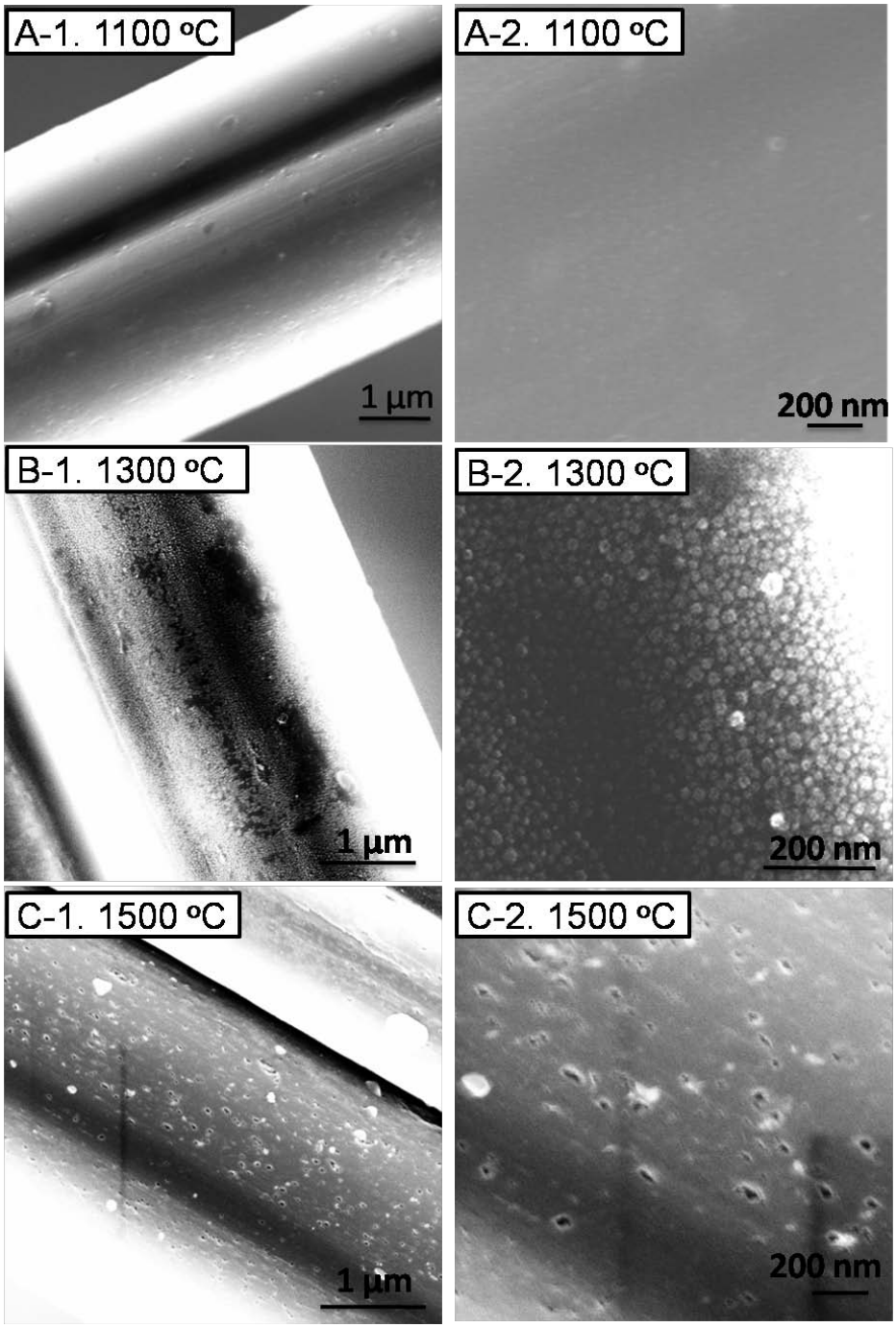

Figure 12. Surface morphologies of carbonized fiber after stabilized at 255 ^{o}C for 260 min under 35 MPa. A: Carbonized at 1100 ^{o}C; B: Carbonized at 1300 ^{o}C; C: Carbonized at 1500 ^{o}C. The carbon fiber carbonized at 1100 ^{o}C exhibits smooth surface, while the carbon fiber carbonized above 1100 ^{o}C have rough surface or pore structure, indicating thermal degradation occurred during carbonization. In current study, the exposure time (for carbonization) of the stabilized fiber at above 1000 ^{o}C is more than 4 hr including cooling time, which is excessively long. By comparison, typical carbonization residence time for commercial carbon fiber (continuous line) is known to be on the order of minutes.